(2)

PL-TR-92-2068

THE EFFECTS OF TRAVEL PATH AND SOURCE STRUCTURE ON THE CHARACTER OF REGIONAL DISTANCE SEISMOGRAMS FROM NUCLEAR EXPLOSIONS

Terry C. Wallace

University of Arizona
Department of Geosciences, Bldg #77
Tucson, AZ 85721

27 December 1991

Final Report
October 1989 - February 1992

PHILLIPS LABORATORY
AIR FORCE SYSTEMS COMMAND
HANSCOM AIR FORCE BASE, MASSACHUSETTS 01731-5000

SPONSORED BY
Defense Advanced Research Projects Agency
Nuclear Monitoring Research Office
ARPA ORDER NO. 5307

MONITORED BY
Phillips Laboratory
Contract F19628-89-K-0023

The views and conclusions contained in this document are those of the authors and should not be interpreted as representing the official policies, either expressed or implied, of the Defense Advanced Research Projects Agency or the U.S. Government.

This technical report has been reviewed and is approved for publication.

JAMES F. LEWKOWICZ
Contract Manager
Solid Earth Geophysics Branch
Earth Sciences Division

JAMES F. LEWKOWICZ
Branch Chief
Solid Earth Geophysics Branch
Earth Sciences Division

DONALD H. ECKHARDT, Director
Earth Sciences Division

This report has been reviewed by the ESD Public Affairs Office (PA) and is releasable to the National Technical Information Service (NTIS).

Qualified requestors may obtain additional copies from the Defense Technical Information Center. All others should apply to the National Technical Information Service.

If your address has changed, or if you wish to be removed from the mailing list, or if the addressee is no longer employed by your organization, please notify PL/IMA, Hanscom AFB, MA 01731-5000. This will assist us in maintaining a current mailing list.

Do not return copies of this report unless contractual obligations or notices on a specific document requires that it be returned.

REPORT DOCUMENTATION PAGE

Form Approved
OMB No 0704-0188

1. AGENCY USE ONLY (Leave blank)	2. REPORT DATE	3. REPORT TYPE AND DATES COVERED
	27 December 1991	Final: October 1989 - February 1992

4. TITLE AND SUBTITLE
The Effects of Travel Path and Source Structure on the Character of Regional Distance Seismograms from Nuclear Explosions

5. FUNDING NUMBERS
PE 61101E
PR 9A10
TA DA
WU AS

Contract:
F19628-89-K-0023

6. AUTHOR(S)
Terry C. Wallace

7. PERFORMING ORGANIZATION NAME(S) AND ADDRESS(ES)
University of Arizona
Department of Geosciences, Bldg. #77
Tucson, AZ 85721

8. PERFORMING ORGANIZATION REPORT NUMBER

9. SPONSORING/MONITORING AGENCY NAME(S) AND ADDRESS(ES)
Phillips Laboratory
Hanscom AFB, MA 01731-5000

Contract Manager: James Lewkowicz/GPEH

10. SPONSORING/MONITORING AGENCY REPORT NUMBER
PL-TR-92-2068

11. SUPPLEMENTARY NOTES

12a. DISTRIBUTION/AVAILABILITY STATEMENT
Approved for public release;
distribution unlimited

12b. DISTRIBUTION CODE

13. ABSTRACT *(Maximum 200 words)*

A comprehensive or low-yield threshold test treaty will require monitoring at regional distances, and the seismograms are very difficult to deterministically model. The character of the phases *Pg* and *Lg* shows a very strong dependence on travel path. We have conducted a number of observation-based experiments to develop empirical path corrections or scaling relations for regional phase excitation and propagation.

We determined the gross crustal structure of the western syntaxis and performed empirical studies of the blockage of *Pg* and *Lg* in the region. We also used 18 events from the 1986 Chalfant Valley earthquake sequence to examine the effects of source magnitude, depth, and rock properties on the regional distance spectra of *Pg*, *Lg*, and *Pn*. For all three variables, the spectral ratios discriminant behaves in a linear fashion.

We also reviewed the effects of tectonic release on seismic body waves generated by underground nuclear explosions.

14. SUBJECT TERMS
Pn, Pg, Lg, tectonic release, blockage

15. NUMBER OF PAGES
96

16. PRICE CODE

17. SECURITY CLASSIFICATION OF REPORT	18. SECURITY CLASSIFICATION OF THIS PAGE	19. SECURITY CLASSIFICATION OF ABSTRACT	20. LIMITATION OF ABSTRACT
Unclassified	Unclassified	Unclassified	SAR

TABLE OF CONTENTS

CHAPTER 1

Crustal Thickness and Upper Mantle Velocities in the Western Syntaxis of the Himalayas From the Inversion of Regional *Pnl* Waveforms

by

Laura L. Cathcart and Terry C. Wallace

ABSTRACT

A comprehensive or low-yield threshold test treaty will require monitoring at regional distances, and the seismograms at these distances are very difficult to deterministically model. The character of the phases *Pg* and *Lg* shows a very strong dependence on travel path. Although scattering is apparently very important in controlling the character of these phases, the gross features of the crustal waveguide, such as crustal thickness, *Pn* velocity, and "continuity" of the waveguide, have a strong signature on the efficiency of *Pg* and *Lg* propagation. It has been shown that *Lg* (and to a lesser extent, *Pg*) can be blocked by certain geologic structures such as grabens or mountain ranges. Further, the efficiency of *Pn* propagation strongly depends on the uppermost mantle velocity structure. For these reasons it is important to empirically characterize the efficiency of regional distance propagation in areas in which seismic monitoring is important.

We have determined the gross crustal structure of the western Himalayan syntaxis and performed empirical studies of the blockage of *Lg* and *Pg* in the region. We studied 36 *Pnl* waveforms from earthquakes recorded on WWSSN, IRIS/IDA and CDSN stations which had travel paths across the Tien Shan and the western Himalayan syntaxis. We used the procedure of Wallace (1986) to invert the long-period waveforms from crustal thickness and *Pn* velocity in a 12-block regionalization of the area. Fourteen events recorded at KIV or WMQ were used to map the blockages of regional phases. As expected, the correlation between rapid crustal thickness changes and blockage of *Lg* (and to a lesser extent, *Pg*) was good, but surprisingly there is also a strong correlation with low *Pn* velocity. We attempted to reproduce the spectral ratios (*Pn* to *Pg* and *Pn* to *Lg*) by generating regional distance synthetics for a suite of structural models. In particular, we investigated the effects of slight negative or positive velocity gradients below the Moho. We found that most of the regions with low *Pn* velocities have small positive velocity gradients below the Moho. We found that most of the regions with low *Pn* velocities have small positive gradients or no gradients, while the higher *Pn* velocities always have positive velocity gradients. This significantly affects spectral ratios.

INTRODUCTION

There is little dispute that the Indian and Eurasian plates collided 40 million years ago to form the Himalayan mountain chain. There is, however, disagreement on the dynamics of the collision process, namely the mode of accommodation of the Eurasian plate to the subducting Indian plate. A data set of 36 *Pnl* waveforms for travel paths across the western syntaxis region of the Himalayas is utilized to investigate the crustal thickness and upper mantle velocity in this area.

The data set was recorded at regional distances. The raypaths cross the Zagros, Hindu Kush and Pamirs, the Quetta syntaxis, and the Makran. A regionalized block model is developed for the tomographic inversion of average crustal thicknesses and upper mantle velocities from these waveforms. The results of this study provide a picture of gross crustal thicknesses and upper mantle velocities in these areas and constraints on the degree of shortening and/or crustal thickening of the Eurasian plate in its collision with India.

DATA AND METHOD OF ANALYSIS

The *Pnl* waveform is recorded at regional distances (2°–12°) and is strongly affected by the waveguide nature of the crust. It consists of two parts: the first arrival, which is composed of *Pn* and multiply reflected headwaves, and the P_L wavetrain. The P_L phase may be described as the total sum of the mode-converted and reflected *P* and *SV* energy that is trapped in the crust. The interference of this mode-converted and reflected energy within the crustal waveguide strongly affects the shape of the *Pnl* waveform.. A change in crustal thickness causes changes in arrival time of different phases, thus changing the waveform shape.

If the source parameters are known, the *Pnl* synthetics may be parameterized in terms of crustal thickness and upper mantle velocity. An optimal match of the *Pnl* synthetic to the observed regional distance waveform indicates the average thickness of the crustal waveguide. Subsequently, upper mantle velocities can be determined if the absolute travel time, crustal thickness, source depth, and distance from the source are known.

The model used for this study, developed by Langston and Helmberger (1975), consists of a layer over a half-space that correspond to the crust and mantle, respectively. It has been demonstrated (Helmberger and Engen, 1980; Wallace, 1986b) that for periods greater than a few seconds, a single-layer model is sufficient for accurate long-period *Pnl* synthetics for most continental paths. The match to the *Pnl* synthetic is thus an indication of gross crustal thickness and not of detailed crustal structure.

To obtain an optimal match of the *Pnl* synthetic waveform to the observed regional distance waveform, each *Pnl* waveform was inverted for the average crustal thickness sampled along the entire path. Wallace (1986a) has shown that if the path samples along a laterally heterogeneous or dipping Moho, then the average of the crustal thickness sampled along the entire path can be recovered from the inversion of the *Pnl* waveform.

A norm was chosen, defined as an error function, as follows:

$$e_0 = 1 - \left[\frac{\int fg}{\left(\int f^2\right)^{1/2} \left(\int g^2\right)^{1/2}} \right] \qquad (1)$$

where f is the observed regional distance *Pnl* waveform and g is the corresponding synthetic waveform. The limits of integration correspond to the starting and ending time of the window over which the waveform was inverted. In several cases this window was as long as 100 sec, but in general it was around 85 sec. When $e_0 = 0$, this indicates that the observed and synthetic waveform shapes are identical, while $e_0 = 2$ indicates the waveforms are completely out of phase. The error function was minimized with respect to the average crustal thickness and *Pn* velocity. This minimization involves the computation of numerical derivatives with respect to the crustal thickness:

$$\frac{\partial e}{\partial Th_i} = \frac{e(Th_i + \Delta Th_i) - e(Th_i)}{\Delta Th_i} \tag{2}$$

where Th_i is the crustal thickness for the i^{th} iteration and ΔTh_i is the change in crustal thickness of the model. A change in crustal thickness or upper mantle velocity only alters the timing of the headwave and reflected waves for each raypath, but does not change the shape of the single raypath response (Wallace, 1986b); therefore, the computation of numerical derivatives is simplified. Since it is not necessary to recompute the entire synthetic response for a new structure, the procedure is very efficient computationally.

For a given crustal thickness, the *Pn* velocity can be computed from the absolute travel time assuming a spherical Earth:

$$t = p\Delta + \left[\int_{r_t}^{r_s} r^{-1}\left(\gamma^2 - p^2\right)^{1/2} + \int_{r_t}^{r_0} r^{-1}\left(\gamma^2 - p^2\right)^{1/2}\right] dr \tag{3}$$

where p, the ray parameter, is equal to r_t/Pn, r_0 is the radius of the Earth, r_t is the radius to the Moho, r_s is the radius to the assumed source depth, and $\gamma = r/v(r)$. The origin times were obtained from the ISC and EDR catalogues. For those raypaths in which the optimum modeling depth differed from that listed in these catalogues, a correction to the travel time was made. This amounted to subtracting the travel time difference between the two source depths from the origin time. Because origin times are calculated assuming a crustal thickness of 33 km, a further correction was needed. The travel time difference of a ray traveling through the mantle (8.0 km/sec) of thickness Th_i – 33 km was subtracted from the origin time. As in Holt and Wallace (1989), this resulted in an increased travel time and a decreased *Pn* velocity.

Based on known topography and tectonics in the area of a given raypath, a starting crustal thickness is chosen. With the absolute travel time, source depth, and crustal thickness, a *Pn* velocity is calculated. A synthetic *Pnl* waveform is then generated, and an error function is

computed. The crustal thickness is then altered (ΔTh_i = 2 km), and a new synthetic and error function are computed. Taking the partial derivative of e, the error function, with respect to crustal thickness, followed by inversion, indicates the amount of the change in crustal thickness that will drive the error in the solution to a minimum. This new crustal thickness becomes the starting model, and the procedure is repeated for 3–5 iterations until an acceptable value for the error function is obtained. For inversions of paths that crossed the Zagros and the Makran region, a crustal velocity of 6.0 km/sec was used, with the exception of paths associated with 1965.6.21 and 1968.9.14, both of which required a crustal velocity of 6.2 km/sec to fit the observed waveform. Barazangi and Ni (1986) noted the thick layer of sediments in the Zagros region and also used a low crustal velocity for their body wave modeling. Prevot et al. (1980) found a P velocity of 6.2 km/sec for events in eastern Afghanistan in the depth range of 7–25 km, while Chatelain et al. (1980) found the optimum crustal P velocity in the Hindu Kush to be 6.4 km/sec. For the raypaths in the northwest Himalayas, therefore, a mean crustal velocity of 6.2 km/sec was chosen.

DATA

A total of 16 earthquakes in the Hindu Kush, the Pamirs, the Zagros, Turkey and the Quetta syntaxis, which were recorded at one or more WWSSN (WUE and SHI), IRIS/IDA (GAR) and CDSN (WMQ) stations at regional distances, provided 36 travel paths. Figure 1 shows the study area, the seismic stations, the earthquakes used, and a series of blocks used to regionalize the area. Table 1 lists the source parameters for the events used.

Parameters for the event of 1972.8.6 in the Makran were taken from Jackson and McKenzie (1984), those for 1968.6.23 in the Zagros were taken from Jackson and Fitch (1981), and those for 1968.9.14 were taken from Ni and Barazangi (1986). The event of 1968.4.29 was modeled after McKenzie (1972), the solution for 1965.6.21 was taken from Ni and Barazangi (1986), and the solution for 1965.2.2 was taken from Chandra (1978).

Earthquakes which occurred on 1965.4.10, 1965.4.2, 1965.12.3, and 1972.1.28 did not have previously determined focal mechanisms. Source parameters for these earthquakes were obtained from the ISC and the EDR. The focal mechanisms determined by Chandra (1978) in the Hindu Kush and Pamirs were carefully studied. The mechanism of 1965.2.2 was used for 1965.4.2 and 1965.4.10 as a starting model. It was found through the inversion procedure that a dextral sense of slip for 1965.4.10 yielded a good fit to the observed waveform but the steep dip was taken to the north instead of the south as in the 1965.2.2 mechanism.

The earthquake on 1965.4.2 occurred just north of the Herat fault in the Hindu Kush. Its mechanism was assumed to be right lateral strike slip in the same sense as this fault. The fault plane was assumed to have a northerly trend and a shallow dip (30°).

An event on 1974.10.4 at 26.29°N, 66.54°E, within 100 km of the 1972.1.28 earthquake, has been interpreted as one of right lateral strike slip with a northwesterly trending nodal plane (Quitmeyer et al., 1979). This mechanism was used for 1972.1.28, which was located in the southern Kirthar Range. The dip direction was taken to the south, and while 1974.10.4 was more steeply dipping (40°), the synthetic waveform most closely fit the observed waveform with a dip of 20°. The mechanism of 1965.3.14 (Chandra, 1978) was taken as the starting model for the event on 1965.12.3. After the inversion, it became clear that a polarity reversal was necessary, indicating a normal-faulting event.

Sources from Jackson and McKenzie (1984) were obtained from first-motion arrivals on mostly long-period vertical WWSSN instruments plotted on the focal sphere with an assumed source velocity of 6.8 km/sec. Chandra (1978) also obtained solutions by plotting first-motion arrivals of mostly long-period WWSSN instruments. Ni and Barazangi (1986) improved solutions of Jackson and McKenzie (1984) by *P*-waveform modeling and/or analyzing *S*-wave polarization data.

Holt and Wallace (1989) have demonstrated that uncertainties in the range of ±20° in strike, dip, and rake do not significantly affect the inversion results for *Pn* velocity and crustal thickness. They have deduced that uncertainties of ±20° in strike, dip, and rake for dip-slip mechanisms also

present no serious problems for the inversion results. Small inaccuracies in time function length (of the order of 50%) should not alter the inversion results much and increase the error only slightly (Holt and Wallace, 1989).

TECTONIC BACKGROUND

The convergence rate between India and Eurasia, calculated at 50 mm/yr (Molnar and Tapponnier, 1975), cannot be accounted for solely by the rate of underthrusting at the Himalayas (10s of millimeters per year, Molnar and Qidong, 1984). Part of India's penetration may be absorbed by conjugate strike-slip faulting. Slip-line field theory has been proposed (Molnar and Tapponnier, 1975) to account for the missing amount of convergence in the Himalayas. By this theory, as India (a rigid indentor) collided with Eurasia to the north, this produced slip lines (strike-slip faults) in a plastic body (Eurasia). Along these strike-slip faults, material is squeezed out to the east and west.

In the western Himalayas these strike-slip faults are the Chaman fault (left lateral) and the Herult fault (right lateral). Movement of material along these faults may prevent crustal thickening and allow further northward movement of India beneath Eurasia. Holt and Wallace (1989) postulated the presence of an upper mantle lid defined by a gradual increase in velocity down to a low-velocity zone (the top of the asthenosphere) beneath Tibet based on a positive upper mantle velocity gradient beneath this region. The high *Pn* velocities beneath southern Tibet suggested that underthrusting of India beneath Eurasia was the dominant mechanism of uplift of the Tibetan Plateau rather than uniform thickening, although Holt and Wallace's (1989) seismic data did not exclude the mechanism of uniform thickening. Assuming a rate of 2–2.5 cm/yr of underthrusting, Holt and Wallace (1989) concluded that the remaining amount of northward movement is taken up by shortening within Asia by the mechanism of crustal extrusion and thickening.

In this paper the transition in crustal thickness and upper mantle velocity from the Hindu Kush and Pamirs to as far west as eastern Turkey is examined. Numerous studies have been done

of the Hindu Kush and Pamirs. Menke and Jacob (1976) found *P* velocities of 6.5 km/sec and *Pn* velocities of 8.35 km/sec at the western Indian plate margins. Chatelain et al. (1980) used crustal velocities and upper mantle velocities of 6.0 km/sec and 8.0 km/sec, respectively, in the Hindu Kush. Velocity inversion of the Chatelain (1980) data indicated that the best fit was for a *P* velocity of 6.4 km/sec (Roecker, 1982). In their analyses of *S*–*P* residuals, Chen and Molnar (1981) found evidence for high upper mantle velocity in the northwest Himalayas. The inversion for gross crustal thickness and *Pn* velocity yielded a *Pn* velocity of 8.3 km/sec in the Hindu Kush and Pamirs region (Holt and Wallace, 1989). Most workers agree on a 45- to 70-km-thick crust beneath the northwest Himalayas and the Hindu Kush (Maruyssi, 1964; Khurshid et al., 1984; Chatelain et al., 1980; Roecker, 1982).

Velocities and thicknesses in the Quetta syntaxis and in the Makran region of southern Pakistan and southeast Iran are not very well known. There has been some work done, however, in the Zagros Mountains of Iran. Analysis of Rayleigh wave dispersion suggests thick crust (45 km) in the Iranian Plateau (Asudeh, 19481, 1982a,b). In the Zagros, the upper mantle velocity is believed to be high (Asudeh, 1982b), and the efficient propagation of *Sn* (Kadinsky-Cade et al., 1981) agrees with this velocity. It is also noted (Kadinsky-Cade, 1981) that the crust in the Zagros thickens to 50 km north of Shiraz, Iran. A thick basement is believed to be present in the southern Caspian Sea with a *P* velocity of 6.6 km/sec (Kadinsky-Cade, 1981), and the efficient propagation of *Sn* along with the poor propagation of *Lg* is believed to indicate oceanic basement in this region.

INVERSION RESULTS

The average crustal thickness and upper mantle velocity were determined for each block by performing a linear weighted least squares inversion using the crustal thickness and *Pn* velocity results for the individual paths. The average thickness and slowness ($1/Pn$) of a given path are

assumed to be the sum of the fraction of path length in a given block multiplied by the thickness or slowness of the block:

$$X_j = \sum_{i=1}^{n} \left(X_i d_{ij} \right) / D_j \tag{4}$$

where X_j is the average crustal thickness or slowness obtained from each inversion of the *Pnl* waveform along travel path j, X_i is the same parameter for block i, d_{ij} is the distance traveled in block i by raypath j, and D_j is the total raypath length. The *a priori* variance-covariance matrix is assumed to be a diagonal matrix composed of the variance from crustal thickness and the slowness obtained from the individual inversions for each path. Holt and Wallace (1989) have determined that errors in crustal velocity of ±0.1 km/sec can lead to errors in crustal thickness estimates of ±5% of the true thickness. On the basis of experience with inversions in the Tibet and China region, it is assumed that the average standard deviations for crustal thickness and *Pn* velocity are ±2.5 km and ±0.1 km/sec, respectively. Uncertainties in *Pn* velocity are due to errors in origin time of hypocenter location.

Table 2 lists the results of the regionalized inversion. These results are shown in Figures 2 and 3. The standard deviation of each parameter was obtained from the *a posteriori* model variance-covariance matrix after the inversion was performed. Figure 4 shows the results for crustal thickness.

Block 1 has an estimated crustal thickness of 33 km. It must be recognized that the northwestern portion of this block is poorly sampled. The *Pnl* waveform averages the crustal thickness it encounters along its path. An average value of 33 km for crustal thickness is geologically possible. Jackson and McKenzie (1984) found that the deformation in western Turkey is dominated by the movement of continental material laterally away from the Lake Van region in eastern Turkey along the Anatolian faults. This need not be incompatible with a relatively normal crustal thickness in this region. It has also been postulated that subducting or thickening

the continental crust can be avoided by moving material away from the collision zone (the Zagros) along strike-slip faults subparallel to the regional trend (northwest-southeast). Hence Turkey moves west relative to Eurasia along the north and east Anatolian faults (Jackson and McKenzie, 1984). The rethickening of previously stretched basement (Arabian) is an important mechanism in Iran and allows shortening without creating abnormally thick crust (Jackson and McKenzie, 1984). Additionally, Ni and Barazangi (1986) indicate that the Zagros are currently in an earlier stage of continental collision than the Himalayas, and the style of deformation is therefore much different.

Block 2 is indisputably the most poorly resolved block in this study. Since a block is better resolved with an increased density of raypaths and also raypaths in more than one direction, the lack of data for this block makes the resolution so poor. The *a posteriori* model variance-covariance matrix attests to this (standard deviation of ±12.9 km!). As this parameter is associated with the smallest single value (0.08), it is also the most sensitive to noise. Nevertheless, the thickness value of 60 km, although it is high, can be explained. Central Iran is believed to be relatively rigid (Jackson and McKenzie, 1984), with little or no seismicity. There is considerable evidence for crustal shortening in the Kopet Dag (Jackson and Mckenzie, 1984), where Iran is compressed against the Turan shield. If thickening accompanies this shortening, this anomalously thick crust may be justified. Because this block also encompasses the southern Caspian Sea, the efficient *Sn* propagation attributed to oceanic basement may not be incompatible with a thick crust.

Block 3 is resolved the next most poorly in this study. There are, however, two raypaths in different directions, so the solution is more reliable than that for block 2. A thick (56 km) crust agrees with the well-documented subcrustal seismicity in this area, where the Arabian plate is thrust under the Makran (Quitmeyer and Jacob, 1979; Quitmeyer et al., 1979; Jackson and McKenzie, 1984; Ni and Barazangi, 1986;). Jackson and Mckenzie (1984) discuss evidence for movement of material away from the collision zone in northeast Iran on north-south strike-slip faults toward the Makran, indicating a possible thickening in the Makran region.

Block 4 is well sampled. There has not been much work in this area to constrain the solution of crustal thickness of 50 km; however, northeast of the main Zagros reverse fault there is no seismicity (Jackson and Mckenzie, 1984), so this area may be a stable shield-type region.

Block 5 covers the Quetta syntaxis and the Kirthar Range. The standard deviation for this block is very small, and it is well sampled. The crustal thickness of 30 km seems a little thin, yet the Quetta Transverse Range (Menke and Jacob, 1976) may be a zone of young crustal shortening and lithospheric convergence, as evidenced by ERTS satellite images. The western collisional boundary of India and Eurasian (the Sulaiman and Kirthar Ranges) consists of folding, thrusting, and left-lateral shear (Quitmeyer and Jacob, 1979) and contains scattered seismicity. Not much is known about this region, but this block is well resolved.

Block 6 encompasses the Hindu Kush and Pamirs. A crustal thickness of 75 km agrees with previous estimates of thickness in the area. In particular, it agrees with Roecker (1982) and is close to the result of Holt and Wallace (1989) of 67 km. This region is known for its intermediate-depth seismicity, and Roecker (1982) has suggested that this results from subducted continental lithosphere.

Figure 3 shows the regionalized inversion results for *Pn* velocity. All the results for *Pn* velocity were relatively stable to noise in the data, as they were associated with large single values. Block 1 has a reasonable *Pn* velocity of 8.1 km/sec. This result agrees with the results of Asudeh (1982b), which indicate a high *Pn* velocity for this region, and Kadinsky-Cade et al. (1981), who found the propagation of *Sn* to be efficient. There is not subcrustal seismicity in the Zagros or evidence of any significant amount of subduction (Jackson and McKenzie, 1984). Thus a relatively high *Pn* velocity is not surprising.

Block 2 has a very high *Pn* velocity (8.7 km/sec), and in view of the resolution associated with this block, not much credence should be given to it. The efficient *Sn* propagation and poor *Lg* propagation in the southern Caspian Sea (Kadinsky-Cade et al., 1981) do not disagree with these results, however. The lack of seismicity northeast of the main Zagros fault together with this high *Pn* velocity may indicate the uplift of the Iranian plateau was not caused by thermal means.

Block 3 has a low *Pn* velocity of 7.6 km/sec. This value strongly supports the postulated subduction in the Makran. There are calc-alkali andesitic magmatic centers with a northeast alignment in the central Makran (Jackson and McKenzie, 1984), thus providing geological evidence for a hot mantle beneath this area. The oceanic portion of the Arabian plate is apparently subducted to the north beneath the Makran (Quitmeyer and Jacob, 1979).

Block 4 has a *Pn* velocity of 7.9 km/sec. Jackson and McKenzie (1984) discuss the low *Pn* velocity in northeast Iran and the attenuation of high-frequency *Sn*, evidence that northeast Iran is shortened and sheared. The low *Pn* velocity may reflect this shearing (and also the effect of the Helmond basin).

Block 5 indicates a very low (7.5 km/sec) *Pn* velocity for the Quetta syntaxial region. A large part of this result is controlled by raypath 12, whose *Pn* velocity was particularly low. If this region is one of young crustal shortening and lithospheric convergence as postulated by Menke and Jacob (1976), then a low *Pn* velocity would be expected. The major left-lateral Chaman fault to the west of this block would also provide a way of moving material laterally out of the way of Quetta.

Block 6 has a high *Pn* velocity of 8.2 km/sec, which is slightly lower than that determined by Holt and Wallace (1989) and higher than that assumed by Chatelain et al. (1980) for the Hindu Kush region. A high *Pn* velocity in the northwest Himalayas has been postulated by many workers (Menke and Jacob (1976) and Roecker (1982), among others). Intermediate-depth seismicity has also been documented for this region (Quitmeyer and Jacob, 1979; Chandra, 1978), indicating subduction.

DISCUSSION

The high crustal thickness (56 km) coupled with the low *Pn* velocity (7.6 km/sec) in the Makran region is significant. The active northward subduction of the Arabian plate beneath the Makran may be accommodated by the mechanism of uniform crustal thickening and lithospheric shortening, as the age of the subduction in this area is 70–100 Ma (Jackson and McKenzie, 1979).

In this model the mantle is expected to be hot and weak after thickening has occurred, thus causing the *Pn* velocity to be slow while the crust is thick.

The relatively normal crustal thickness (33 km) in the Turkey/Zagros region may explain how the volcanoes of the Lake Van region are related to the collision of Arabia and Eurasia. Evidence from this study indicates that these volcanoes are related to tension perpendicular to shortening, as postulated by Jackson and McKenzie (1979). They found evidence for the expulsion of northwest Iran eastward from the Lake Van region. This type of extension might cause stretching and a thinner crust, along with a moderate *Pn* velocity.

There is insufficient seismic data in block 2 (central Iran) to make any observations about the crustal structure or upper mantle velocity of this region. The results of block 4 in the Helmond basin and the southern part of the former Union of Soviet Socialist Republics, however, may indicate a stable shield-type region, which is supported by the apparent lack of seismicity in the area of block 4.

The relatively thin crust (30 km) in the Quetta syntaxial region coupled with the extremely low *Pn* velocity (7.5 km/sec) may be explained if the mechanism of young crustal shortening (causing a low *Pn* velocity) and lithospheric convergence (Menke and Jacob, 1976) is to be believed. The crust need not be thick in this region, as the major left-lateral Chaman fault can carry material out of Quetta's way.

Results for the Hindu Kush and Pamirs indicate an extremely thick crust (75 km) and a high *Pn* velocity (8.2 km/sec). These results support the accommodation of subduction by the mechanism of underthrusting in which the mantle behaves in a shield-like manner. This strongly agrees with the conclusion of Holt and Wallace (1989) for this same region.

Results of this study support the theory of Ni and Barazangi (1986), in which the collision of the Arabian and Iranian blocks (shortening and high-angle reverse faulting) represents a younger stage in the cycle of collisional tectonics seen in the Himalayas (i.e., the underthrusting in the Hindu Kush). The crustal thickening in the Makran may represent an intermediate stage in the

transition from high-angle reverse faulting to underthrusting. More investigation into the central Iranian area is necessary to constrain the mode of deformation in this area.

Lg and Pg Efficiency

We investigated the efficiency of the propagation of *Lg* and *Pg* in several ways. The first method is based on the empirical algorithm of Kennet et al. (1985). Each *Lg* train is assigned a numerical code on the basis of *Lg* appearance. Although the size of the *Lg* packet is not simply related to the nature of the crustal structure along the path, the largest effects (such as blockage) come from prominent structural heterogeneity. A similar empirical approach is used to assess *Pg* efficiency. The installation of two very broadband seismic stations in the Soviet Union allowed us to also assess the efficiency of propagation more rigorously. An envelope function was fit to *Pn*, *Sn*, *Pg*, and *Lg*; these envelopes were calculated at 1, 3, and 5 Hz. The ratio of the envelope functions for *Pg* and *Pn* was used to calculate the relative efficiency of *Pg*. Similarly, the ratio of *Lg* to *Sn* was used to calculate the efficiency of *Lg*.

Figure 4 summarizes the *Lg* efficiency. Paths through relatively constant-thickness crust (for example, blocks 2, 3, and 4) were fairly efficient. As expected, when paths crossed regions of rapidly varying crustal thickness, *Lg* was much diminished. For example, raypaths from the Hindu Kush to the Quetta syntaxis were nearly devoid of *Lg*. Similarly, earthquakes in southern Iran recorded at ASH (only two events studied thus far) had poorly developed *Lg*. Figure 5 summarizes the *Pg* efficiency. Again, crustal thickness heterogeneity plays a role in the efficiency of propagation, although the correlation is much less well developed. For example, the *Pg* phase is much more efficiently propagated for the Hindu Kush to the Quetta syntaxis than *Pn*. This is probably the result of very low *Pn* velocities in block 5 (as associated high attenuation of the uppermost mantle).

REFERENCES

Asudeh, I. (1981). The crust and upper mantle structure of Iran, Ph.D. thesis, University of Cambridge, 113 pp.

Asudeh, I. (1982a). Pn velocities beneath Iran, *Earth Planet. Sci. Lett.* **61**, 136-142.

Asudeh, I. (1982b). Seismic structure of Iran from surface and body wave data, *Geophys. J. R. Astron. Soc.* **71**, 715-730.

Chandra, U. (1978). Seismicity, earthquake mechanisms and tectonics along the Himalayan mountain range and vicinity, *Phys. Earth Planet. Inter.* **16**, 109-131.

Chatelain, J. O, S. Roecker, D. Hatzfeld, and P. Molnar (1980). Microearthquake seismicity and fault-plane solutions in the Hindu Kush region and their tectonic interpretation, *J. Geophys. Res.* **85**, 1365-1387.

Chen, W. P. and P. Molnar (1981). Constraints on the seismic wave velocity structure beneath the Tibetan Plateau and their tectonic implications, *J. Geophys. Res.* **86**, 5937-5962.

Helmberger, D. V. and G. R. Engen (1980). Modeling the long-period body waves from shallow earthquakes at regional distances, *Bull. Seism. Soc. Am.* **70**, 1699-1714.

Holt, W. E. and T. C. Wallace (1989). Crustal thickness and upper mantle velocities in the Tibetan Plateau region from the inversion of regional *Pnl* waveforms: Evidence for a thick upper mantle lid beneath southern Tibet, *J. Geophys. Res.* **95**, 12,499-12,525.

Jackson, J. A. and T. J. Fitch (1981). Basement faulting and the focal depths of the larger earthquakes in the Zagros mountains (Iran), *Geophys. J. R. Astron. Soc.* **64**, 561-586.

Jackson, J. A. and D. P. McKenzie (1984). Active tectonics of the Alpine-Himalayan Belt between western Turkey and Pakistan, *Geophys. J. R. Astron. Soc.* **77**, 185-264.

Kadinsky-Cade, K., M. Barazangi, J. Oliver, and B. Isacks (1981). Lateral variations of high frequency seismic wave propagation at regional distances across the Turkish and Iranian plateaus, *J. Geophys. Res* **86**, 9377-9396.

Khurshid, A., G. Yielding, S. Ahmad, I. Davidson, J. A. Jackson, G. C. P. King, and Lin Ban Zuo (1984). The seismicity of northernmost Pakistan, *Tectonophysics* **109**, 209-226.

Langston, C. A. and D. V. Helmberger (1975). A procedure for modeling shallow dislocation sources, *Geophys. J. R. Astron. Soc.* **42**, 117-130.

Marussi, A. (1964). *Geophysics of the Karakorum. Scientific Reports, Italian Expeditions to the Karakorum (K2) and Hindu Kush*, E. J. Brill, Leiden.

McKenzie, D. P. (1972). Active tectonics of the Mediterranean region, *Geophys. J. R. Astron. Soc.* **30**, 109-185.

Menke, W. H. and K. H. Jacob (1976). Seismicity patterns in Pakistan and northwestern India associated with continental collision, *Bull. Seism. Soc. Am.* **66**, 1695-1711.

Molnar, P. and Q. Deng (1984). Faulting associated with large earthquakes and the average rate of deformation in central and eastern Asia, *J. Geophys. Res.* **89**, 6203-6228.

Molnar, P. and P. Tapponier (1975). Cenozoic tectonics of Asia: Effects of a continental collision, *Science* **189**, 419-425.

Ni, J. and M. Barazangi (1986). Seismotectonics of the Zagros continental collision zone and a comparison with the Himalayas, *J. Geophys. Res.* **91**, 8205-8218.

Prevot, R., D. Hatzfeld, S. W. Roecker, and P. Molnar (1980). Shallow earthquakes and active tectonics in eastern Afghanistan, *J. Geophys. Res.* **85**, 1347-1357.

Quitmeyer, R. C., A. Farah, and K. Jacob (1979). The seismicity of Pakistan and its relation to surface faults, in *Geodynamics of Pakistan*, A. Farah and K. DeJong, editors, Geological Survey of Pakistan, Quetta.

Quitmeyer, R. C. and K. Jacob (1979). Historical and modern seismicity of Pakistan, Afghanistan, northwestern India and southeastern Iran, *Bull. Seism. Soc. Am.* **69**, 773-823.

Roecker, S. W. (1982). Velocity structure of the Pamir-Hindu Kush region: Possible evidence of subducted crust, *J. Geophys. Res.* **87**, 945-959.

Wallace, T. C. (1986a). Inversion of long-period regional body waves for crustal structure, *Geophys. Res. Lett.* **13**, 749-752.

Wallace, T. C. (1986b). Some useful approximations to generalized ray theory for regional distance seismograms, *Geophys. J. R. Astron. Soc.* **85**, 349-363.

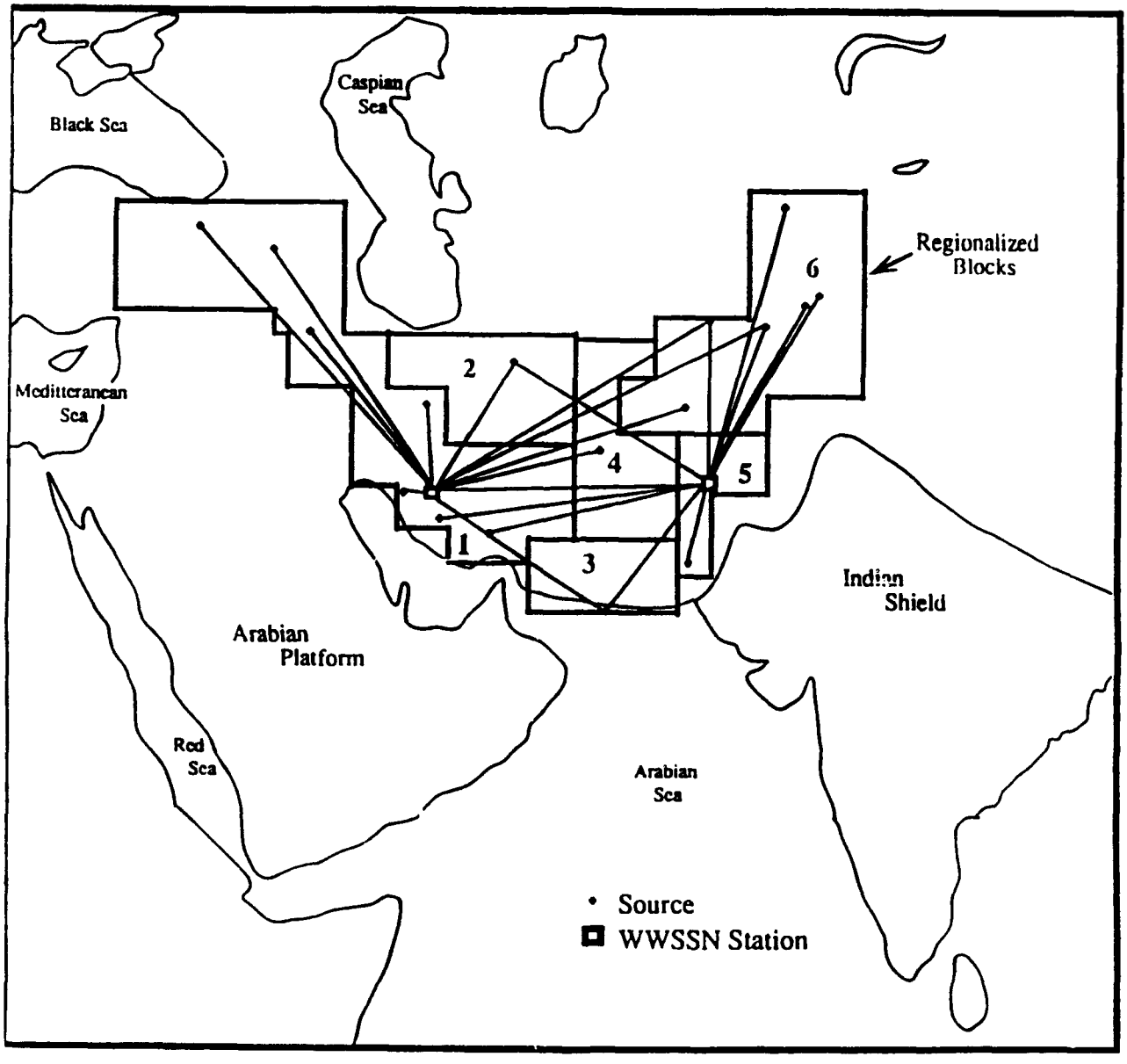

Figure 1. Regionalization of the western Himalayan Syntaxis. The six blocks were chosen on the basis of topography and surface geology. The sources used in this study are designated by diamonds, and the stations used are designated by squares. The ray paths are shown as solid lines between source and receivers.

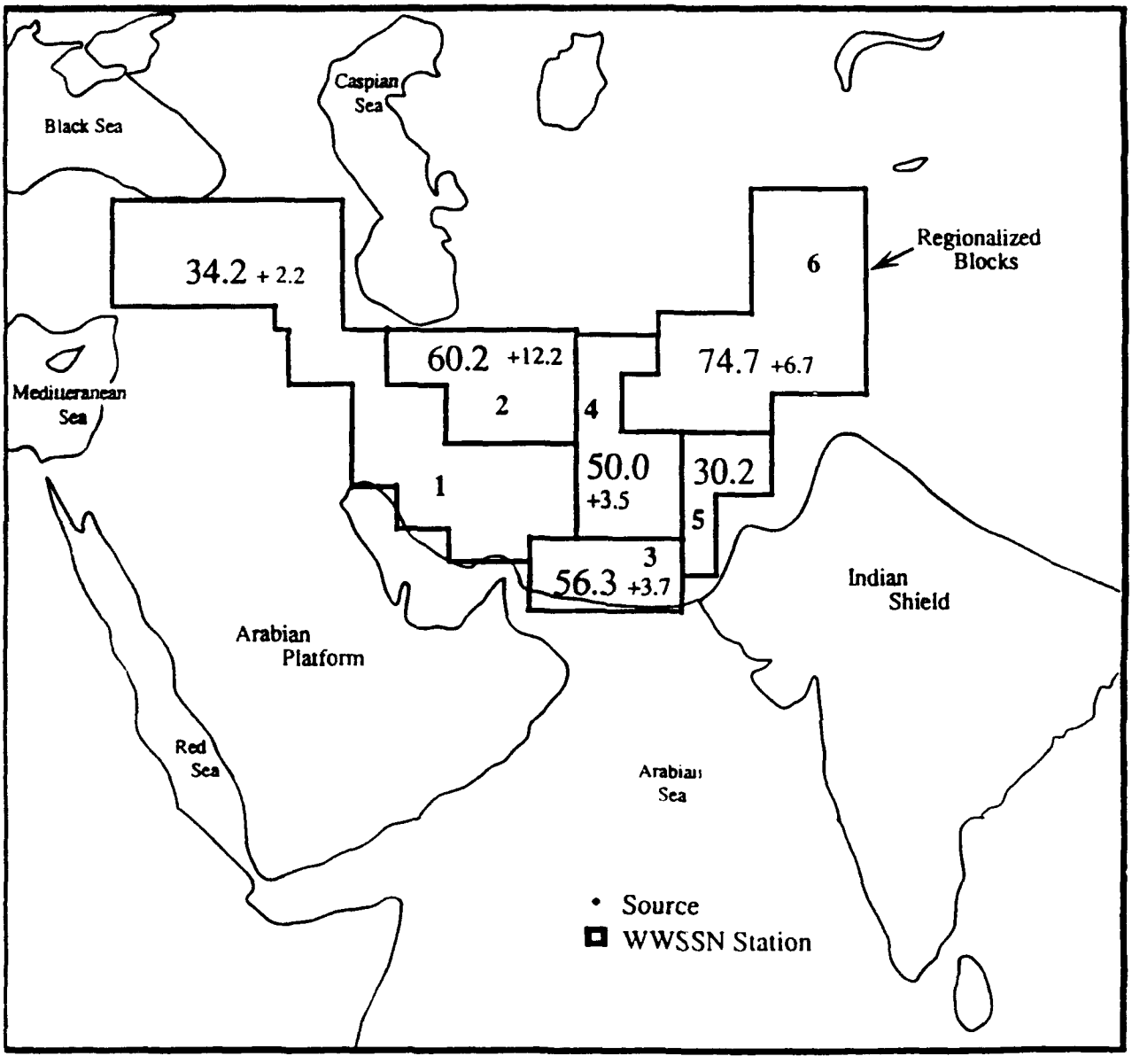

Figure 2. Results of the crustal thickness inversion. Errors are given next to the thickness values (in km).

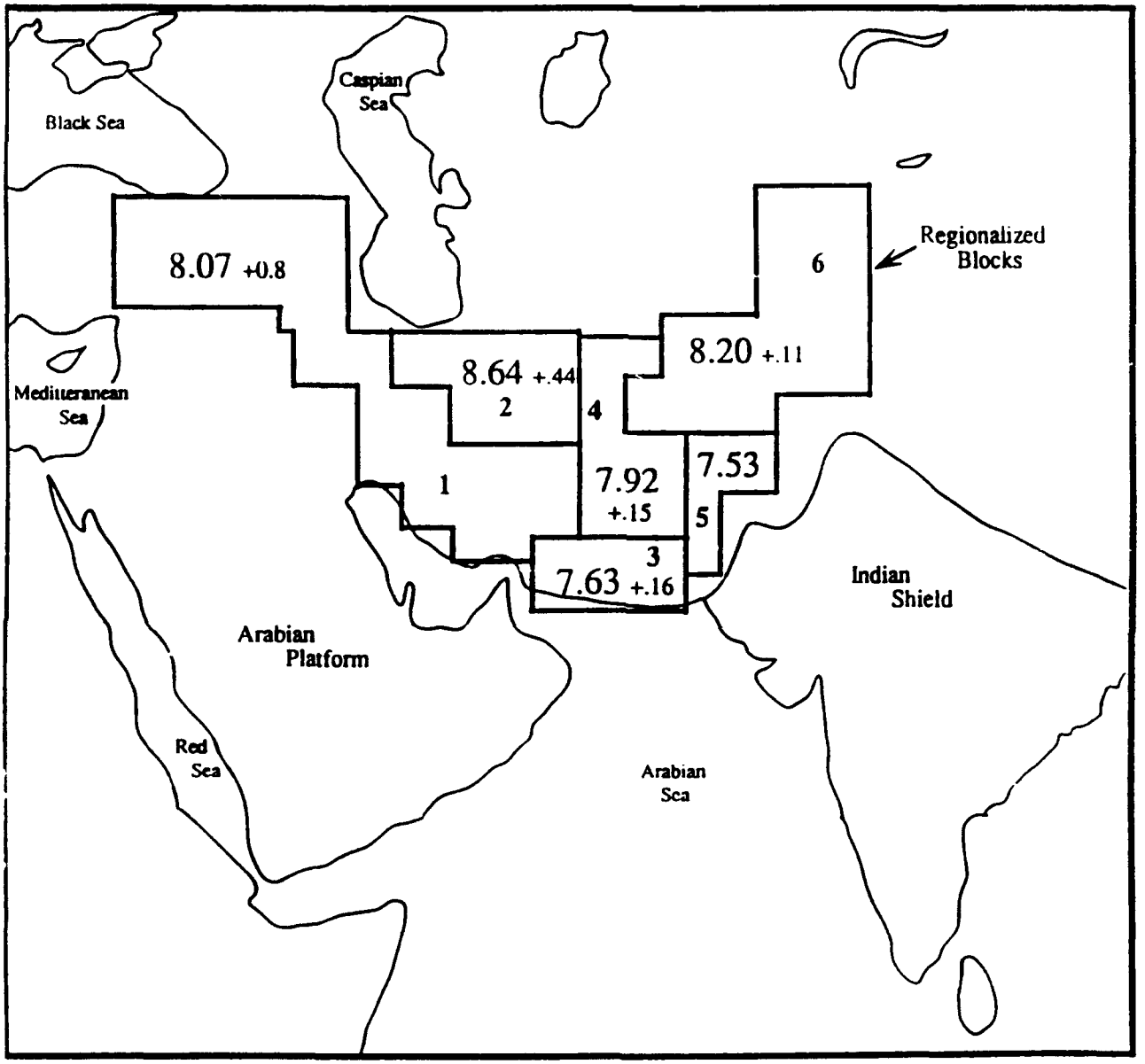

Figure 3. Results of the *Pn* velocity inversions. Errors are given in km/sec.

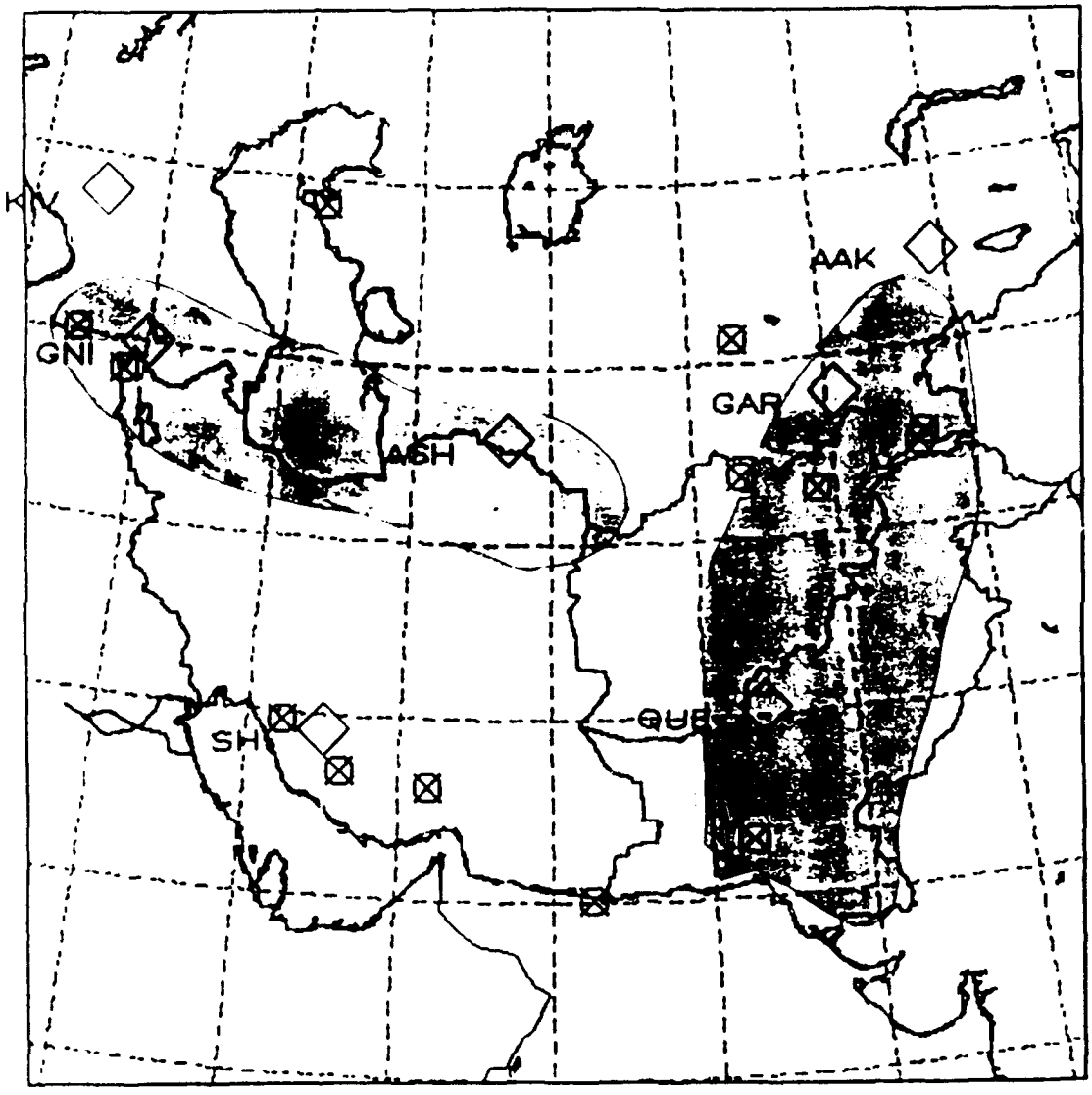

Figure 4. The shaded regions represent the location of significant *Pg* blockage. These regions roughly correspond to regions of inefficient *Sn* propagation as found by Kadinsky-Cade et al. (1981).

CHAPTER 2

The Effect of Source Magnitude, Depth, and Rock Properties on Regional Seismic Spectra of the July 1986 Chalfant Valley Earthquake Sequence

by

Stephen C. Myers and Terry C. Wallace

ABSTRACT

We used 18 events from the July 1986 Chalfant Valley earthquake sequence to examine the effects of source magnitude, depth, and rock properties (parameterized by *P*-wave velocity at the source) on the regional distance spectra of *Pg*, *Lg*, and *Pn*. The data consist of 18 events with M_L's of 1.8–5.8, depths of 4.5–10 km, and *P*-velocities of 5.88–6.06 km/sec recorded regionally at four Sandia broadband seismic stations. Sixteen of the 18 events were located to within ±1 km in depth, providing accurate depth and *P*-wave velocity at the source. The two poorly located events were used only in magnitude correlations. We examined the spectral behavior of each phase via a ratio of the maximum amplitude within a 1 to 2 Hz frequency window with the maximum amplitude within a 6 to 7 Hz window.

Initial results showed a great deal of scatter when the spectral ratio was plotted as a function of source magnitude, depth, and *P*-wave velocity. Scatter was greatly reduced, however, by limiting the range in magnitude when examining the depth and *P*-wave velocity, and vice versa (depth and *P*-wave velocity are inseparable variables in this study). Correlations show that the spectral ratio linearly depends on all three variables for this study. However, the linear fit may change as a greater range in the variables is examined.

At three of the four stations used in this study the spectral ratio decreased as depth and *P*-wave velocity increased. For *Pg* the one station the contradicts this relation has a very low correlation coefficient, and the contradicting station for *Lg* shows a spectral ratio having very little dependence on source depth or *P*-wave velocity at the source, perhaps indicating that these data are noisy. Two stations are beyond *Pn* distance for the Chalfant Valley area. One station shows a spectral ratio decreasing as depth and the *P*-wave velocity increase, and the other station shows the opposite behavior. However, the correlation coefficient at the station that has a decreasing spectral ratio is very high, and the correlation coefficient at the other station is very low, implying that the negative correlation is more reliable. Correlations between spectral ratio and magnitude are contrary from station to station for *Pg* and *Lg*. Two stations have positive correlations for both

phases, and the other two stations have negative correlations. The correlation coefficients were generally equivalent. There was very weak correlation between spectral ratio and magnitude for *Pn*.

INTRODUCTION

The spectral characteristics of seismograms recorded at regional distances have been extensively studied in recent years (Pomeroy et al., 1982; Lilwall, 1988; Bennett et al., 1989; Taylor et al., 1989). The interest stems from the use of seismic spectra to discriminate underground nuclear explosions from earthquakes. Although effective long-period, time-domain methods of discrimination have been developed for larger (M_b > 4.5) teleseismically recorded events, such techniques perform poorly for smaller events that are only recorded out to regional distances (100–1300 km) and at short periods (Taylor et al., 1989). Smaller events therefore necessitate the use of other characteristics of the seismic signal to classify the nature of their source.

At this time, spectral discriminants are some of the most promising short-period regional discriminants. One type of spectral discriminant stems from the observation that the amplitude spectra of explosions decrease with increasing frequency more rapidly than amplitude spectra of earthquakes. In other words, for an explosion and an earthquake that have equal amplitudes at low frequencies, the earthquake tends to be relatively enriched in high frequencies compared with the explosion (Figure 1). The spectral ratio technique exploits this observation by examining the ratio of the maximum amplitude within a low-frequency window (usually 1 to 2 Hz) and the maximum amplitude within a high-frequency window (usually 6 to 8 Hz) for either *Pn*, *Pg*, or *Lg*. *Pn* is a mantle head wave, and *Pg* and *Lg* are crustal waveguide phases for *P* and *S* waves, respectively (Langston, 1982; Kennett, 1986). The spectral behavior explained above predicts that the spectral ratio for an explosion source will be higher than that for an earthquake source, and this is found to be true for most events, as illustrated in Figure 2 (Taylor et al., 1989). An example of another

spectral discriminant is described by Bennett et al. (1989). This discriminant follows the more intuitive argument that earthquakes, being shear dislocations, excite more *S*-wave energy than explosions, which are compressional sources. This hypothesis is exploited by dividing the spectrum of the *Lg* phase, which is associated with shear energy, by the spectrum of *Pg*, which is a compressional phase. As is expected, the ratio is generally greater for earthquakes than for explosions. Bennett et al. (1989) observe the differences in the ratio to be accentuated as frequency increases (Figure 3).

Figures 2 and 3 demonstrate that the spectral discriminant techniques can differentiate between explosion and earthquake sources. However, some outliers occur in the data that evade proper classification when either discriminant is used. The cause of these misclassifications is not well understood. It has been suggested that overburial of an explosion may change the values of spectral discriminants.

Source parameters other than the type of source should affect the spectral behavior of seismic signals. Three such parameters are (1) source depth, (2) the rock properties at the source, and (3) the event magnitude.

Regional distance phases consist of the interference of the direct, reflected (and multiply reflected) and refracted rays (Langston, 1982). The reflections are primarily due to the free surface and the crust–mantle boundary (Moho), with midcrustal impedance contrasts being of variable importance depending on the location and frequency range of interest. Changes in the depth of the source slightly change the arrival time of regional rays. Travel times of direct and surface-reflected rays become slightly longer as depth increases, but the surface-reflected ray is affected more than the direct ray. In contrast, rays which are initially reflected off the Moho will arrive earlier as depth increases. The net effect is to change the interference pattern of the direct, reflected and refracted rays that make up the regionally recorded seismic phase. Because changes in the interference pattern change the spectra of the seismic pulse, the source depth should be important to the spectral behavior of regional distance seismograms. Additionally, energy may be trapped in the uppermost crust for shallow events, causing differences in the character of body and surface waves.

The rock properties at the source are important because they relate directly to the particle velocity at the source. A strong rock (high velocity) should break with a higher stress drop than a weak rock. When higher stresses are released in the breaking of a strong rock, as in the case of an earthquake, the particle velocity at the source should be faster than that of a source in weaker rock. The faster particle velocity makes a shorter-duration seismic pulse, which enrichs the signal in high frequencies. For explosions, changes in rock properties are observed to change spectral characteristics. Overburied explosions and events detonated below the water table are observed to be enriched in high frequencies, lowering the spectral ratio and causing misclassification (Taylor et al., 1988). These changes in rock properties can be parameterized by the seismic velocity at the source. In this case, both increased depth and water saturation increase the *P*-wave velocity, indicating that *P*-wave velocity and the excitation of high frequencies may be directly related. However, this hypothesis has not been thoroughly tested.

Event magnitude should also affect the seismic spectra. The seismic pulse or source time function for earthquakes is thought to be the convolution of two basic components. The first component is particle motion on the fault; the second component is the rupture history of the event (Brune, 1970). For large earthquakes, which generally have large fault planes, the time required to rupture the entire fault is longer than for smaller events. This corresponds to the source being "turned on" longer for a larger event than for a smaller one. If the source is turned on longer, the particle motion component of the pulse (the length of time required for a particle on the fault to move from its initial to its final position) becomes a spike compared with the rupture time. As a result, the source pulse from a larger earthquake should resemble a boxcar function (convolution of a boxcar and a spike). However, for smaller events the particle motion time and the time taken to rupture the fault are nealy equal, so the source pulse from a smaller event should resemble a triangle function (convolution of two boxcars). Because the amplitude spectrum of a triangle function falls off twice as fast as that of a boxcar function (in log-log space) and because the corner frequency is higher for the shorter source time function, a change in event magnitude should

noticeably affect the frequency content of the seismogram. However, frequency-dependent attenuation along the path could lessen the magnitude's effect on the spectra.

The use of spectral characteristics as an explosion/earthquake discriminant is very promising for small, regionally recorded events. However, some events are misclassified. This implies that factors other than the type of source affect the spectral characteristics of regional phases. In this study we use the well-located events of the July 1986 Chalfant Valley earthquake sequence (mainshock m_b = 6.4) to help calibrate spectral discriminants. Our goal is to test three source parameters that could affect the earthquake spectra: source depth, rock properties at the source, and event magnitude. If a correlation is found, we hope to quantify the relationship in order to correct regionally recorded events, enabling correct source identification. If a correlation is not found, then we have eliminated a possible source of scatter in the data.

THE CHALFANT VALLEY EARTHQUAKE SEQUENCE

The 1986 Chalfant Valley earthquake sequence commenced in early July and continued through September of the same year. The main shock occurred on July 1 and had a M_L of 6.4. The earthquake sequence was very energetic, having a foreshock with a M_L of 5.9 and three large aftershocks measuring 5.8, 5.6, and 5.4. Thousands of smaller events occurred, and a large number of those events have a M_L of between 3.0 and 4.0. (Cockerham and Corbett, 1974). These events were well located using records from local arrays operated by the University of Nevada, Reno (UNR) and the U.S. Geological Survey (USGS) (Smith and Priestley, 1988). Most of the UNR stations were within 20 km of the main shock; however, the majority of USGS stations were near Mammoth Lakes, approximately 45 km northwest of Chalfant. We used earthquake locations calculated by workers at the UNR for which depth estimate errors are most often within ±1 km. Because of the large number of events with greatly varying magnitude and the good locations provided by the UNR, the 1986 Chalfant Valley earthquake sequence offers an

excellent opportunity to study the effects that earthquake magnitude, earthquake depth, and rock properties have on the spectra of regional seismic phases.

We parameterized rock properties using the *P*-wave velocity at the source. Figure 4 is a velocity profile of the Chalfant Valley area after Smith and Priestley (1988). Superimposed on the velocity profile are the 18 events we used in this study, which have local magnitudes ranging from 1.5–5.8, illustrating the range in depth and source velocity. From the surface down to about 4 km depth, there is a strong gradient in the seismic velocity, indicating substantial changes in rock properties. From 4.5–10 km depth, *P*-wave velocity gradually increases, possibly due to the compaction of a single lithology. Two of the 18 events have been located within the strong velocity gradient, and these two events give the data set most of its range in *P*-wave velocity. It is important to note, however, that the two most shallow events are poorly located compared with the deeper events, bringing into question the breadth in *P*-wave velocity in this study. However, the well-located events ranging in depth from 4.5 to about 10 km give a good range in depth.

Chalfant Valley is located in eastern California near Bishop, California (see Figure 5). Also shown in Figure 5 are the four Sandia broadband seismic stations from which we obtained records for the 18 Chalfant Valley events we used. The importance of Chalfant Valley's location is its proximity to the Nevada Test Site (NTS). Chalfant is only 100 km west of the NTS. Therefore, the Chalfant Valley events, as recorded at the four Sandia stations, have similar travel paths as explosions at NTS, making this data set particularly well suited for earthquake/explosion discrimination in the western United States. The Chalfant Valley earthquake sequence also occurred within an area of 12-mile radius. So Chalfant events, when at regional distances, had nearly identical paths to individual stations as explosions have. As a result, path effects for events that were recorded at the same station should be nearly identical, and differences in the seismic spectra can be attributed to differences at the source.

DATA AND PROCEDURE

The data were recorded on the Sandia broadband seismic stations at Tonopah, Nevada; Darwin, California; Battle Mountain, Nevada; and Nelson, Nevada. The distances from the Chalfant Valley main shock to the stations, as listed above, are 123 km, 156 km, 347 km, and 416 km, respectively. The stations have a flat frequency response from 1–8 Hz, and all records were recorded digitally at 50 samples/sec. Because of occasional drop-outs in the seismograms, the data were interpolated to 50 samples/sec using the algorithm described by Wiggins (1976). We conducted several tests of the effect that interpolation has on the data's spectra and found no changes in the frequency domain when the interpolator is correcting for drop-outs (i.e., if the interpolater is not increasing the sample rate but only filling in holes, the spectra do not change).

Figure 6 is a record from Battle Mountain, which typifies records from all the stations. It shows that even at the farthest stations the signal-to-noise ratio is very high for all phases. The clarity of the *Pg* phases on the records at all stations was excellent, allowing *Pg* to be identified by inspection. Two stations, Battle Mountain and Nelson, are beyond *Pn* distances for the Chalfant events. The *Pn* phase at these stations was large enough in amplitude to give confident phase picks in the presence of noise. *Pn* was therefore identified by inspection too. The *Lg* phase, however, was quite variable in nature from event to event and from station to station, so *Lg* was chosen to be within a velocity window of 3.0 to 3.5 km/sec.

After the phases were identified, each phase was cut from each seismogram and transferred into the frequency domain. As a check on the behavior of the *Pg* spectra, the amplitude of the "zero frequency" was plotted as a function of event magnitude for all events as recorded at the four stations (see Figure 7). The way in which the zero frequency changes from event to event in very consistent from station to station (the event with a magnitude of approximately 3.2, for example), giving us confidence that the source effect of magnitude is manifesting itself in the seismic spectra regardless of the path. According to Bullen and Bolt (1987) the zero frequency should continually increase with increasing magnitude, and the general trend in Figure 6 confirms that the Chalfant

Valley events used in this study behave as expected. Locally, however, some events show a decrease in the amplitude of the zero frequency as event magnitude increases. This is observed for the same events at all four stations. The inconsistencies give us some idea, perhaps, of the accuracy of magnitude estimates. However, because the inconsistencies are small compared with the overall trend, we find the spectral behavior and magnitude estimates to be good. Importantly, the source magnitude is expressed in the spectra of *Pg* regardless of azimuth.

It is important to look at the phases separately in order to determine whether or not the source parameters affect the different phases differently. The spectral ratios for *Pg* and *Lg* were calculated for the 18 events as recorded at the four stations. Two stations were used to find the spectral ratio for *Pn* because two stations are beyond *Pn* distance. The spectral ratio was calculated by dividing the maximum value within a 1 to 2 Hz window by the maximum value within a 6 to 7 Hz window (see Figure 8). The spectral ratio for all the events was plotted as a function of event magnitude, depth, and *P*-wave velocity at the source. In order to display differences due primarily to source effects, data recorded at the same station were plotted on a single graph. The graphs from all the stations were then displayed as panels on a single figure for *Pn*, *Pg*, and *Lg* so correlations from station to station could be observed.

RESULTS

Figures 9 through 17 display the spectral ratio of *Pg*, *Lg*, and *Pn* as a function of event magnitude, depth, and P-wave velocity at the source as recorded at the four Sandia stations. The most prominent characteristic of the data is the wide range of scatter, which can be from one-half to two orders of magnitude, depending on the variable and the station of interest. The scatter makes correlations difficult to identify in this data set. However, correlations do exist, and much of the scatter may be due to the spectral ratio's dependence on many variables, not only the variable we would like to make correlations with.

If the spectral ratio is equally affected by two independent variables and the data have wide ranges in both variables, the change in the spectral ratio as a result of one variable will be seen as scatter when examining correlations between the spectral ratio and the other variable. For example, if many events have the same magnitude but widely varying depths, then the changes in the spectral ratio due to depth will result in many different values of the spectral ratio at that magnitude. As a result of the relation being multivalued, the initial conclusion may be that spectral ratio does not have a strong correlation with magnitude, because any attempt at correlating spectral ratio with magnitude will result in a poor fit to the data. This problem can occur in reverse as well. Events with the same depth may have differing magnitudes, resulting in widely varying spectral ratios at a given depth. One solution to this dilemma is to choose events that have the same depth when correlating spectral ratios with magnitudes and vice versa. In this study we have 18 events to work with, so we want to avoid the exclusion of any data if possible. We decided to make correlations using both all the data and using a limited population that minimized the effect of other variables. A magnitude range of 3.0–3.5 was used when correlating depth and velocity with spectral ratio, and a depth window of 7–8 km, which corresponds to a velocity window of 6.02–6.04 km/sec, was used when correlating magnitude with spectral ratio. These windows were chosen because, for this data set, they allow the widest range in the variable of interest while limiting other variables the most. We found that in all cases but one, spectral ratio versus magnitude for *Pn*, that the limited data set reduced scatter significantly (see Figures 18 through 26). Because velocity and depth are not independent variables, it was impossible to separate the two variables.

Another problem stems from the two shallow events that are poorly located. The two events provide most of the range in the *P*-wave velocity variable, but if the depth estimates are far from the true depths, then we would do better to ignore them. Realizing this problem, we conducted a test to determine whether the two shallow events change the correlation between depth and spectral ratio, there being a good range in depth without the poorly constrained events. We found that the correlation between spectral ratio and depth was changed greatly when the two shallow events were included in the analysis. This indicates that the two shallow events do not

follow the behavior of the well-located events. Because we do not wish to base our correlation on poorly constrained data, the two shallow events were not used when correlating spectral ratio with depth and with *P*-wave velocity at the source.

We attempted to quantify the spectral ratio's dependence on event magnitude, depth, and *P*-wave velocity at the source. We did this by fitting the most appropriate curve to plots of spectral ratio as a function of the three variables. The most appropriate curve is the lowest-order polynomial that satisfactorily fits the data. By satisfactory we mean identifying trends and removing scatter or noise. To determine the most appropriate curve we fit a least-squares line to the data (second-order polynomial). Then two polynomials with three and four model parameters were fit to the data. Using an *F*-test that takes into account the number of degrees of freedom and the misfit between the model and the data (Hearns, 1984), we found that a linear regression statistically fit the data better than a third- or fourth-order polynomial at a confidence level of 95% for all but one case. The one case was the spectral ratio versus magnitude for *Pg* at the Battle Mountain station when all the data were used, for which a parabola fit best. However, we believe that the one parabolic fit is simply a fortuitous distribution of noise because it was the only nonlinear correlation and the *F*-test is a statistical qualifier that does allow for some amount of misidentification. The true relation may well be a higher-order polynomial, but the scatter in the data along with the limited range in the source variables, as in the case of *P*-wave velocity at the source, may be preventing us from statistically identifying such correlations. We therefore conclude that a linear relation best describes the dependence of spectral ratio and event magnitude, depth, and *P*-wave velocity at the source for this data set. This finding holds true when the correlation is performed using all the events and when the effect of other variables on the correlation is minimized. Tables 1 through 6 contain the *y* intercept, slope, and correlation coefficient of linear regressions for spectral ratio as a function of magnitude, depth, and *P*-wave velocity at the source at the four seismic stations for both all the data and the data set that minimizes the effects of other variables.

SPECTRAL RATIO VERSUS MAGNITUDE

Pg

Figure 27 shows the slope of the least-squares line fit to spectral ratio versus magnitude plots for the *Pg*, *Lg*, and *Pn* phases as recorded at the four seismic stations. When all the data are used in the correlation, changes in the spectral ratio as function of event magnitude are very small, with very weak correlation coefficients for three of the four stations. Only at Tonopah is there a weak correlation. The trend at Tonopah is for spectral ratio to decrease as magnitude increases (a negative correlation).

When spectral ratio and magnitude are correlated using events which lie between the depths of 7–8 km, the correlation coefficients are much improved, and the change in spectral ratio as a function of event magnitude increases dramatically. This indicates that the effects of depth and/or velocity are being seen as noise in the magnitude correlation. However, at Battle Mountain and Tonopah the relation is negative, whereas at *Darwin and Nelson the correlation is positive.* The correlation coefficients at the stations with negative dependence are stronger than those at the positively correlated stations. Thus the best-fitting data show the spectral ratio to decrease s magnitude increases. It is vexing, however, that the four stations give contradicting results. Station distance does not appear to be important, as the sets of positively and negatively correlated stations consist of one close and one distant station. It is interesting to note that the positively correlated stations are northeast of Chalfant, whereas the negatively correlated stations are southeast of Chalfant (see Figure 5). This brings up the question of whether or not spectral ratio is azimuthally dependent. As will be discussed later, only when the spectral ratio is correlated with magnitude is there a hint of azimuthal dependence. We also discussed above that the relative amplitude of the zero frequency as a function of event magnitude for nearly every event is consistent from station to station (relative amplitude being the amplitude minus the DC shift at a particular station). This implies that radiation pattern must be frequency dependent if the spectral

ratio is a function of radiation pattern. Any dependence of the spectral ratio on the radiation pattern is difficult to identify and should be studied further.

Because there is a weak correlation between event magnitude and spectral ratio when all the station are used and contradictory results when noise introduced by depth and velocity variables is minimized, we cannot make any definitive conclusions about how spectral ratios change as a function of event magnitude. However, at stations where the spectral ratio decreases as event magnitude increases, the strongest correlation coefficients are seen, and as was explained above, the more boxcar-shaped source time function (gradual amplitude fall-off with increasing frequency) of a large event should give a lower spectral ratio than the more triangle-shaped source time function (sharp amplitude fall-off with increasing frequency) of the smaller event.

Lg

Both using all of the events and events within a limited depth/velocity range yielded similar results for *Lg* and *Pg*, but limiting the depth/velocity strengthened the correlation. Again, the Battle Mountain and Tonopah stations gave negative correlations, and the stations at Darwin and Nelson gave positive correlations. However, for *Lg*, positively correlated stations have the higher correlation coefficient on the average. As with *Pg*, the contradictory nature of the data does not afford a definable relationship between *Lg* spectral ratio and event magnitude.

Pn

When all the data are used, both stations beyond *Pn* distance show a positive correlation between spectral ratio and event magnitude. The two correlation coefficients are small and moderate. Surprisingly, when source depth is limited, the strength of correlation greatly diminishes at both stations. Perhaps depth and source velocity do not affect the *Pn* spectral ratio as much as they do the spectral ratios of *Pg* and *Lg*. As a result, the larger data set better defines the

trend. Whether using all of the data or a limited depth range, the correlation between *Pn* spectral ratio and magnitude is very weak.

SPECTRAL RATIO VERSUS DEPTH

Pg

For the analysis of spectral ratio as a function of depth we have eliminated the two shallow events that are poorly located for the reasons explained above. In addition to the analysis using only the best-located events, we also performed the correlations using only events with magnitudes between 3.0 and 3.5 to eliminate scatter caused by magnitude variations. Unlike magnitude, for which the minimization of noise due to other variables often changed the slope of the linear regressions considerably, limiting the effect of magnitude on the spectral ratio versus depth correlation never changed the sign of the slope, but in every case limiting the magnitude range boosted the correlation coefficient. Therefore, we only present here the results from the data set with a limited range in magnitude. Figure 20 shows the slope of the least-squares line fit to spectral ratio versus depth plots for the *Pg*, *Lg*, and *Pn* phases as recorded at the four seismic stations.

Three of the four stations show a least-squares line fit to the spectral ratio versus depth plots having a slope of about −0.06/km. The negative slope indicates that the spectral ratio decreases as depth increases, or high frequencies are relatively enriched as depth increases. Although the slope of the least-squares line is small, correlation coefficients are high, giving us some confidence in the negative slope. The one station with a positive slope, Nelson, has the lowest correlation coefficient of any station, implying that the positive correlation could possibly be due to noisy data.

Lg

As with *Pg* analysis, at three of the four stations the spectral ratio decreases as depth increases. For *Lg*, the line fit to the data at the three stations with negative correlations has an average slope of –0.1/km. The one station that contradicts the negative correlation is at Tonopah, which is not the same station that contradicted the correlation for *Pg*. The correlation coefficient for the negatively correlated stations are generally higher than that of the one positively correlated station.

Pn

Pn correlations between depth and spectral ratio at the Nelson station gave a high correlation coefficient and a slope of –0.15/km, but the station at Battle Mountain gave a very low correlation coefficient with a slope of 0.04/km. Once again the two stations yield contradictory results, with the negatively correlated data having a much better correlation coefficient.

SPECTRAL RATIO VERSUS *P*-WAVE VELOCITY AT THE SOURCE

Pg

Because *P*-wave velocity is a function of depth, we expect the correlation between spectral ratio and *P*-wave velocity at the source to be similar to the correlation between spectral ratio and depth. This is found to be true. We find that the slope of the lines fit to the spectral ratio versus velocity plots are much greater (absolute value) than lines fit to plots whose independent variable is depth. The correlation coefficients are roughly the same when spectral ratio is correlated with source velocity and depth. Again, this is for the analysis using events whose magnitudes lie between 3.0 and 3.5. Even though the dependence of spectral ratio on source velocity appears to be strong, we emphasize the data's narrow range in source velocity when the two poorly located events are excluded from the analysis, which they are here. Because *P*-wave velocity changes little over the wide range in depth that these data cover, a slow change in spectral ratio due to depth

manifests itself as a very strong dependence on *P*-wave velocity at the source. The fact that the dependence of velocity on depth is nearly linear over the depth range of the events used in correlations makes it impossible to discern the degree to which each variable affects the spectral ratio. As a result, for this data set, depth and *P*-wave velocity at the source are inseparable variables. Figure 21 shows the slope of the least-squares line fit to spectral ratio versus *P*-wave velocity for the *Pg*, *Lg*, and *Pn* phases as recorded at the four seismic stations.

The correlation of *Pg* spectral ratio and *P*-wave velocity at the source is much the same as the spectral ratio/depth correlation. The slope of the lines fit to the plots with velocity as the independent variable are 1.75–2.0 sec/km, which is a very strong dependence. As was the case for the depth correlation, the station at Nelson gave a positive correlation, contradicting the other stations. However, the correlation coefficient at Nelson is much smaller than at any of the other stations.

Lg

For *Lg*, the slope of the lines fit to the spectral ratio versus velocity plot are –2.0 to –2.5 sec/km for three of the four stations. The station at Tonopah has a slope of 0.9 sec/km and a correlation coefficient that is as strong as that of most of the other stations.

Pn

At the Nelson station the slope of the spectral ratio versus velocity regression is –3.75 sec/km, with a correlation coefficient of –0.703, both of which are the largest values (absolute value) we calculated for any case. At Battle Mountain the slope is 1.1 sec/km with a correlation coefficient of 0.209. The two stations contradict each other, but the correlation coefficient at Nelson is much better than at Battle Mountain.

CONCLUSIONS

The use of spectral discriminants to distinguish underground nuclear explosions from earthquakes is a promising regional distance technique. However, source parameters other than the type of source appear to influence the spectral behavior of regionally recorded events. Event magnitude and some combination of source depth and the *P*-wave velocity at the source appear to affect the spectral ratio of regional seismic phases from the 1986 Chalfant Valley earthquake sequence.

We found that for the range in magnitude, depth, and *P*-wave velocity at the source of the events used in this study, a linear regression fit the change in spectral ratio as a function of the three variables as well as a third- or fourth-order polynomial. Statistically, the higher-order terms were fitting noise. Scatter in the data, when looking at spectral ratio as a function of one variable, can result from the dependence of the spectral ratio on other variables. Scatter was considerably decreased by limiting the range in event magnitude when correlating depth and *P*-wave velocity at the source with spectral ratio and vice versa.

We found at three of the four stations from which records were used that the spectral ratio of *Pg* and *Lg* decreased as depth and *P*-wave velocity increased. Because for both *Pg* and *Lg* one station contradicted the findings at the other stations, we cannot claim the decreasing ratio with increasing depth/velocity to be universal behavior. However, for *Pg* the one contradicting station has a correlation coefficient far lower than at the other stations, implying the data are noisy. The two stations beyond *Pn* distance gave contradicting results for spectral ratio correlations with depth and velocity, but the station showing the spectral ratio to decrease with increasing depth/velocity had a very high correlation coefficient whereas the other station had a very poor correlation coefficient. Correlations between spectral ratio and magnitude were contradictory from station to station for *Pg* and *Lg*. Records from Battle Mountain and Tonopah showed the spectral ratio to decrease as event magnitude increased, whereas records from Darwin and Nelson showed spectral

ratio to increase as magnitude increased. For *Pn* the spectral ratio correlation with magnitude was very weak.

The changes in spectral ratio as a function of source magnitude, source depth, and *P*-wave velocity at the source that have been calculated using the Chalfant Valley events show that if spectral discriminants take these source variables into account (particularly the depth/velocity variable), we can classify sources (earthquake or explosion) more accurately. We found a strong tendency for the spectral ratio to decrease as *P*-wave velocity at the source increased and a weaker tendency for spectral ratio to decrease as source depth increased. Unfortunately, the Chalfant Valley data set does not allow us to separate the effects that source depth and *P*-wave velocity at the source have on the spectral ratio of regional phases. We believe that the effect these source variables have on seismic spectra can be better defined as more regional, broadband data from Basin and Range events become available. This study has served to identify the relation between source variables and spectral ratio in a rough manner with the hope that these results will eventually lead to a well-constrained relation between spectral behavior and event magnitude, depth, and rock properties at the source.

REFERENCES

Bullen, K. E. and B. A. Bolt (1987). *An Introduction to the Theory of Seismology*, University of Cambridge Press, New York.

Bennett, T. J., B. W. Barker, K. L. McLaughlin, and J. R. Murphy (1989). *Regional Discrimination of Quarry Blasts, Earthquakes and Underground Nuclear Explosions*, S-Cubed report SSS-TR-89-10395, technical report under contract no. GL-TR-89-0114. ADA223148

Brune, J. N. (1970). Tectonic stress and the spectra of seismic shear waves from earthquakes, *J. Geophys. Res.* **75**, 4997-5009.

Cockerham, R. S., and E. J. Corbett (1987). The 1986 Chalfant Valley, California, earthquake sequence: Preliminary results, *Bull. Seism. Soc. Am.* **77**, 280-289.

Hearns, T. M. (1984). *Pn* travel times in southern California, *J. Geophys. Res.* **89**, 1843-1855.

Kennett, B. L. N. (1986). *Lg* waves and structural boundaries, *Bull. Seism. Soc. Am.* **76**, 1133-1141.

Langston, C. A. (1982). Aspects of *Pn* and *Pg* propagation at regional distances, *Bull. Seism. Soc. Am.* **72**, 457-471.

Lilwall, R. C. (1988). Regional m_b:M_S, *Lg*, *Pg* amplitude ratio and *Lg* spectral ratio as criteria for distinguishing between earthquakes and explosions: A theoretical study, *Geophys. J.* **93**, 137-147.

Pomeroy, P. W., W. J. Best, and T. V. McEvilly (1982). Test Ban Treaty verification with regional data—A review, *Bull. Seism. Soc. Am.* **72**, S89-S129.

Smith, K. D., and K. F. Priestley (1988). The foreshock sequence of the 1986 Chalfant, California, earthquake, *Bull. Seism. Soc. Am.* **78**, 172-187.

Taylor, S. R., N. W. Sherman, and M. D. Denney (1988). Spectral discrimination between NTS explosions and western United States earthquakes at regional distance, *Bull. Seism. Soc. Am.* **78**, 1563-1579.

Taylor, S. R., M. D. Denney, E. S. Vergino, and R. E. Glaser (1989). Regional discrimination between NTS explosions and western United States earthquakes, *Bull. Seism. Soc. Am.* **79**, 1142-1176.

Wiggins, R. A. (1976). Interpolation of digitized curves, *Bull. Seism. Soc. Am.* **66**, 2077-2081.

TABLE EXPLANATIONS

Tables 1–3 show the y intercept, slope and correlation coefficient of the least-squares line fit to spectral ratio of Pg, Lg, and Pn versus magnitude, depth, and velocity, respectively. These regressions are for the data sets that are limited with respect to other variables (see text).

Tables 4–6 show the y intercept, slope, and correlation coefficient of the least-squares line fit to spectral ratio of Pg, Lg, and Pn versus magnitude, depth, and velocity, respectively. These regressions are for the data sets that include all the data.

TABLE 1.

Correlation with Magnitude

Phase	Station	*y* Intercept	Slope	Correlation Coefficient
Pg				
	Battle Mountain	1.710	–0.325	–0.783
	Darwin	0.163	0.255	0.679
	Nelson	0.941	0.066	0.115
	Tonopah	2.150	–0.313	–0.717
Lg				
	Battle Mountain	1.574	–0.235	–0.376
	Darwin	0.449	0.142	0.526
	Nelson	–0.720	0.521	0.687
	Tonopah	1.169	–0.120	–0.691
Pn				
	Battle Mountain	0.943	–0.046	–0.043
	Nelson	0.695	0.041	–0.264

TABLE 2.

Correlation with Depth

Phase	Station	*y* Intercept	Slope (1/km)	Correlation Coefficient
Pg				
	Battle Mountain	0.930	–0.063	–0.430
	Darwin	1.141	–0.053	–0.517
	Nelson	0.647	0.043	0.391
	Tonopah	1.290	–0.057	–0.471
Lg				
	Battle Mountain	1.629	–0.125	–0.484
	Darwin	1.609	–0.144	–0.517
	Nelson	1.595	–0.063	–0.403
	Tonopah	0.398	0.039	0.460
Pn				
	Battle Mountain	–0.017	0.041	0.146
	Nelson	1.888	–0.149	–0.688

TABLE 3.

Correlation with Velocity

Phase	Station	*y* Intercept	Slope (sec/km)	Correlation Coefficient
Pg				
	Battle Mountain	10.132	−1.611	−0.409
	Darwin	14.230	−2.203	−0.632
	Nelson	−2.611	0.594	0.291
	Tonopah	9.923	−1.509	−0.506
Lg				
	Battle Mountain	16.730	−2.669	−0.391
	Darwin	19.398	−3.105	−0.625
	Nelson	11.804	−1.779	−0.454
	Tonopah	−4.545	0.871	0.450
Pn				
	Battle Mountain	0.943	−0.046	−0.043
	Nelson	o.695	0.041	−0.264

TABLE 4.

Correlation with Magnitude

Phase	Station	*y* Intercept	Slope	Correlation Coefficient
Pg				
	Battle Mountain	0.519	0.004	0.009
	Darwin	0.808	0.041	0.086
	Nelson	0.791	0.068	0.157
	Tonopah	1.283	−0.133	−0.327
Lg				
	Battle Mountain	1.204	−0.121	−0.254
	Darwin	−0.004	0.262	0.511
	Nelson	0.307	0.236	0.426
	Tonopah	0.977	−0.079	−0.406
Pn				
	Battle Mountain	−0.203	0.177	0.240
	Nelson	−0.082	0.234	0.404

TABLE 5.

Correlation with Depth

Phase	Station	*y* Intercept	Slope (1/km)	Correlation Coefficient
Pg				
	Battle Mountain	0.664	–0.010	–0.165
	Darwin	1.658	–0.093	–0.502
	Nelson	0.757	0.039	0.232
	Tonopah	1.308	–0.058	–0.314
Lg				
	Battle Mountain	3.121	–0.381	–0.414
	Darwin	1.266	–0.046	–0.006
	Nelson	1.713	–0.073	–0.268
	Tonopah	0.472	0.029	0.262
Pn				
	Battle Mountain	0.287	0.023	0.091
	Nelson	1.678	–0.113	–0.087

TABLE 6.

Correlation with Velocity

Phase	Station	*y* Intercept	Slope (sec/km)	Correlation Coefficient
Pg				
	Battle Mountain	3.408	–0.472	–0.137
	Darwin	17.197	–2.700	–0.548
	Nelson	–5.908	1.158	0.292
	Tonopah	9.530	–1.441	–0.304
Lg				
	Battle Mountain	43.256	–7.145	–0.302
	Darwin	9.267	–1.388	–0.008
	Nelson	10.571	–1.565	–0.211
	Tonopah	–4.182	0.810	0.287
Pn				
	Battle Mountain	3.408	–0.472	–0.192
	Nelson	–5.908	1.158	0.147

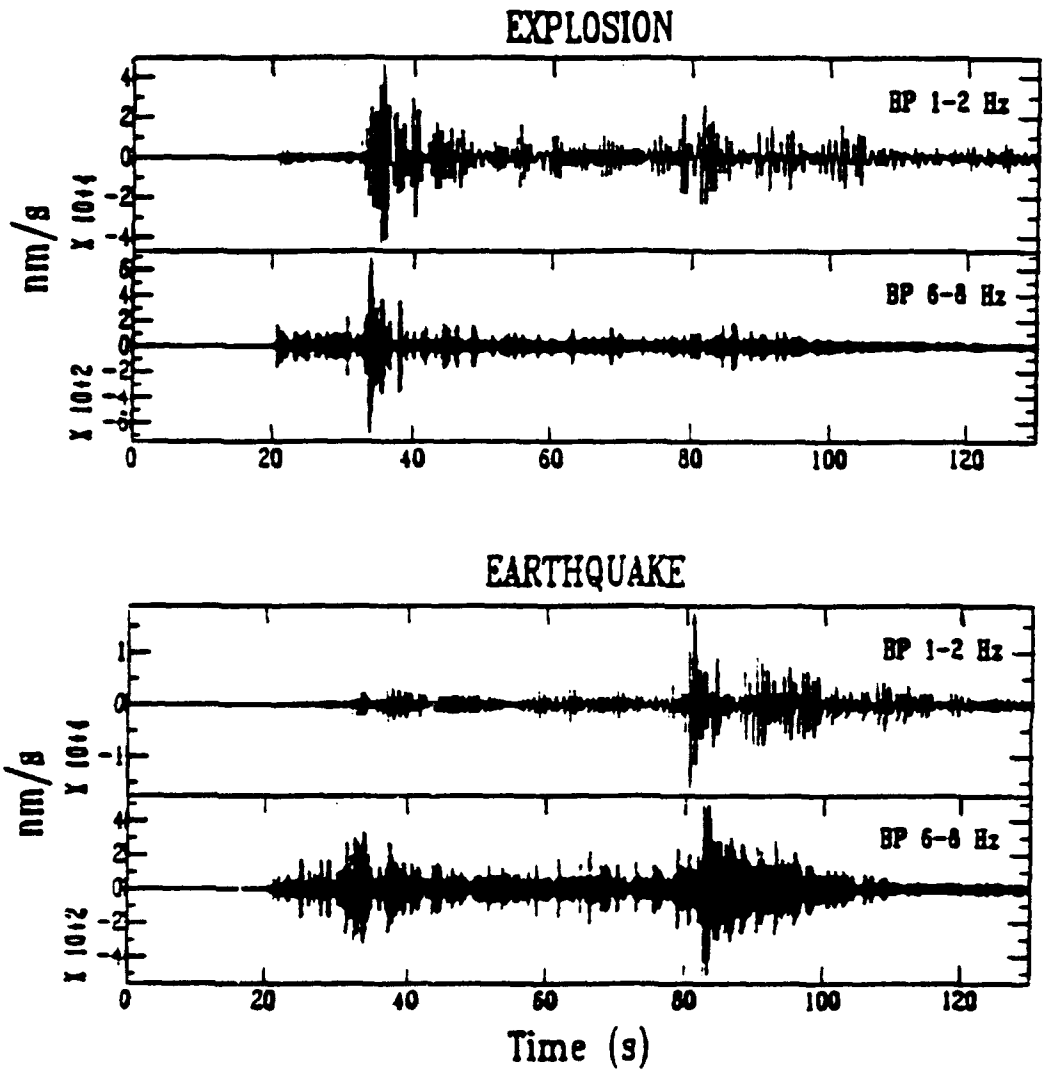

Figure 1. Bandpass seismograms from Taylor et al. (1986) illustrate the difference between amplitudes in low- and high-frequency windows for explosions (larger difference) and earthquakes (smaller difference).

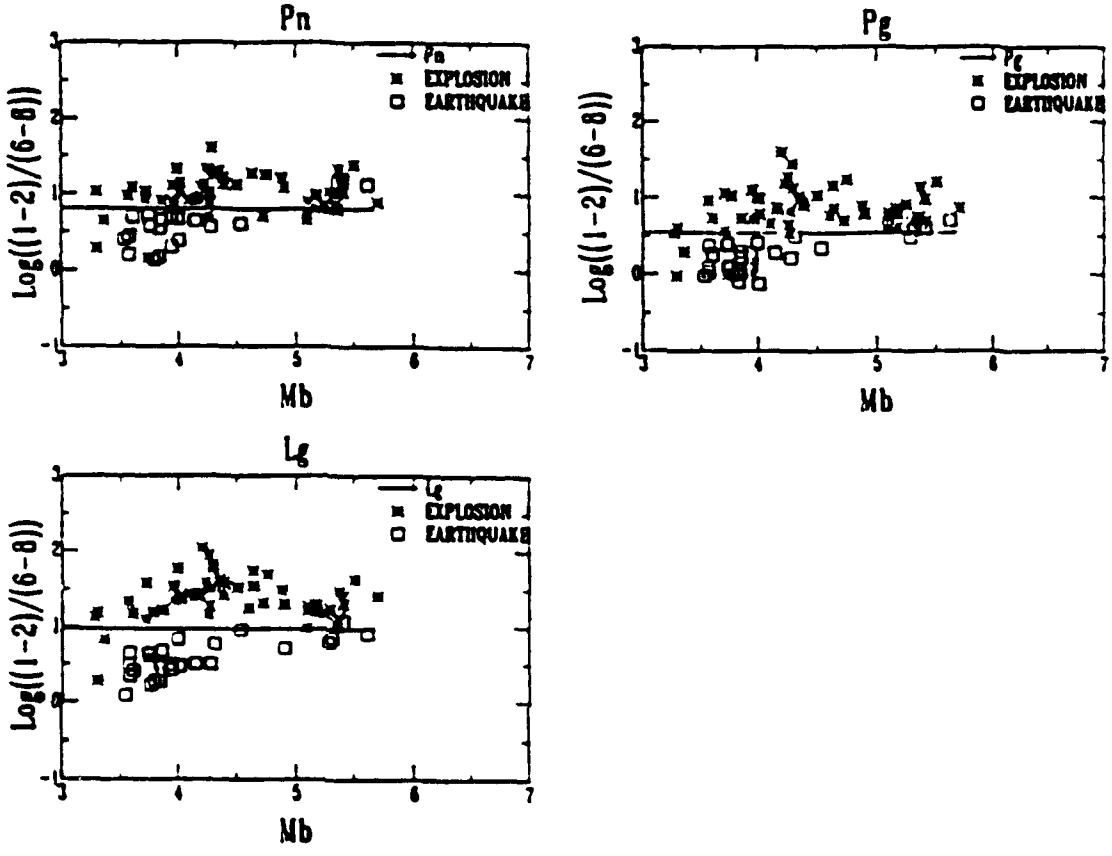

Figure 2. The spectral ratio discriminant for a single phase (*Pn*, *Pg*, and *Lg*) shows the generally higher spectral ratio for explosions compared with earthquakes.

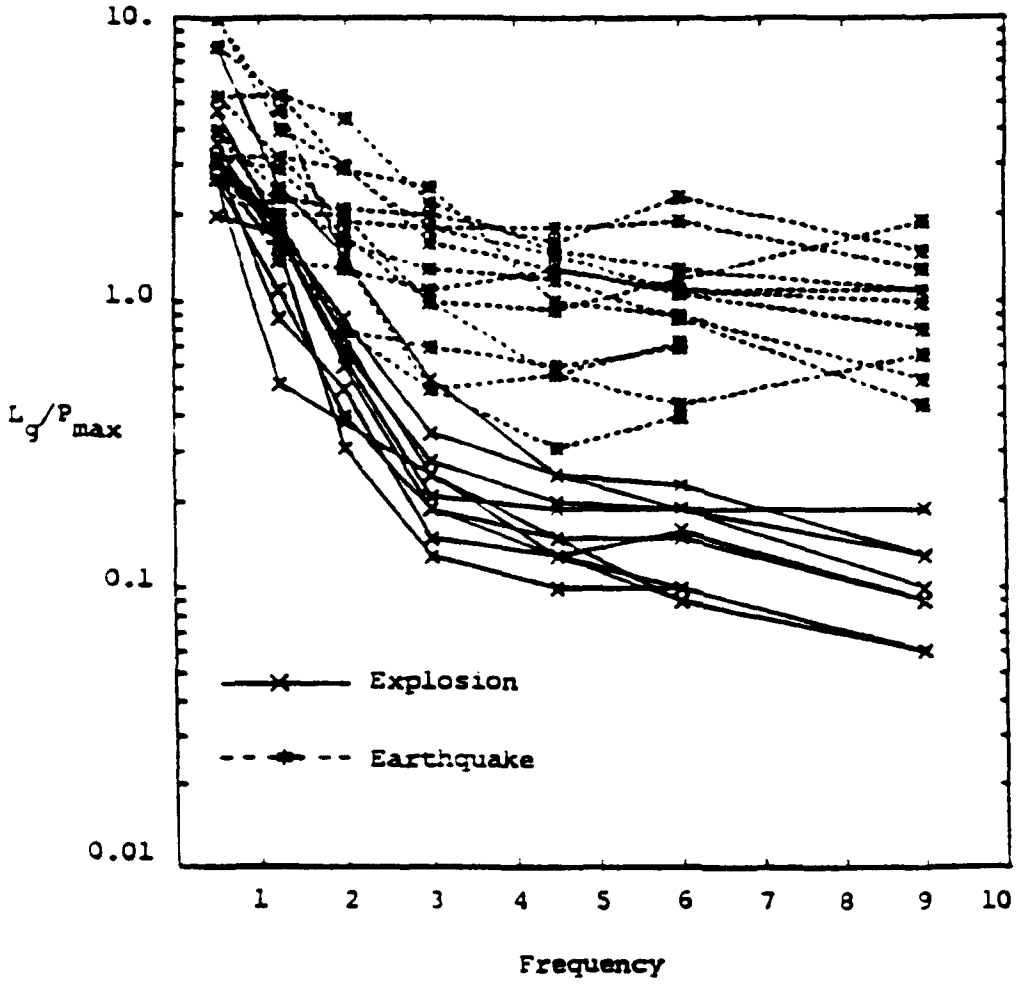

Figure 3. The amplitude ratio of *Lg* and *Pg* for earthquakes and explosions is shown as a function of frequency. Note that at higher frequencies the separation of earthquake and explosion *Lg/Pg* ratios is enhanced (from Bennett et al., 1989).

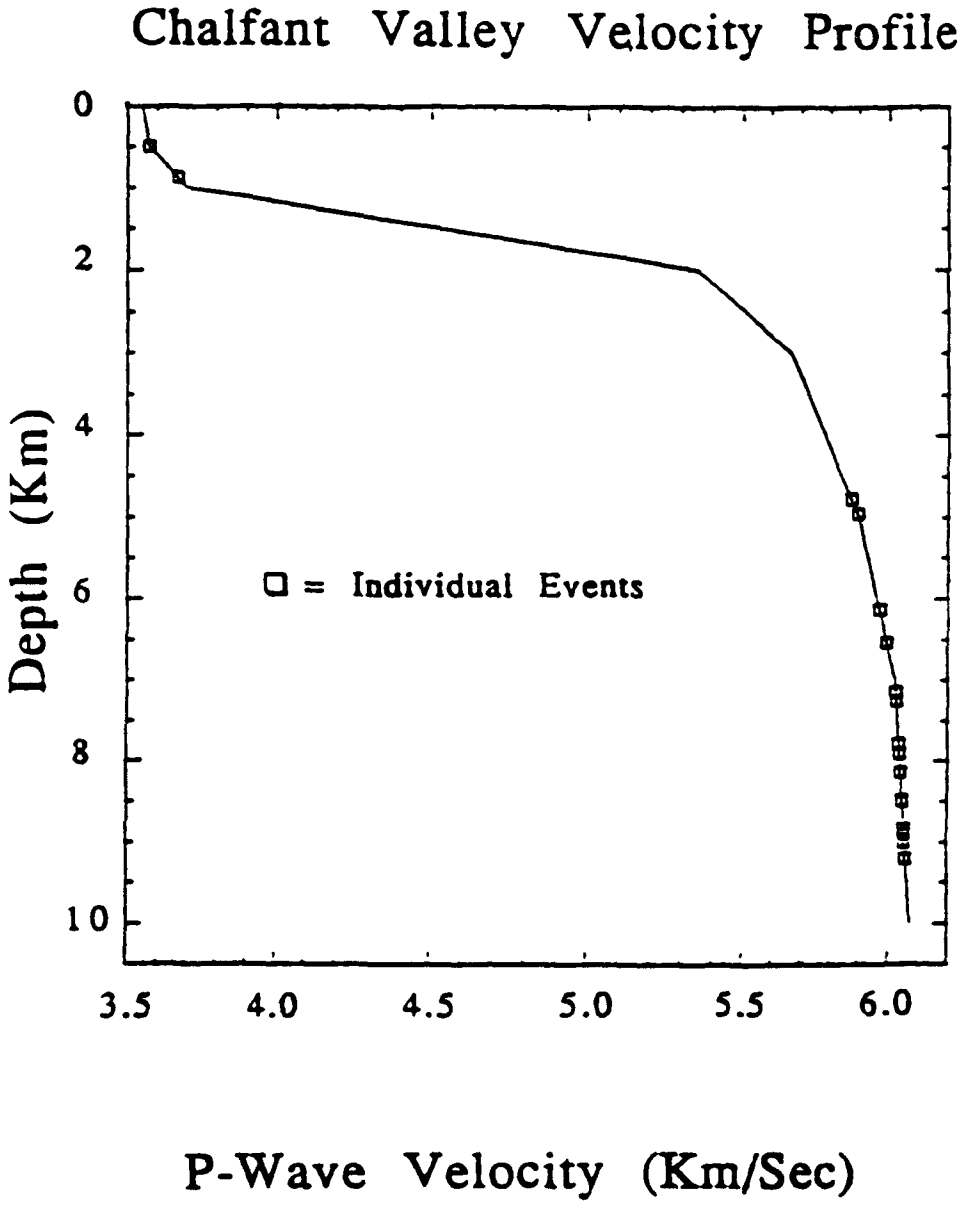

Figure 4. The 18 events used in this study superimposed on the velocity profile for the Chalfant Valley vicinity shows the range in depth and *P*-wave velocity at the source of the events used in this study. (The velocity model is from Smith and Priestley, 1988.)

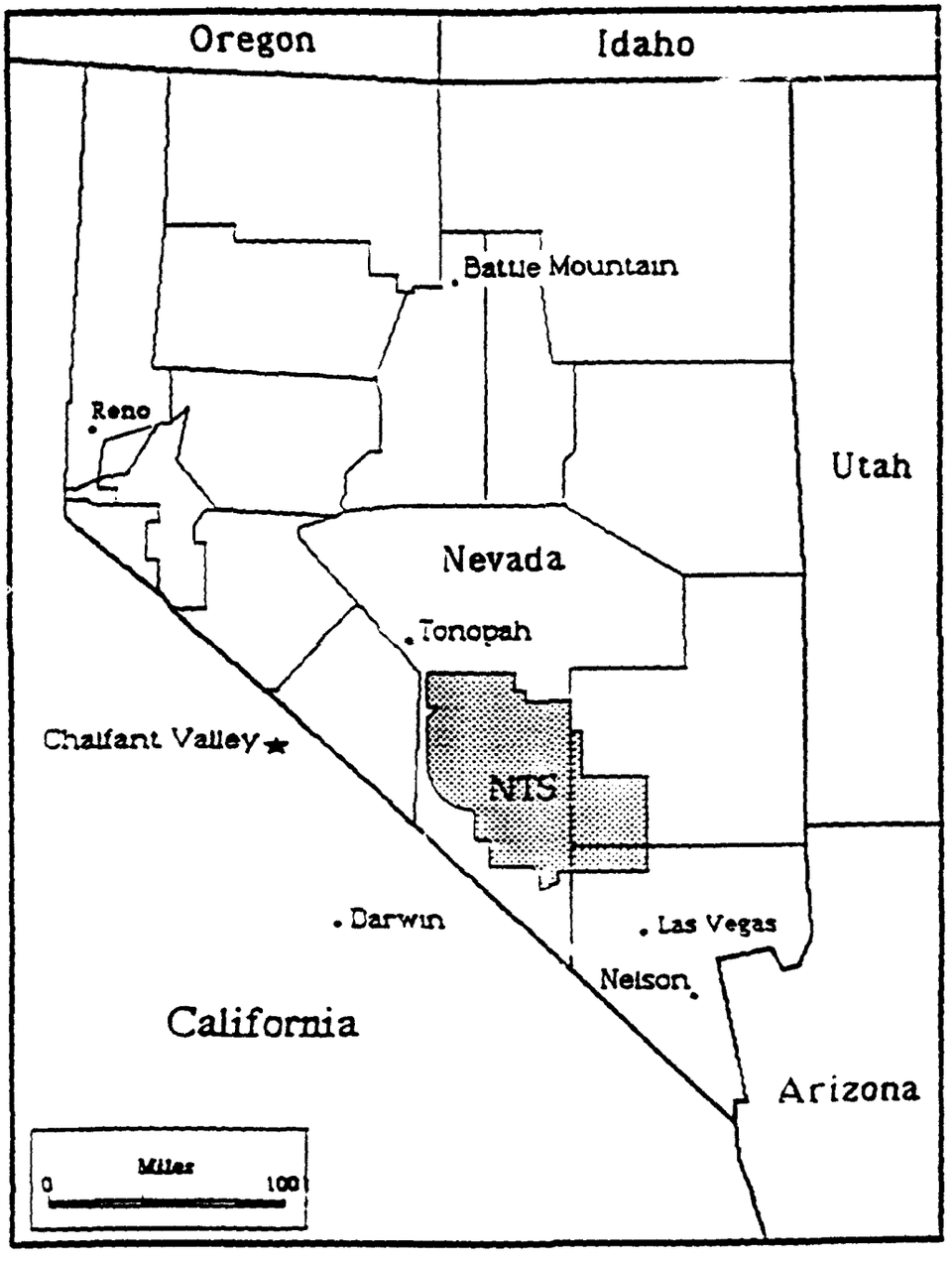

Figure 5. Chalfant Valley and the four Sandia seismic stations (Battle Mountain, Nevada; Darwin, California; Nelson, Nevada; Tonopah, Nevada), whose records were used in this study, are shown in map view. Note Chalfant's proximity to the Nevada Test Site (NTS). Seismic waves from the Chalfant events, as recorded at the Sandia stations, traveled through the same crust as NTS explosions.

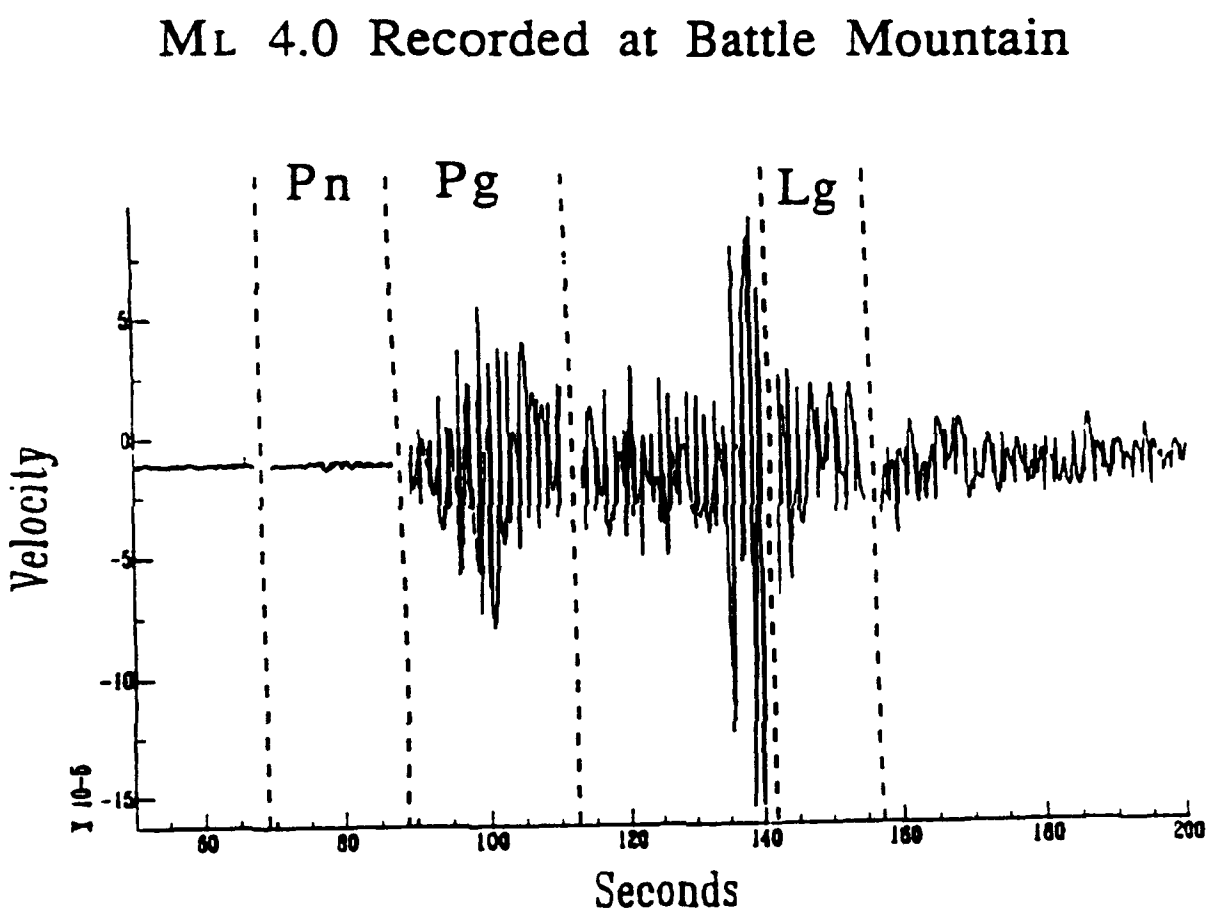

Figure 6. This record shows the good signal-to-noise ratio of *Pn*, *Pg*, and *Lg* as recorded at Battle Mountain, Nevada (357 km from Chalfant Valley) for a $M_L \approx 4.0$ event and typifies the seismograms used in this study.

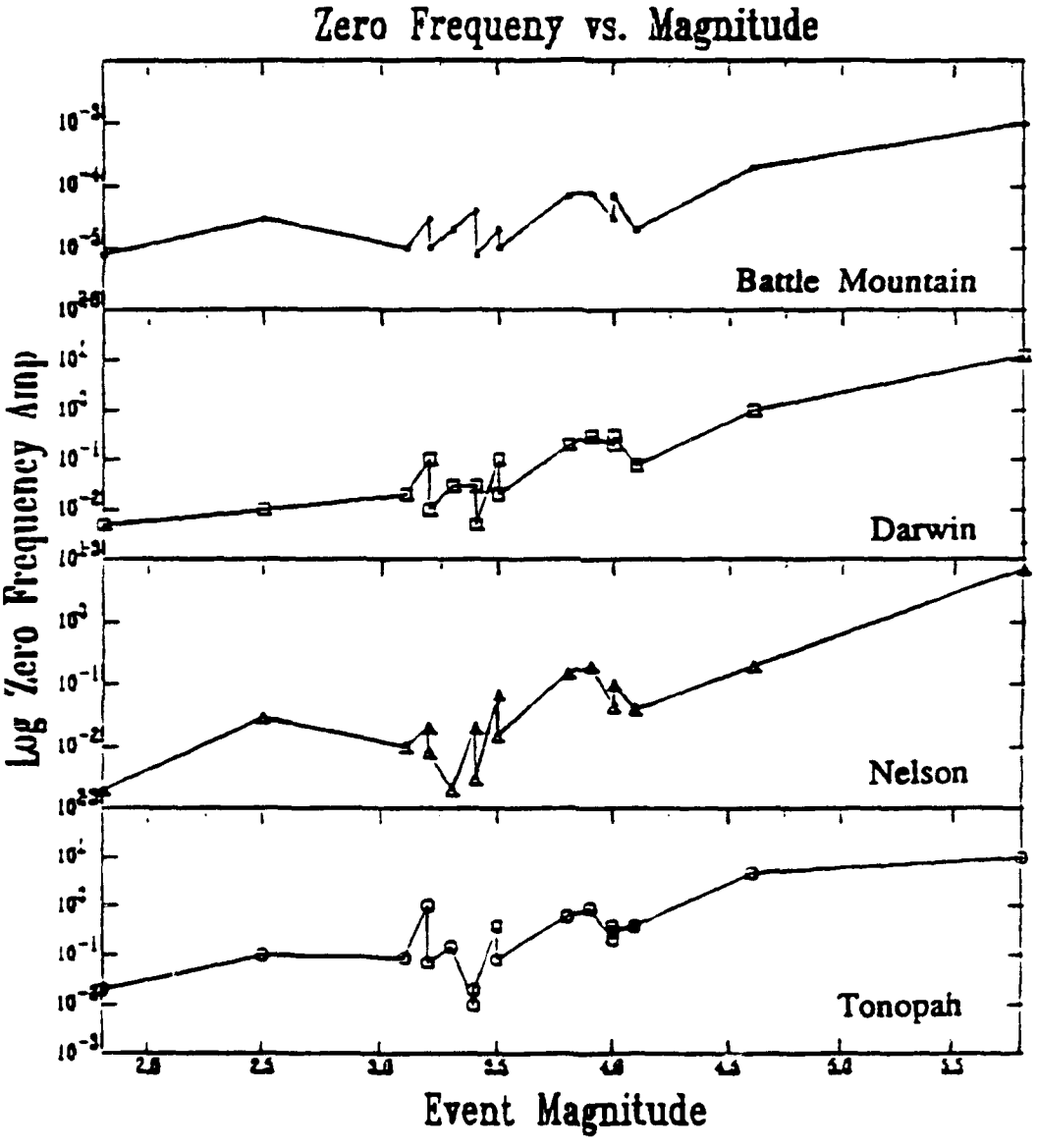

Figure 7. Zero frequency is seen to generally increase with increasing magnitude at all stations. Also, the relative amplitude of the zero frequency does not appear to change significantly from station to station, indicating that radiation pattern is not affecting the relative zero frequency of these events.

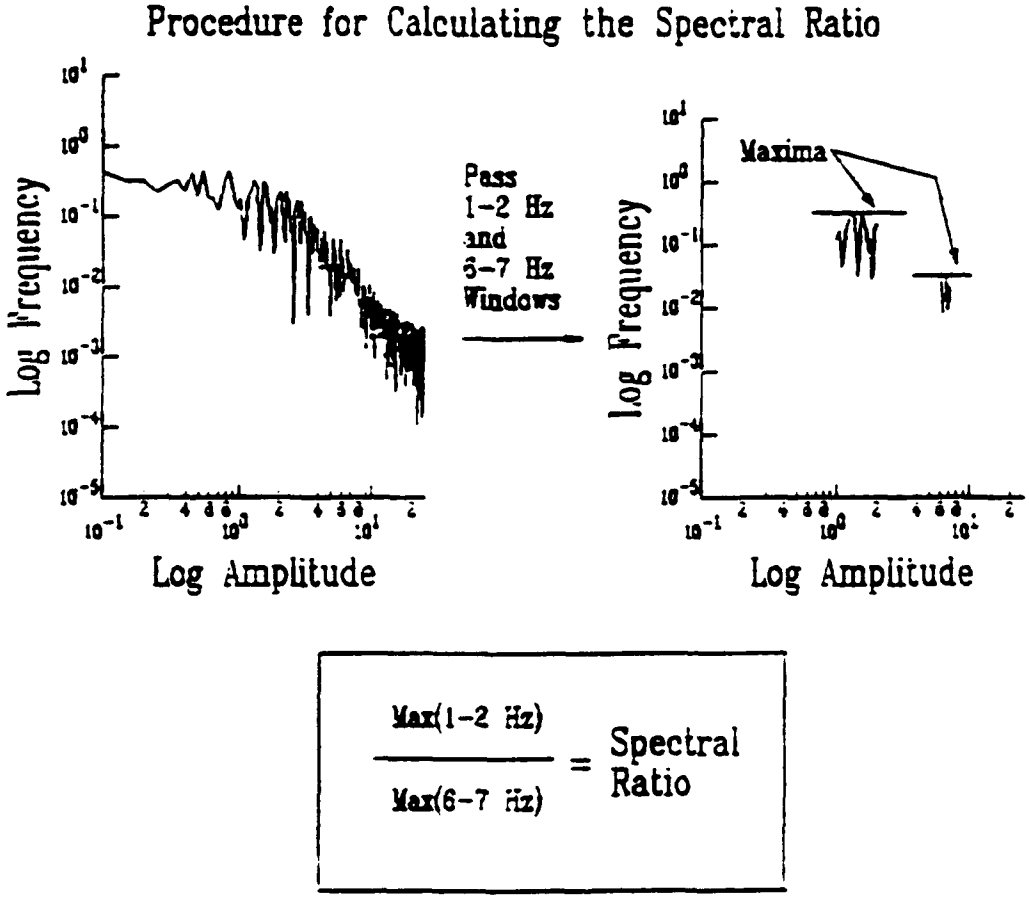

Figure 8. Illustration of procedure. After cutting each phase from each seismogram and transforming the phase into the frequency domain, the maximum amplitude within a 1 to 2 Hz window was divided by the maximum amplitude within a 6 to 7 Hz window, yielding the spectral ratio.

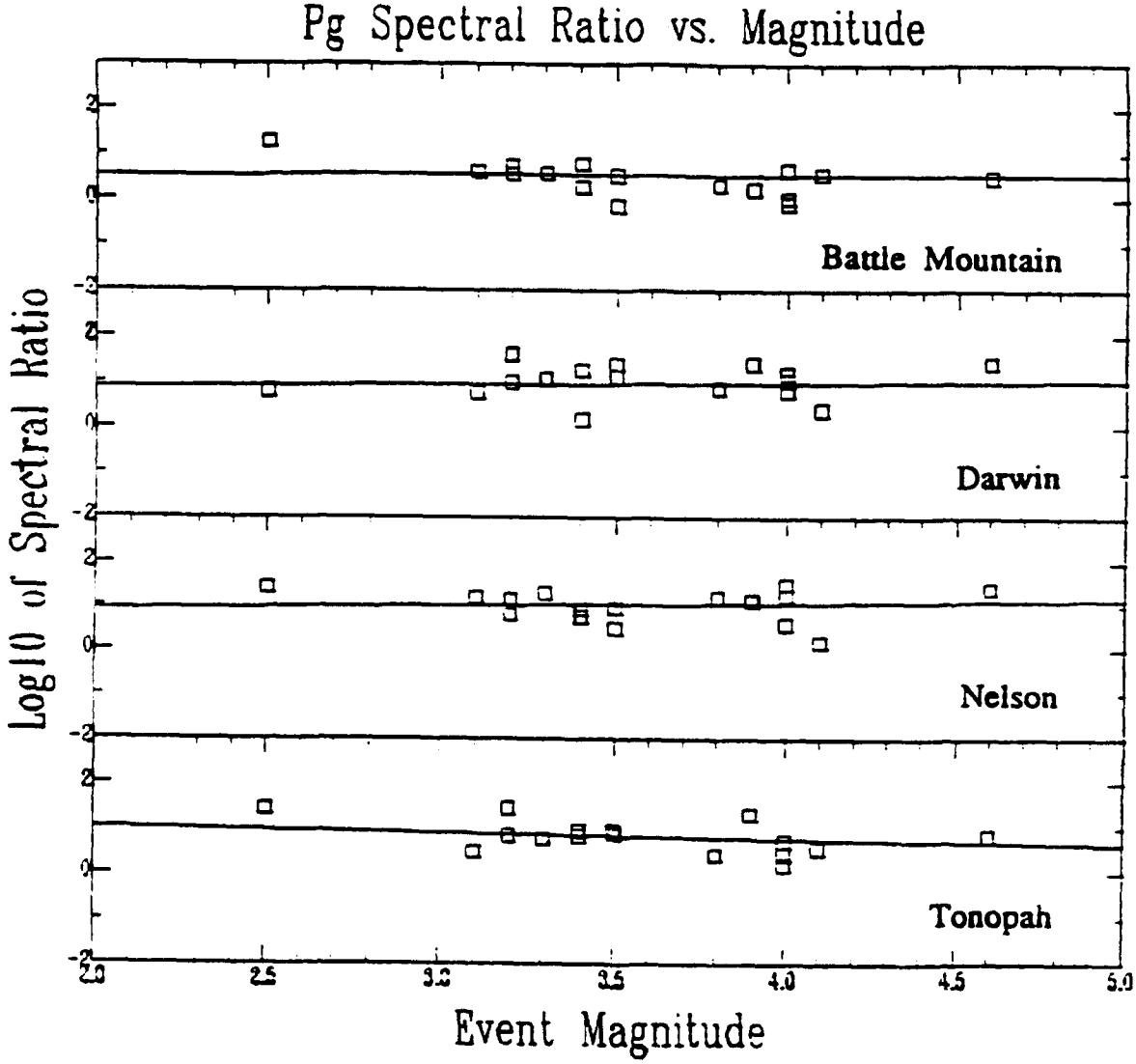

Figure 9. Figures 9–17 show the spectral ratio of Pn, Pg, and Lg as a function of source magnitude, source depth, and P-wave velocity at the source. Also shown is the least-squares linear fit to the data.

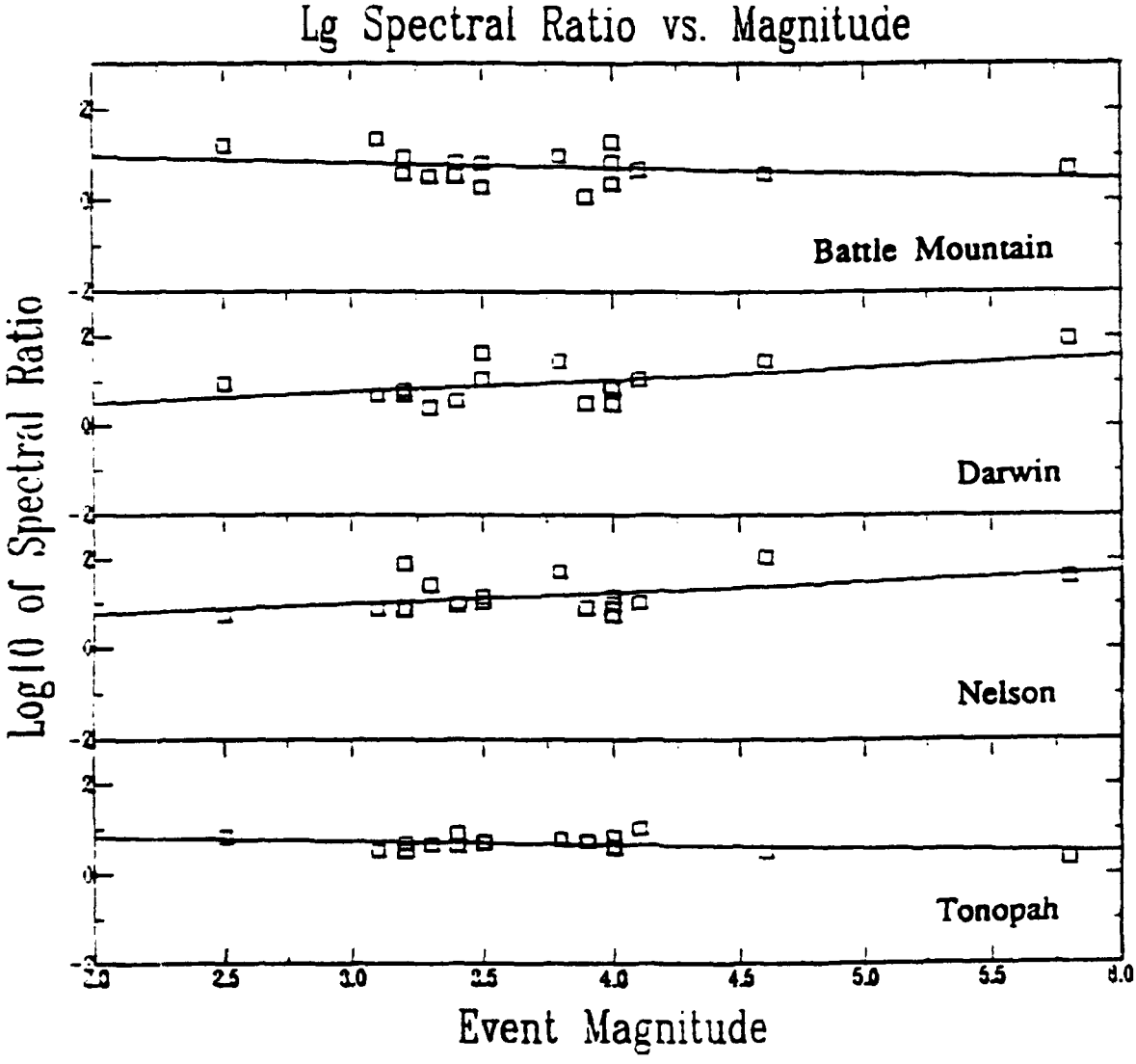

Figure 10. See Figure 9 for explanation.

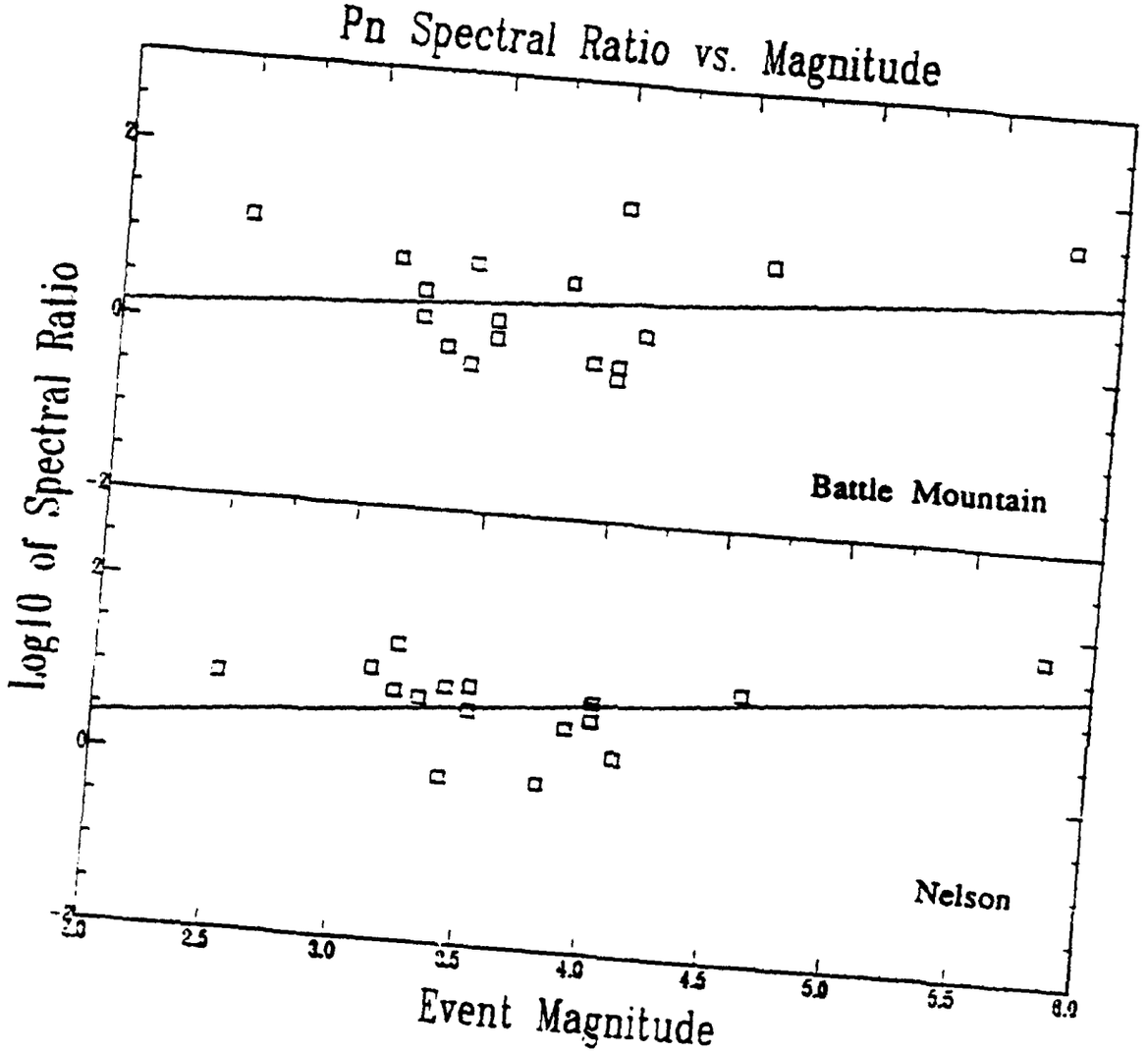

Figure 11. See Figure 9 for explanation.

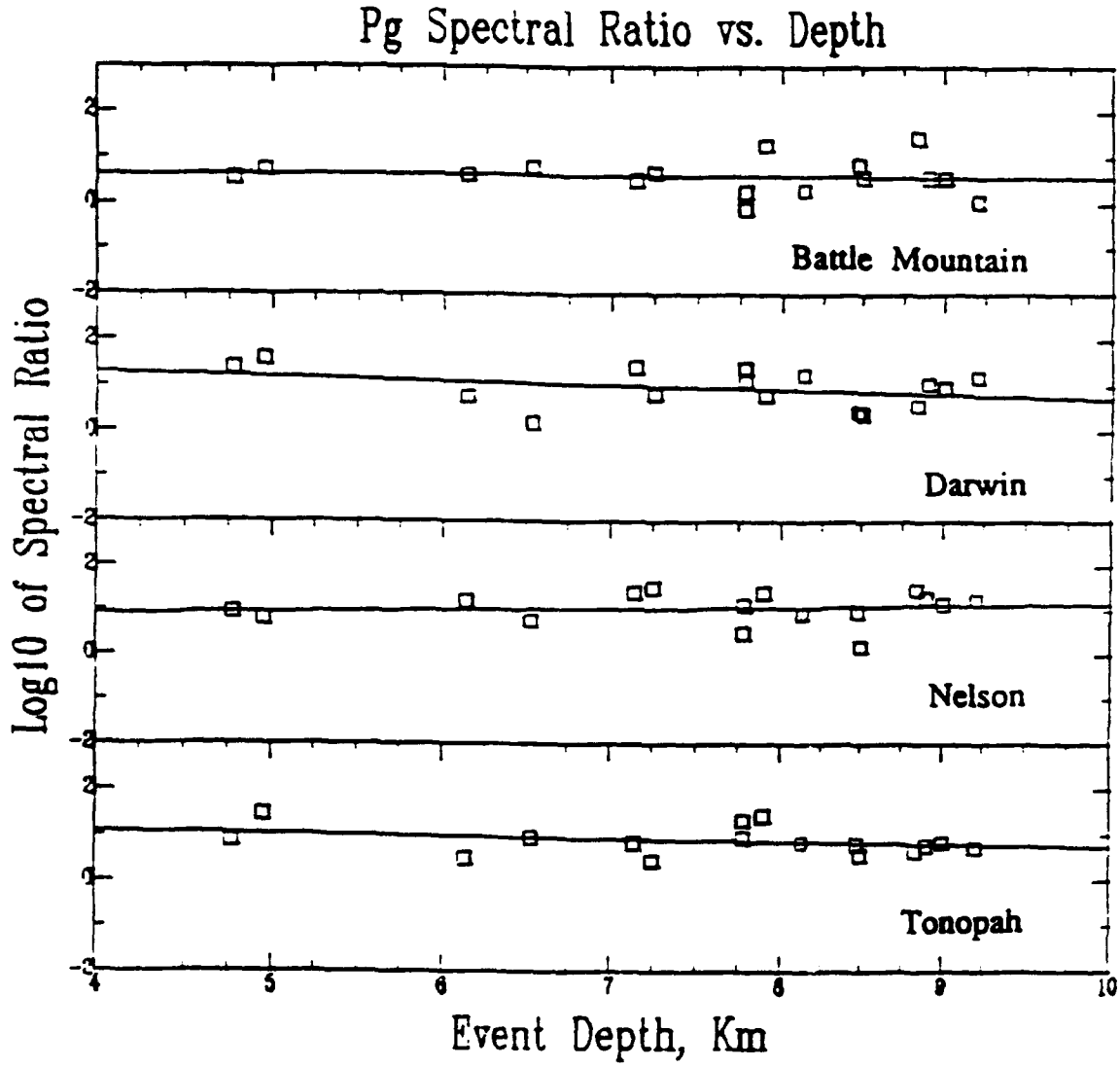

Figure 12. See Figure 9 for explanation.

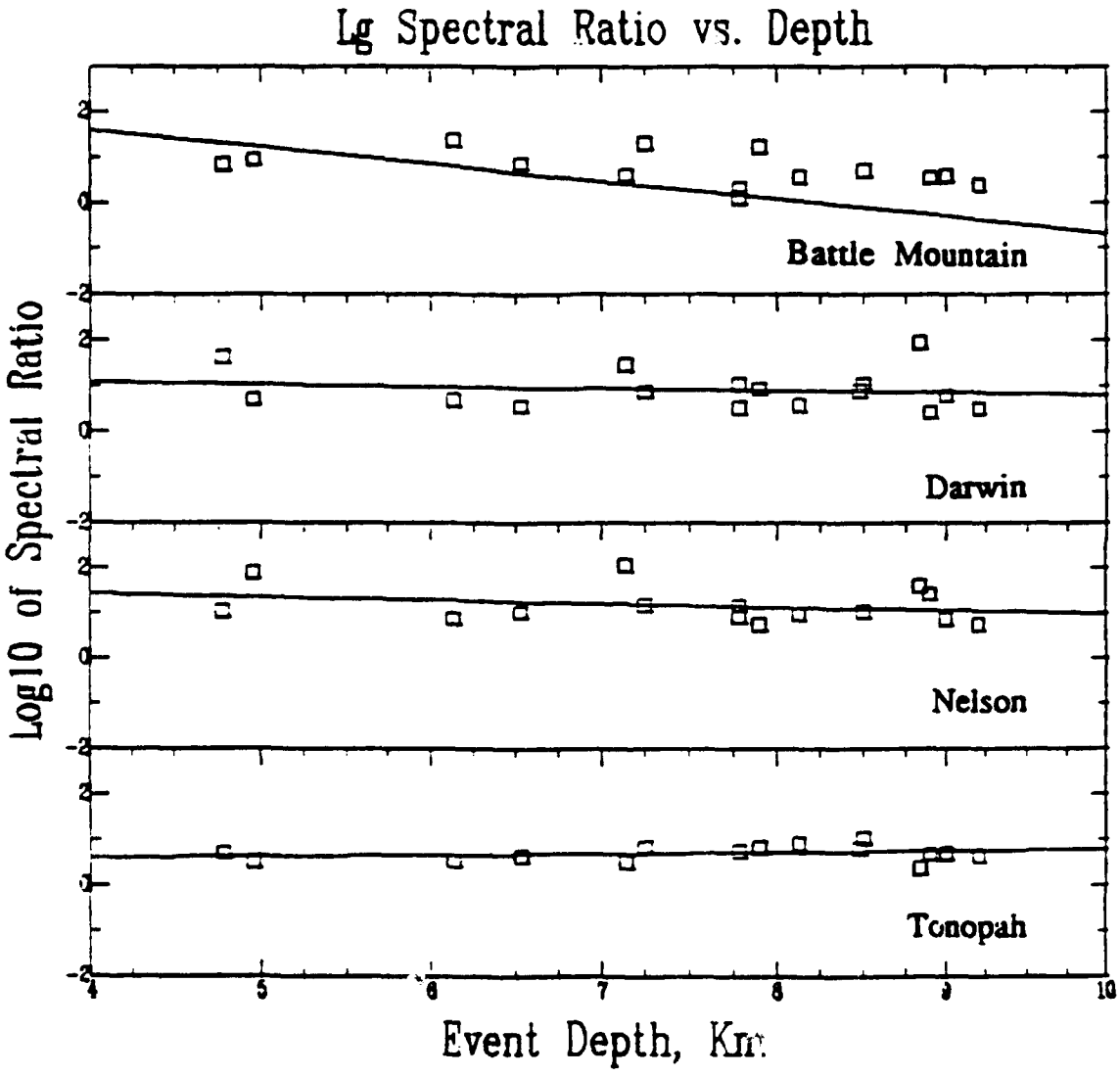

Figure 13. See Figure 9 for explanation.

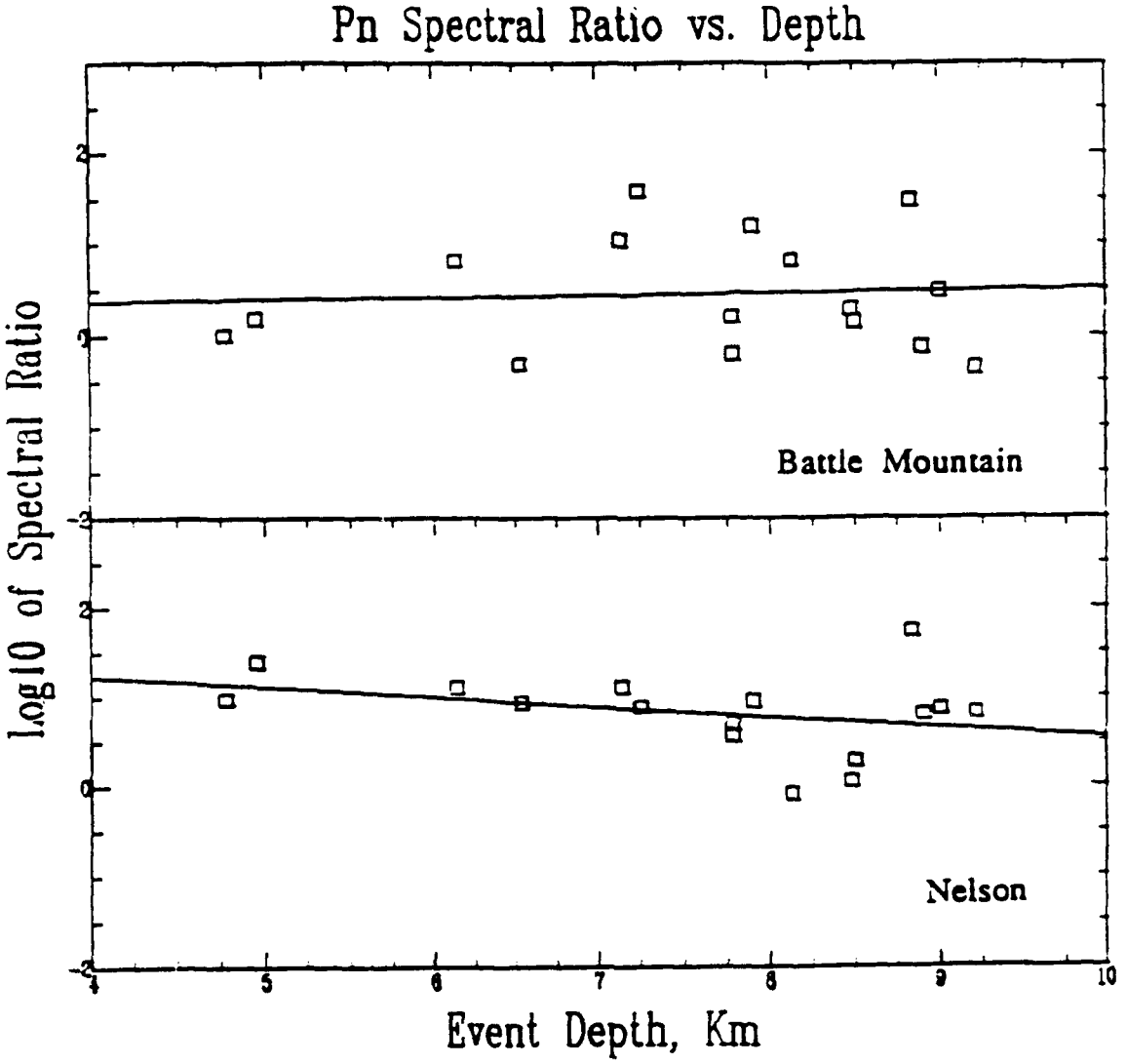

Figure 14. See Figure 9 for explanation.

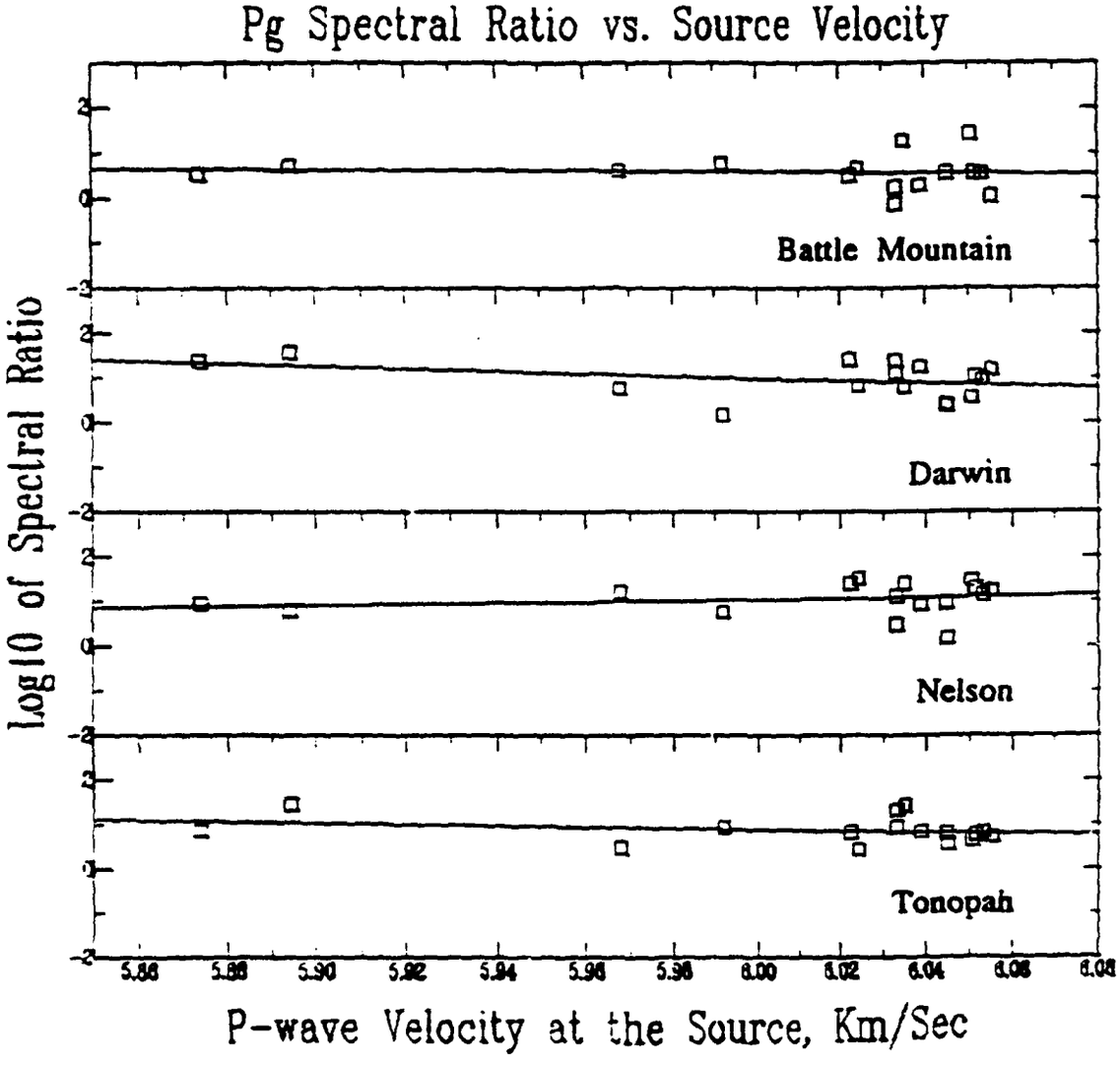

Figure 15. See Figure 9 for explanation.

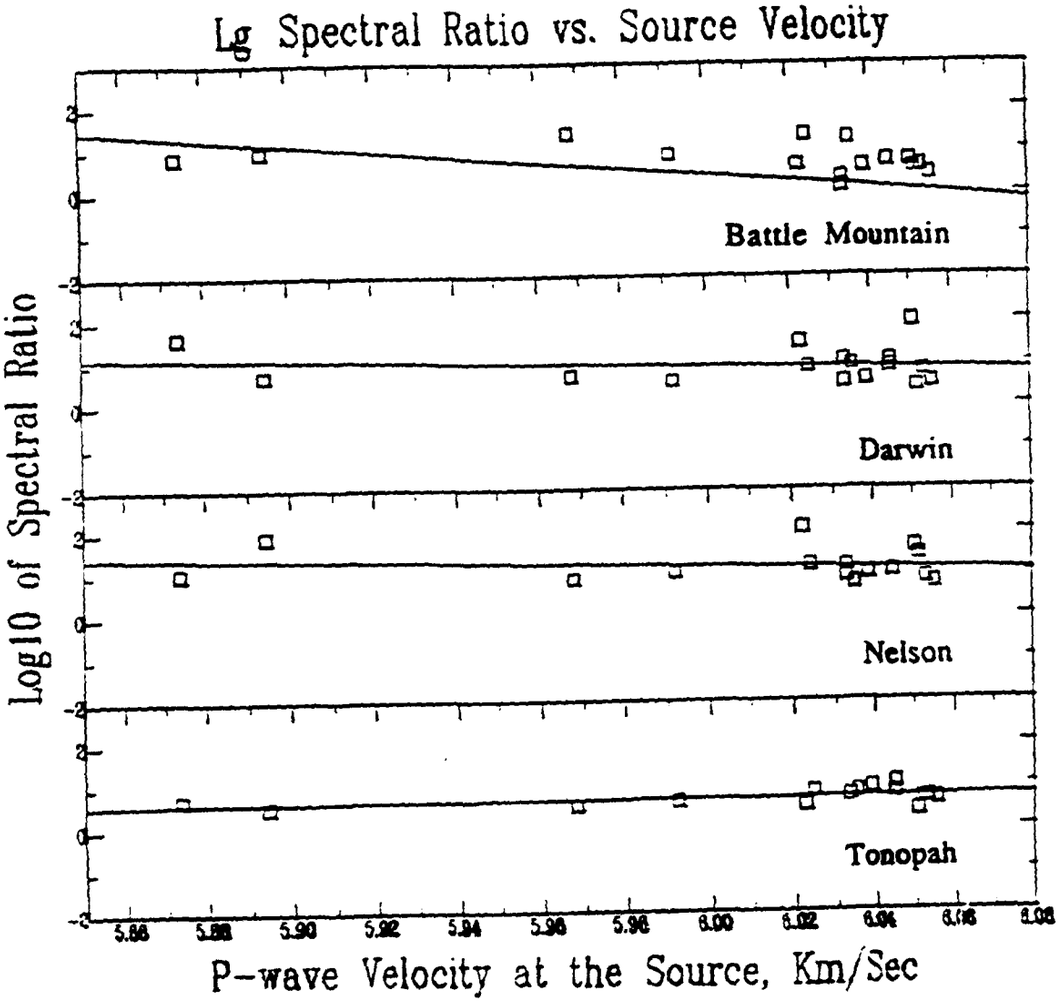

Figure 16. See Figure 9 for explanation.

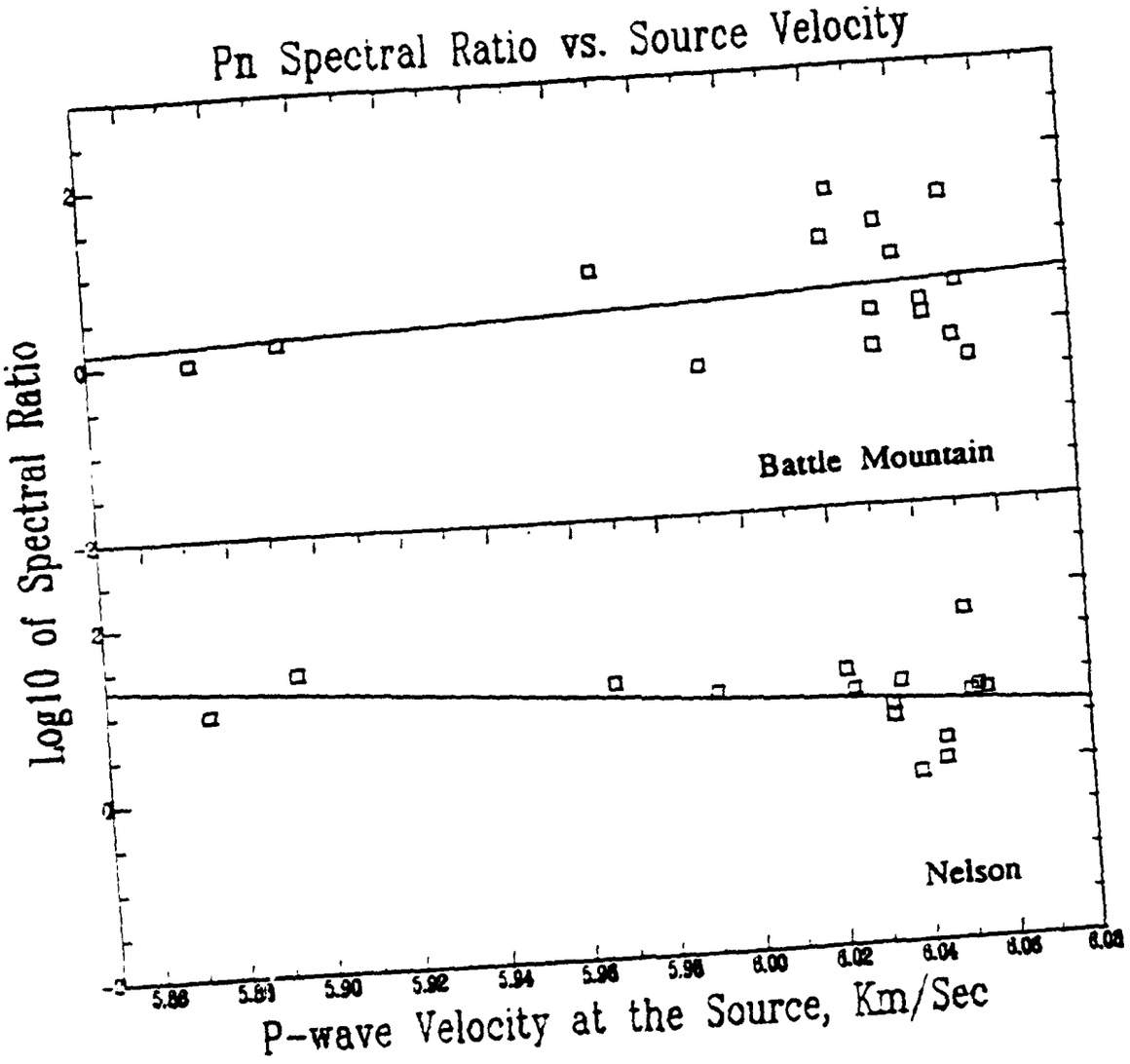

Figure 17. See Figure 9 for explanation.

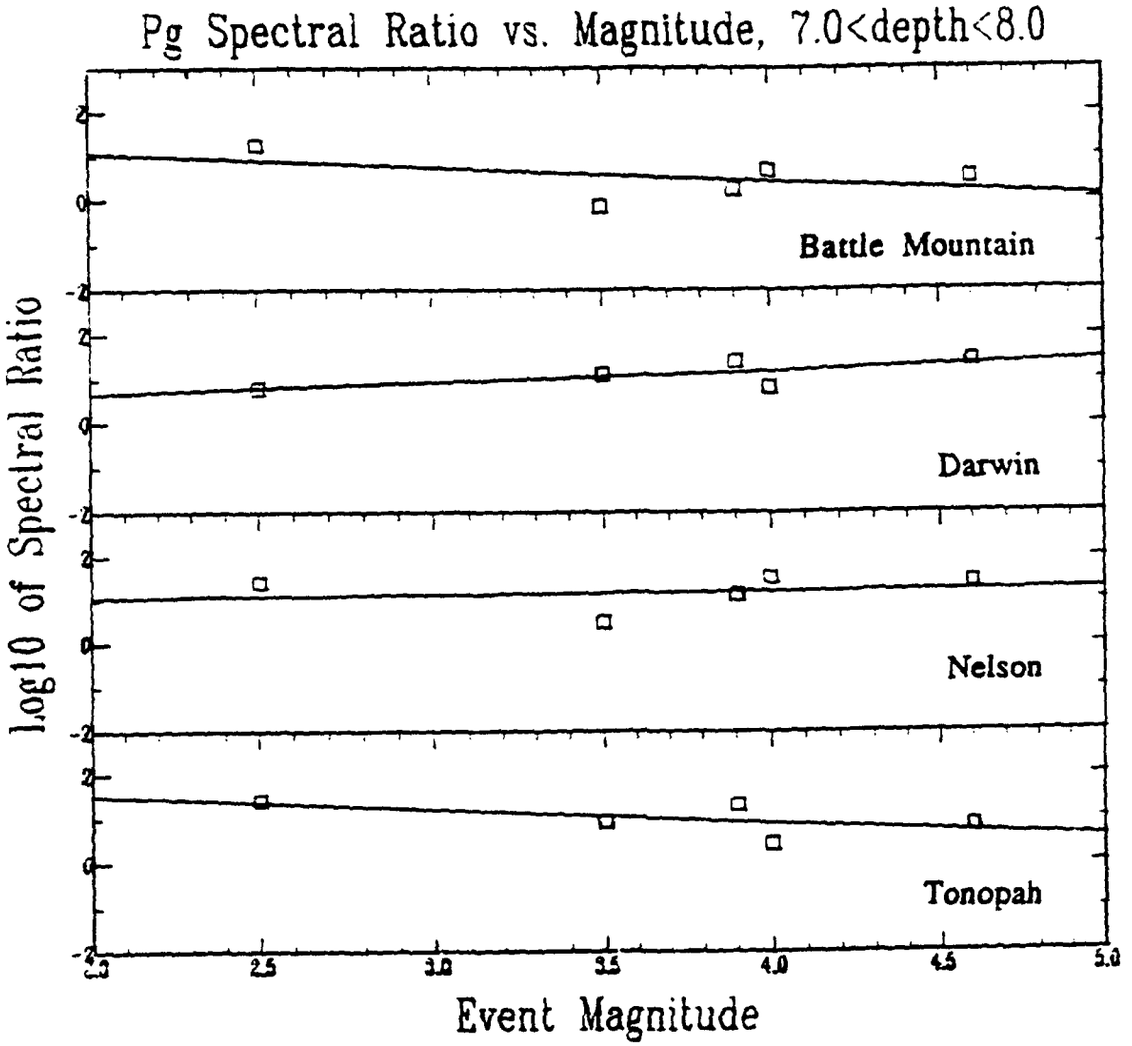

Figure 18. Figures 18–26 show the spectral ratio of *Pn*, *Pg*, and *Lg* as a function of source magnitude, source depth, and *P*-wave velocity at the source when minimizing the effects that other independent variables have on spectral ratio. When correlating depth and velocity with spectral ratio, the magnitude of the events was between 3.0 and 3.5 When correlating magnitude with spectral ratio, the depth was held between 7.0 and 8.0 km. Also shown is the least-squares linear fit to the data.

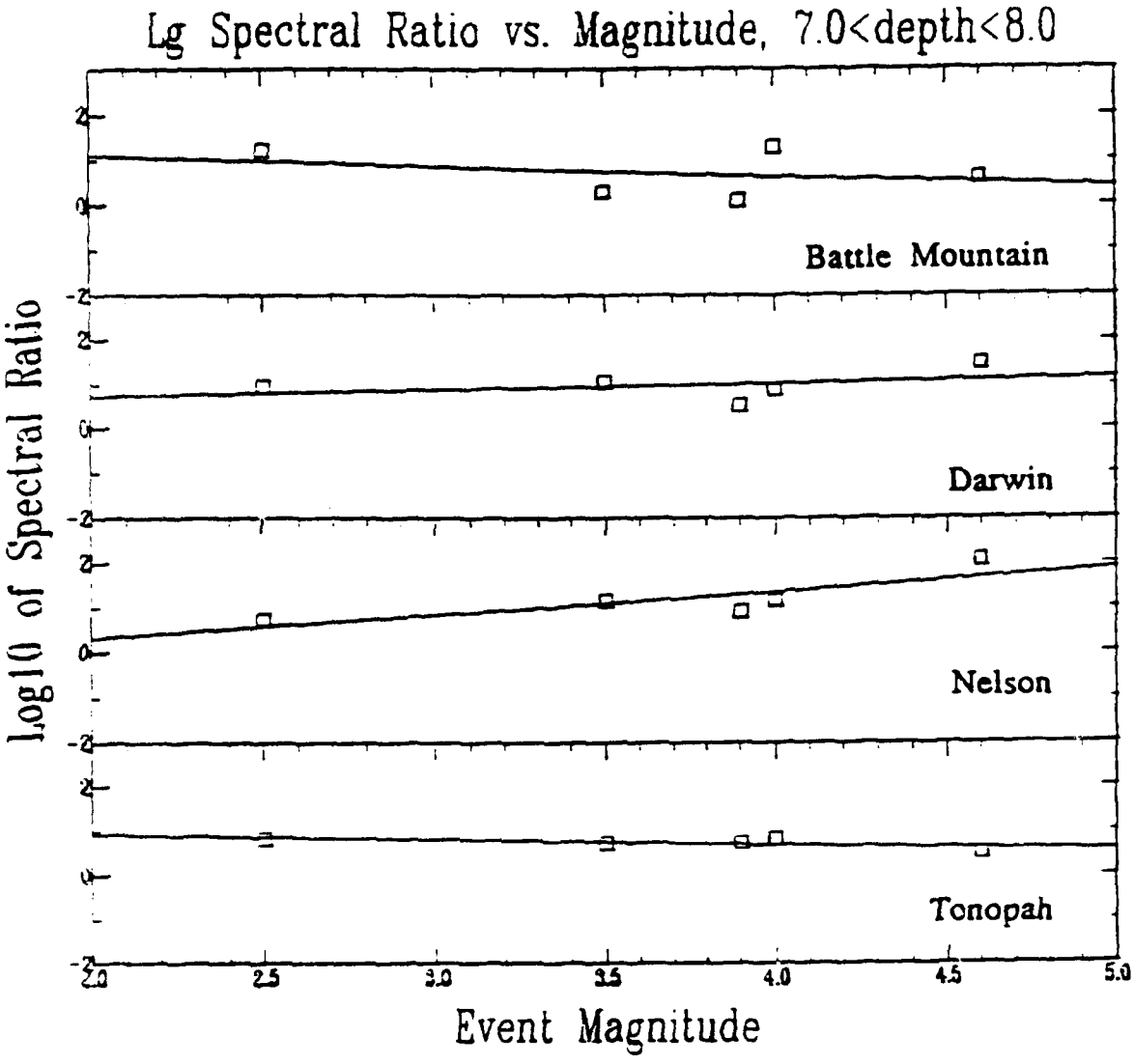

Figure 19. See Figure 18 for explanation.

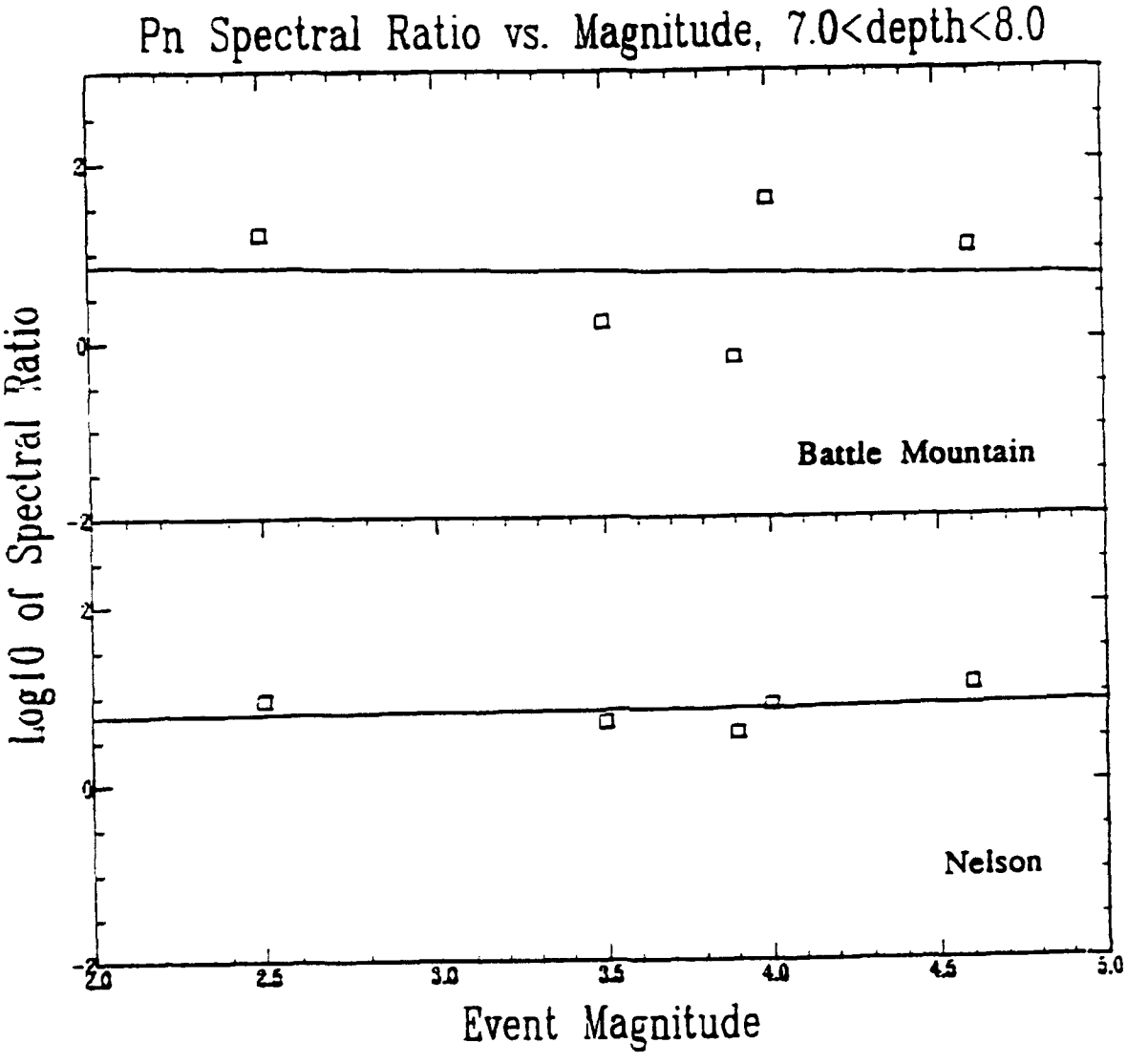

Figure 20. See Figure 18 for explanation.

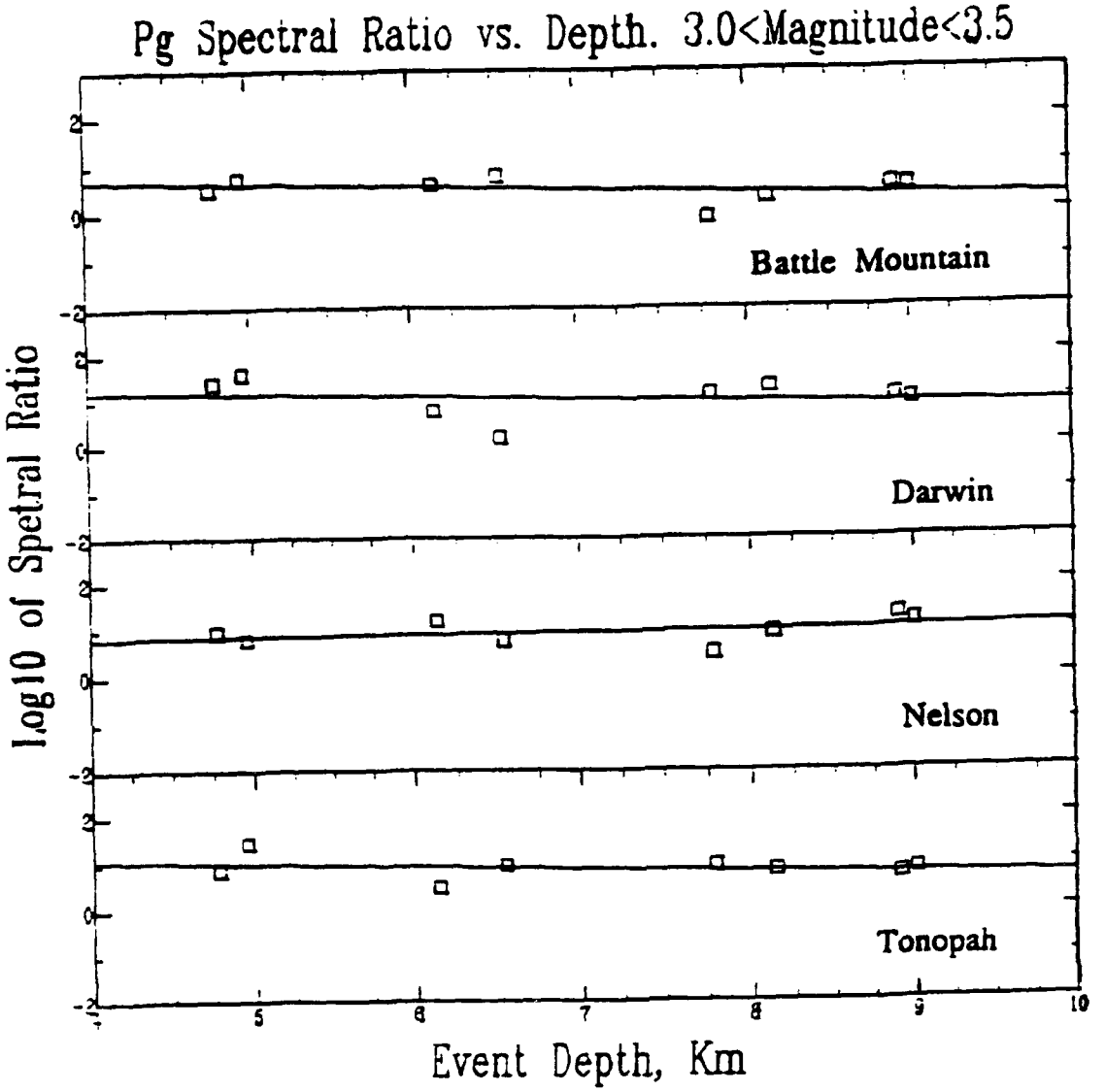

Figure 21. See Figure 18 for explanation.

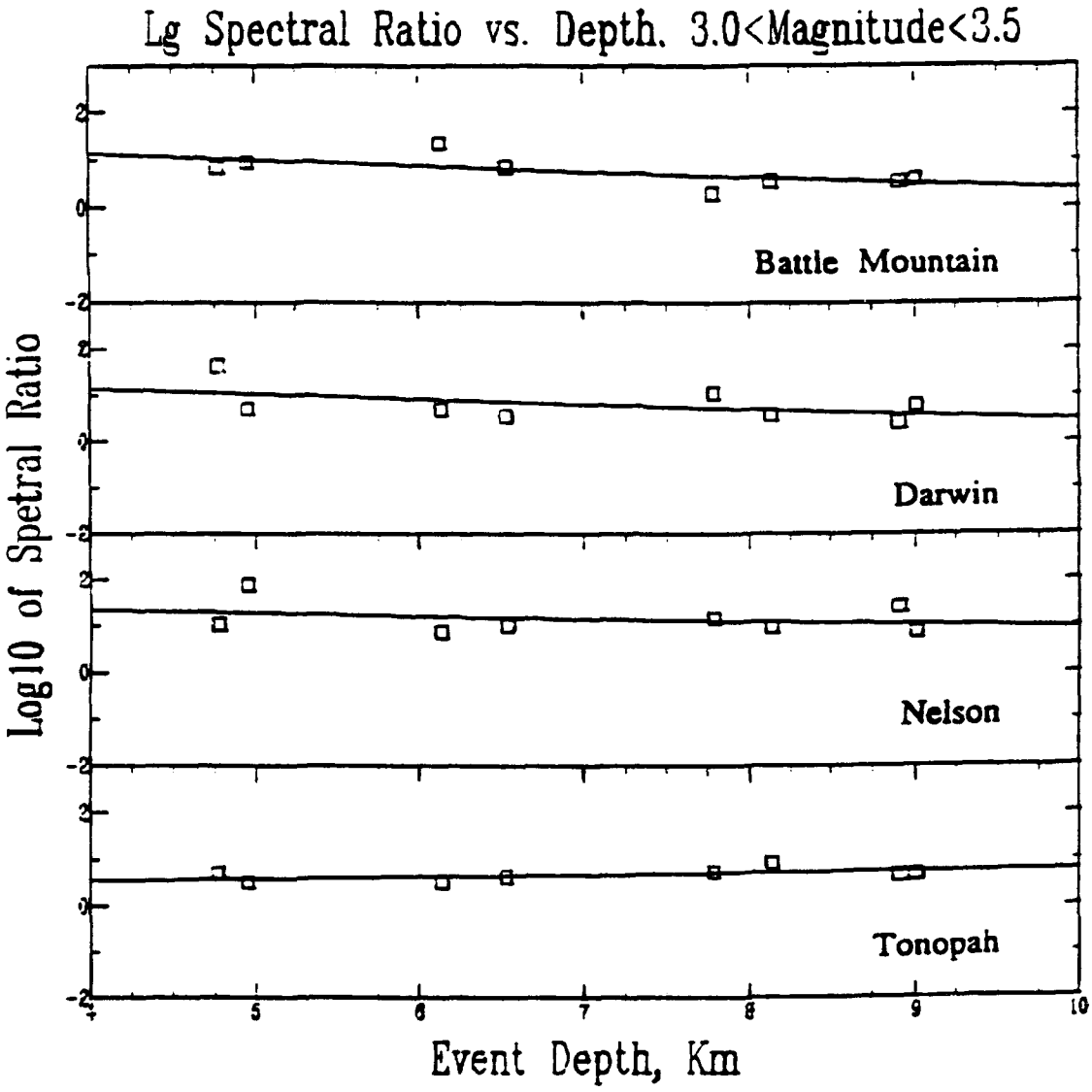

Figure 22. See Figure 18 for explanation.

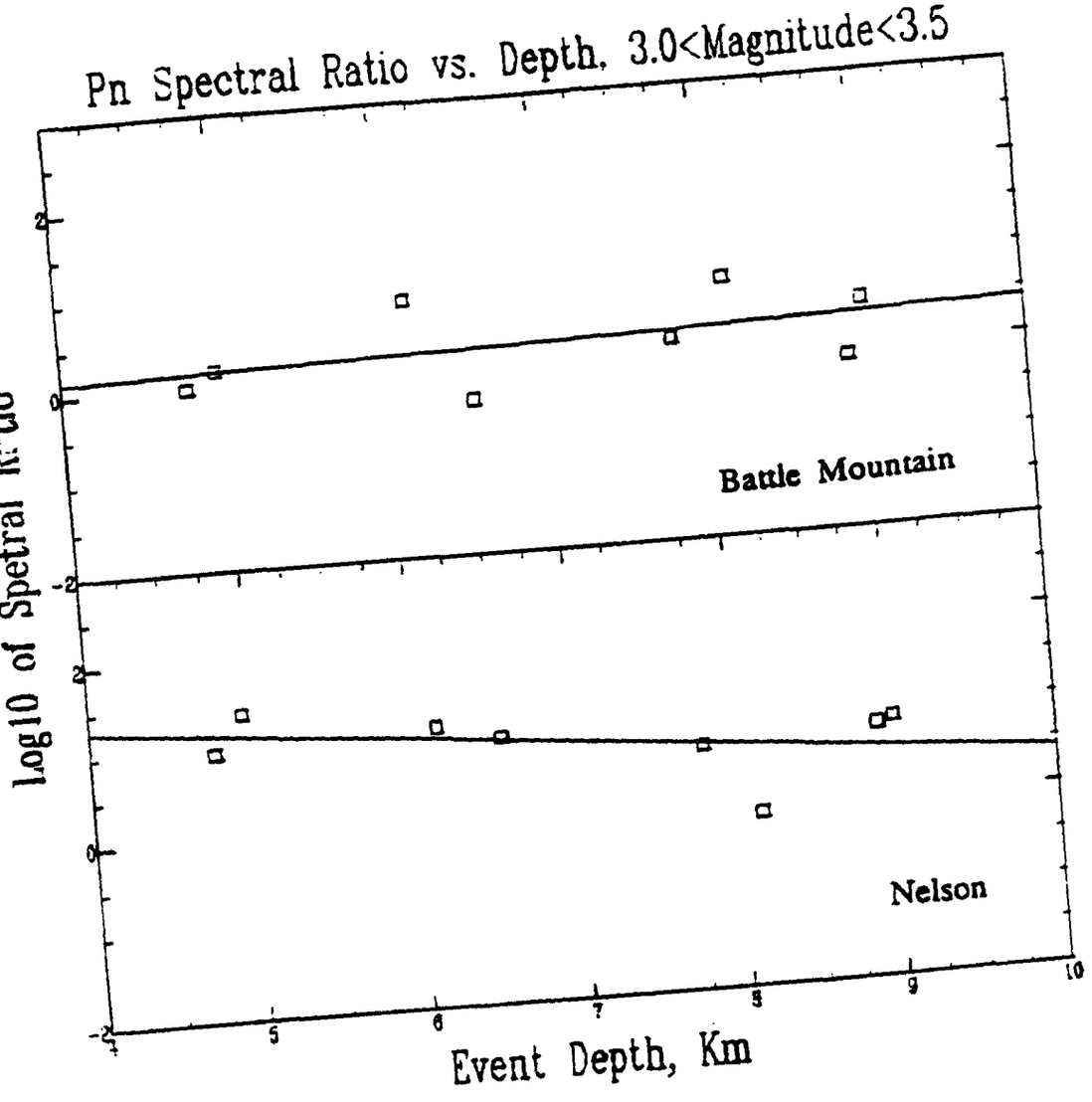

Figure 23. See Figure 18 for explanation.

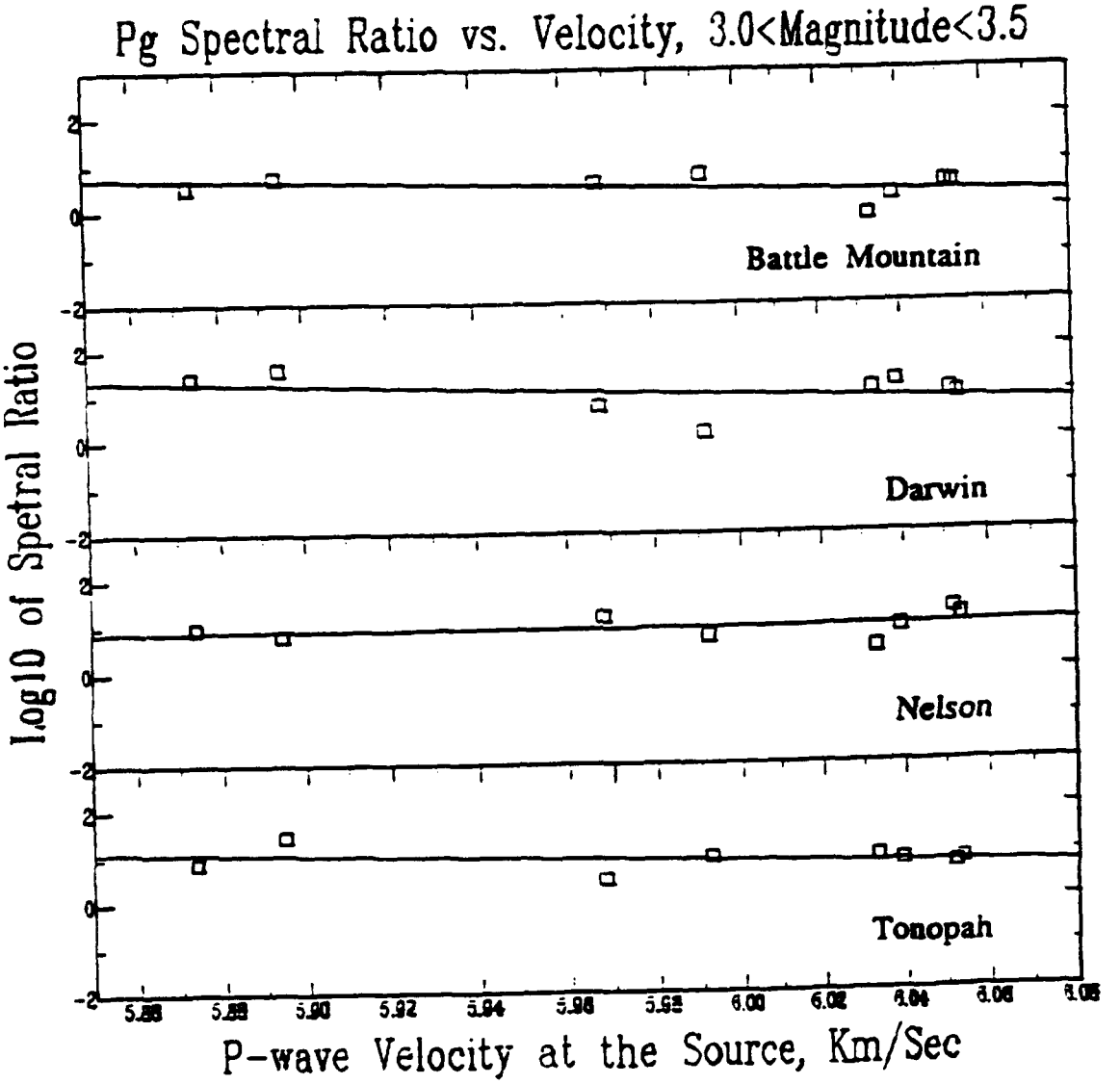

Figure 24. See Figure 18 for explanation.

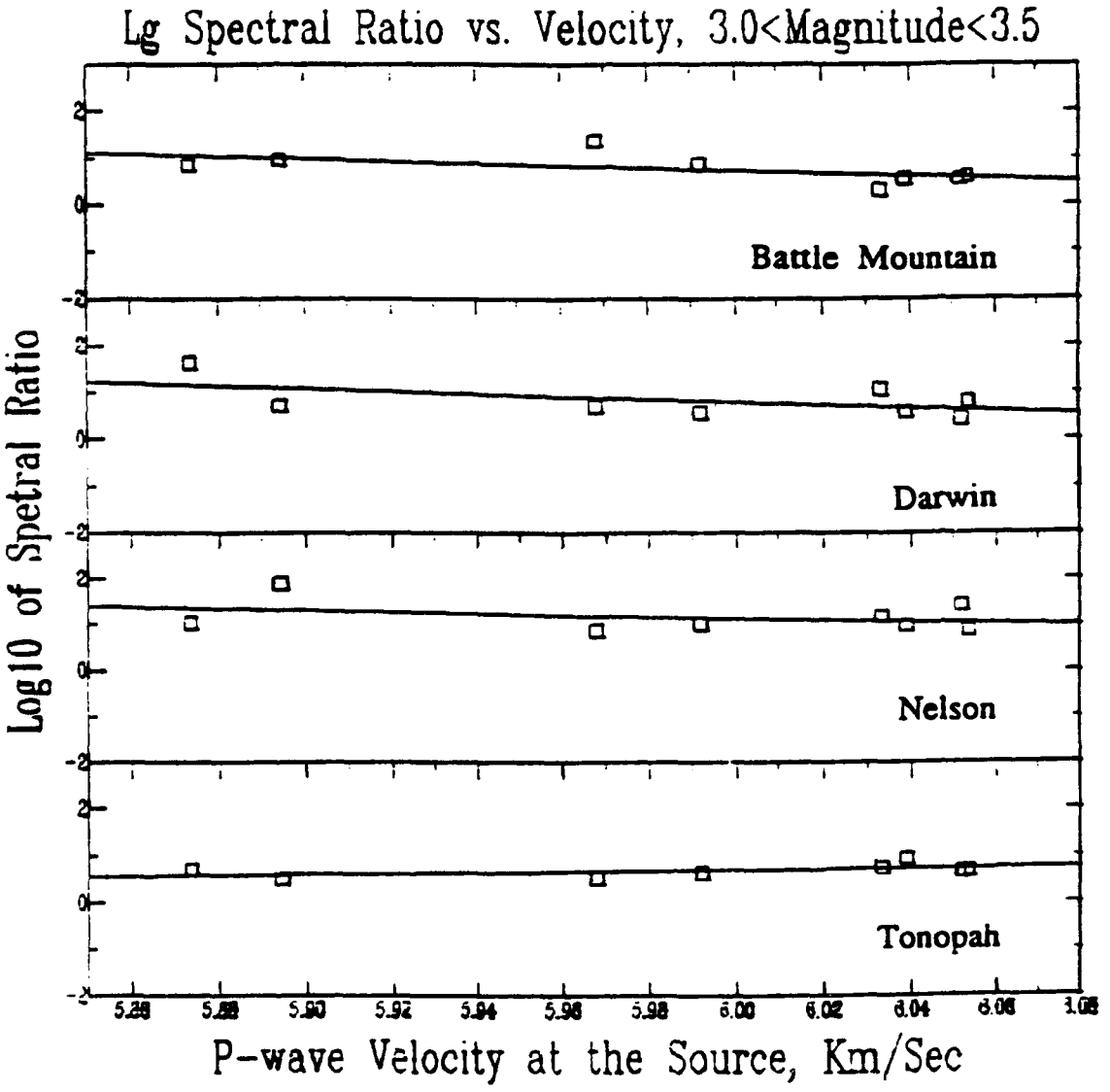

Figure 25. See Figure 18 for explanation.

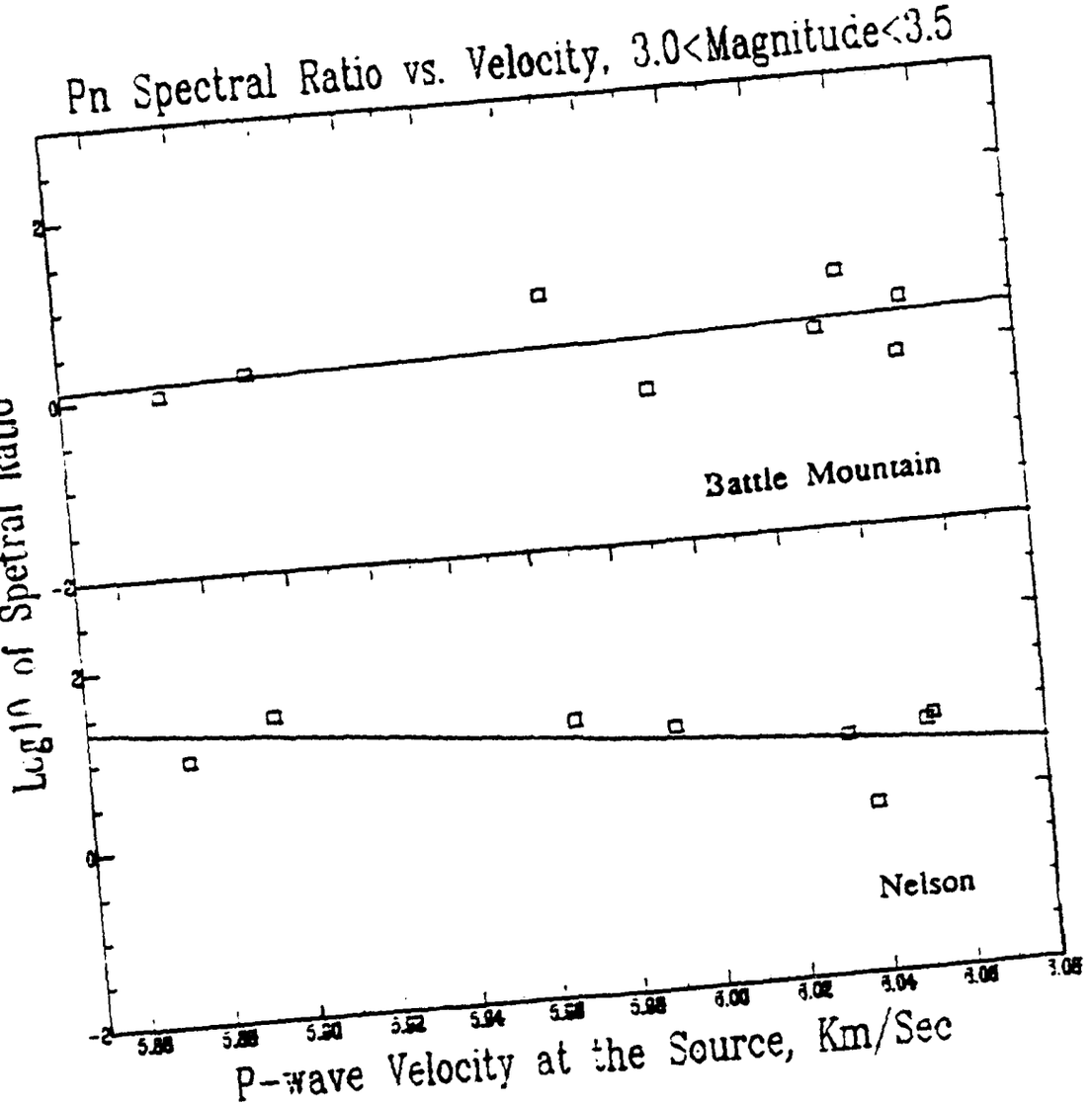

Figure 26. See Figure 18 for explanation.

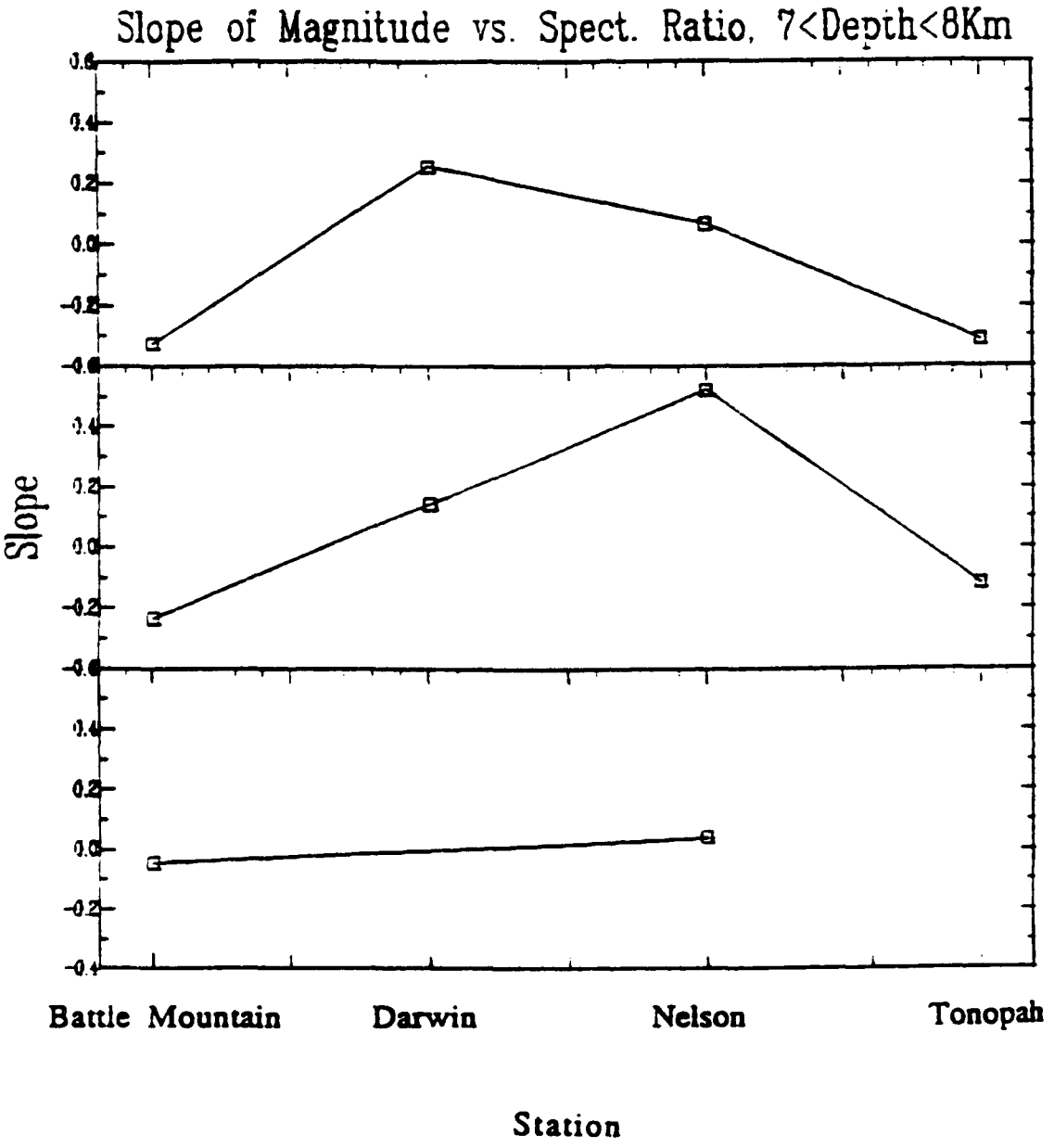

Figure 27. Shown are the slopes of least-squares lines that have been fit to the spectral ratio versus magnitude plots for *Pg*, *Lg*, and *Pn*. The correlation coefficients for each linear regression are displayed adjacent to each point to illustrate the goodness of fit (higher correlation coefficients indicate less misfit between the linear regression and the data). Negative slopes imply that the spectral ratio decreases with increasing magnitude. Positive slopes imply that the spectral ratio increases with increasing magnitude.

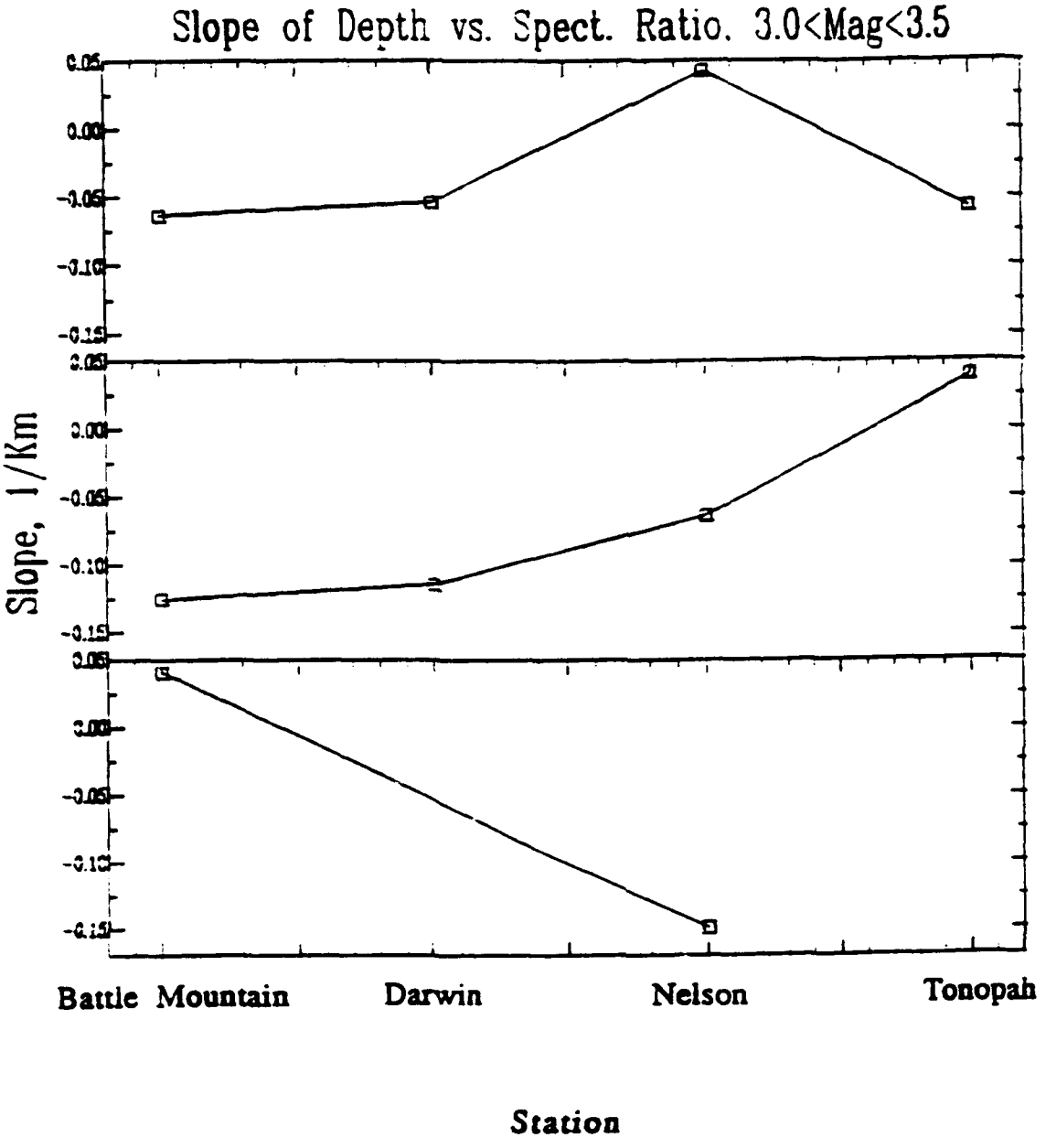

Figure 28. Shown are the slopes of least-squares lines that have been fit to the spectral ratio versus depth plots for *Pg*, *Lg*, and *Pn*. The correlation coefficients for each linear regression are displayed adjacent to each point to illustrate the goodness of fit (higher correlation coefficients indicate less misfit between the linear regression and the data). Negative slopes imply that the spectral ratio decreases with increasing depth. Positive slopes imply that the spectral ratio increases with increasing depth.

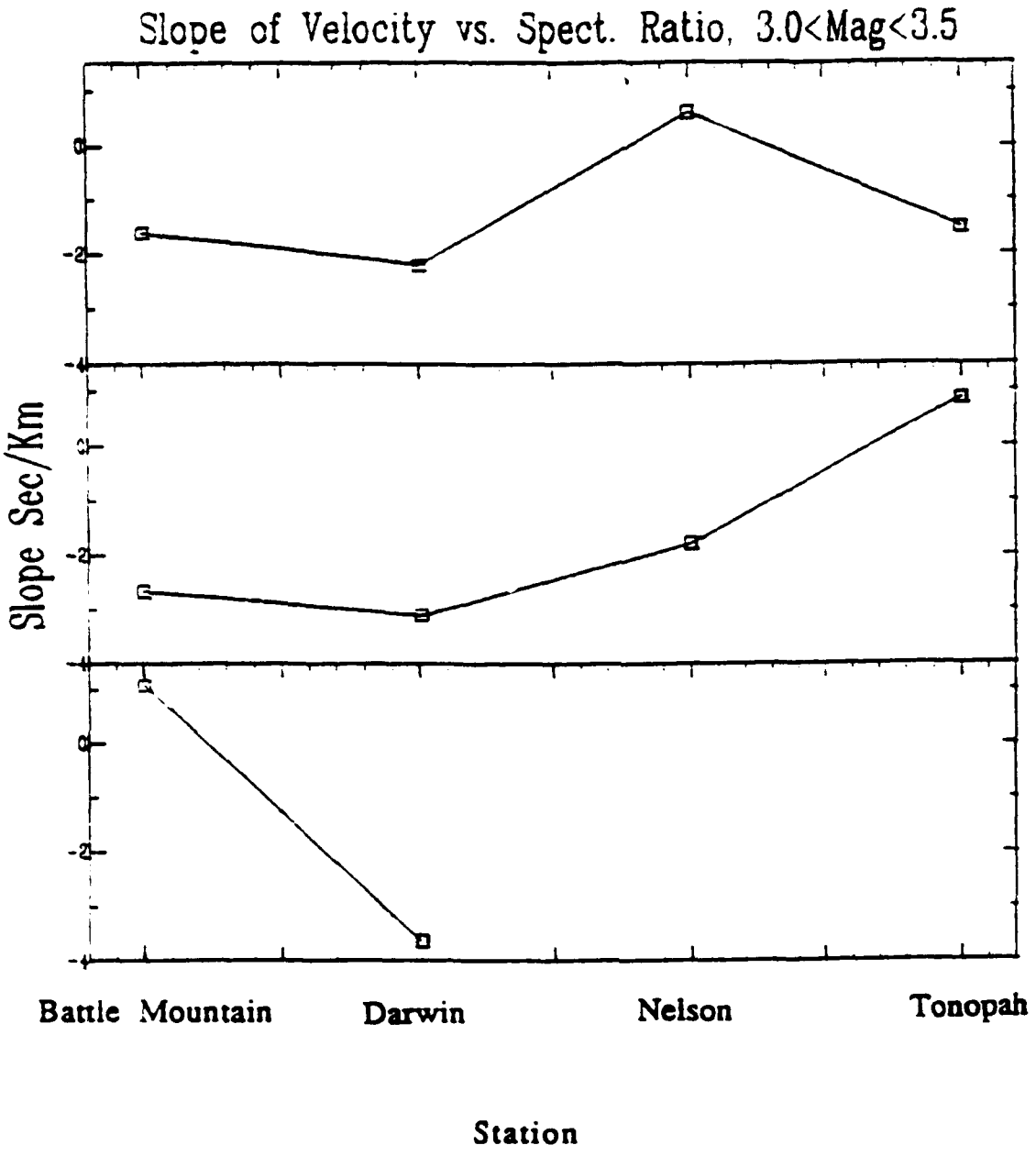

Figure 29. Shown are the slopes of least-squares lines that have been fit to the spectral ratio versus *P*-wave velocity at the source plots for *Pg*, *Lg*, and *Pn*. The correlation coefficients for each linear regression are displayed adjacent to each point to illustrate the goodness of fit (higher correlation coefficients indicate less misfit between the linear regression and the data.). Negative slopes imply that the spectral ratio decreases with increasing *P*-wave velocity at the source. Positive slopes imply that the spectral ratio increases with increasing *P*-wave velocity at the source.

CHAPTER 3

Body Wave Observations of Tectonic Release

by

Terry C. Wallace

BODY WAVE OBSERVATIONS OF TECTONIC RELEASE

Terry C. Wallace

Department of Geosciences, University of Arizona, Tucson, Arizona 85721

Abstract. Nearly all underground nuclear explosions have a component of non-isotropic seismic radiation which can be explained in terms of such phenomena as scattering, spall and tectonic release. Tectonic release is defined as the release of pre-existing strains in a material around an explosion. At long periods the tectonic release produces a wavefield which is identical to that of an earthquake. Theoretically, the only long-period surface waves produced by an explosive source are Rayleigh waves, yet for some explosions in granite the Love waves are larger than the Rayleigh waves. SH and sP phases from large explosions can be used to constrain the orientation of the tectonic release. The orientation for large explosions appears to be controlled by the regional stress regime. Strike-slip, normal-slip and thrust motion tectonic release have been observed for various U.S. and Soviet test sites. Tectonic release is a volumetric source, and is related to: (1) the size of the explosion and depth of burial, (2) the proximity to the source volume of previous explosions, (3) the regional stress pattern and (4) the source material.

The evidence for a short-period body wave tectonic release signature is indirect. There are systematic patterns in the ab amplitudes of teleseismic short-period P waves which are consistent with predictions from long-period tectonic release, but identifiable phases (such as sP) are absent. The short-period observations favor a distributed source for the tectonic release. The distributed source model also provides an explanation for the incoherence of near-field tangential strong ground motions.

Introduction

Precise and accurate yield determination from seismic waveforms requires detailed knowledge of all the processes which are contributing to the waveform. Besides the explosion source, other important processes include spall, "nonelastic" pP, scattering, and tectonic release. Tectonic release is observed as nonisotropic seismic radiation; the presence of SH and Love waves is a fairly common observation on the seismic records of many underground nuclear explosions. In fact, the first deeply buried explosion at NTS (RAINER, 9/19/57) produced significant SH-type radiation [Oliver et al., 1960] which started a vigorous scientific debate as to its origin [Press and Archambeau, 1962; Smith, 1963; Brune and Pomeroy, 1963]. The earliest theories on generation of the SH-type radiation called for a mode conversion during transmission, namely the conversion of SV and Rayleigh waves to SH and Love waves due to nonplanar structure or heterogeneity along the travel path [Oliver et al., 1960]. Brune and Pomeroy [1963] later showed that this scattering mechanism was not responsible for the long-period SH-type waves by comparing the waveforms from explosions (strong Love and Rayleigh waves) and the waveforms from cavity collapse (negligible Love waves, strong Rayleigh waves). This led to the conclusion that the SH-type energy was generated by a "tectonic" component, namely the release of pre-existing strain by the detonation of the explosion. There are two basic models for this strain release: (1) through triggered movement on nearby faults [Brune and Pomeroy, 1963; Aki et al., 1969; Aki and Tsai, 1972], and (2) stress relaxation in the highly fractured zone immediately around the detonation point [Press and Archambeau, 1962; Archambeau and Sammis, 1970; Archambeau, 1972]. For either of the stress release models, the long-period teleseismic radiation pattern can be represented by an equivalent double-couple source. Depending on the orientation and size of the tectonic release, the seismic waveforms from underground nuclear explosions can be significantly modified from what is expected from an isotropic source.

The effects of tectonic release are best documented in the surface waves of underground explosions. Figure 1 shows the Rayleigh and Love waves from the two explosions recorded at Weston, Massachusetts [from Toksöz and Kehrer, 1972]. Note that the Love wave amplitude is actually larger than the Rayleigh wave for these events. Toksöz et al. [1964] defined the "F factor" as the ratio of the Rayleigh wave amplitude generated by the explosion to that generated by the tectonic release. The F factor can be related to the ratio of explosion and tectonic release energy by the approximate relation (assuming a Poisson solid):

$$E_{tect}/E_{exp} = \frac{4}{3} F^2 \qquad (1)$$

or in terms of moment

$$M_o^{tect} / M_o^{exp} = \frac{2}{3} F \qquad (2)$$

where the moment of the explosion is given by [Müller, 1973]

$$M_o^{exp} = 4\pi\rho\alpha^2\psi_\infty \qquad (3)$$

where ρ and α are the density and P wave velocity at the source respectively and ψ_∞ is the reduced displacement potential. The NTS explosions with the largest F factors were detonated in granite: PILE DRIVER (F = 3.2) and HARDHAT (F = 3.0) [Toksöz and Kehrer, 1972]. For these events the seismic energy from the tectonic release was an order of magnitude larger than that released by the explosion itself. The implication of large tectonic release for yield determination from M_s is obvious. If the tectonic release is favorably oriented, and M_s is determined from stations at azimuths which the Rayleigh waves from the tectonic release are maximized, the yield could be over or underestimated by a significant amount. If the orientation of a double-couple representation of the tectonic release is known, then it is possible to correct the surface wave amplitudes for the effects of the tectonic release. Surprisingly, for PILEDRIVER and HARDHAT there was only a small effect on the value of M_s due to the tectonic release. The reason for this is twofold: (1) a good azimuthal distribution of seismic stations was used

Explosion Source Phenomenology
Geophysical Monograph 65

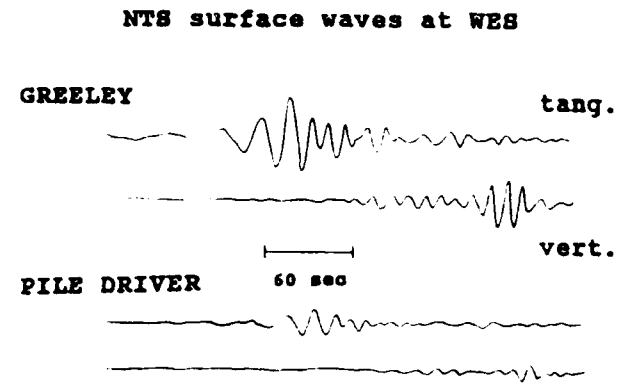

Fig. 1. Love and Rayleigh waves from two nuclear explosions with high levels of tectonic release (PILE DRIVER and GREELEY) recorded at WES (a WWSSN long-period seismic station). The vertical and tangential components are on the same scale. From Toksöz and Kehrer [1972].

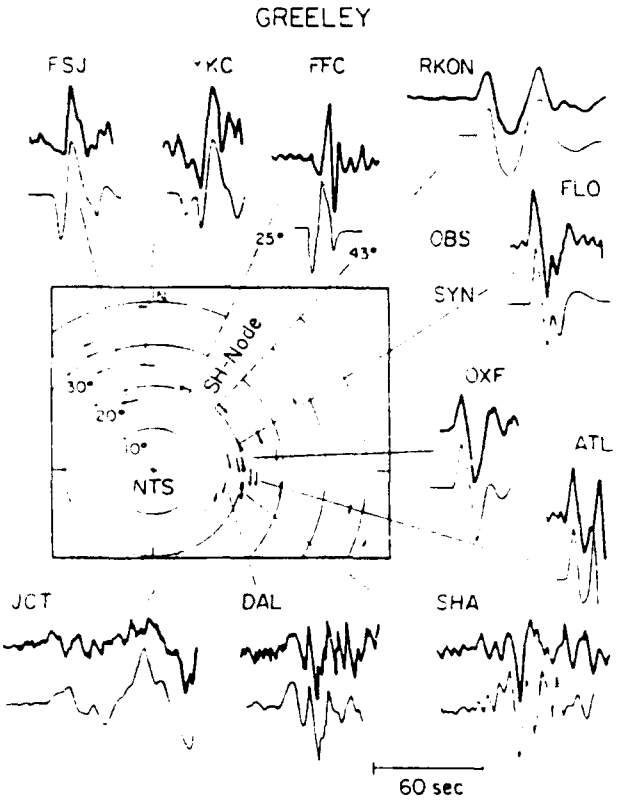

Fig. 2 The observed SH waveforms for GREELEY (top trace of seismogram pair) and waveforms from the Homestead Valley earthquake or a synthetic waveform (at FLO, RKON and OXF). The SH wave changes polarity between FFC, and RKON. From Wallace et al. [1985].

to determine M_s, and (2) the orientation of the tectonic release was equivalent to a strike-slip fault. The Rayleigh wave radiation pattern for a strike-slip fault is four-lobed; in two quadrants the explosion Rayleigh wave is enhanced, and in two quadrants it is reduced. Thus the tectonic-release effects are "averaged" out.

Despite the abundance of evidence for tectonic release in SH and surface wave observations, there is very little documentation of its influence on P waves, especially at high frequencies. Johnson et al. [1982] have shown that moment tensor inversions of three-component, strong motion data (both P and S waves) can be interpreted in terms of an explosion plus a double-couple for HARZER, although the signature of the tectonic release is no obvious. Murphy and Archambeau [1986] have suggested that normal faulting tectonic release with a large stress drop (>300 bars) produced a systematic m_b anomaly for RULISON of Δm_b = 0.3. In general, the short-period tectonic release signature is small, and its effect on m_b is still a scientific issue. Lay et al. [1984] looked at the first cycle (the ab amplitude) of teleseismic short-period P waves from many NTS explosions and found an azimuthally varying pattern which could be explained by tectonic release, although uppermost mantle structure could also be a possible cause. In this paper, we review the evidence for tectonic release in body waves, discuss the implications for the model of tectonic release, and the consequences for yield determination.

Observations of Tectonic Release in Long-Period Body Waves

Many investigators have noted the striking similarity of tangential records from nuclear explosions and those from shallow earthquakes in the frequency passband of the WWSSN long-period seismometer. Figure 2 [Wallace et al., 1985] shows a comparison of the SH waves from GREELEY (12/20/66; m_b = 6.3, F = 1.6 [Toksöz and Kehrer, 1972]) and the Homestead Valley, California earthquake (March 15, 1979, m_b = 5.5) recorded at WWSSN stations in the distance range of 13° to 28°. The stations were chosen such that the travel paths for the explosion and earthquake were essentially identical. The waveform similarity is remarkable. Note that the SH wave polarity changes between RKON and FFC, indicating that an SH node is between N43°E and N25°E. This strongly suggests that the tectonic release mechanism for GREELEY can be modeled with an earthquake source, or double-couple representation, similar to that of the Homestead Valley earthquake (vertical strike-slip). SH data are extremely valuable in constraining the orientation of the tectonic release double-couple. Although surface wave observations are the most common evidence cited for tectonic release, they can rarely be used to determine a unique orientation for the double-couple. This is because the Love wave radiation pattern for a vertical strike-slip fault and a 45° dip-slip fault (with a strike rotated 45° from that of the strike-slip fault) is identical. Although the radiation pattern is the same for both fault orientations, the seismic moments required to match the observed amplitude differ by a factor of two. Rayleigh waves can add information only if the moment of the explosion is small compared to the tectonic release. Otherwise, it is possible to adjust the source depth and size of the tectonic release such that the combined explosion and tectonic release Rayleigh wave spectra are identical. Aki and Tsai [1972] document this for BOXCAR (4/26/68), BENHAM (12/19/66) and BILBY (9/13/63).

Nonisotropic seismic radiation is also a common observation for Soviet explosions. For the Shagan River region of the Eastern Kazakh Test Site, explosions which are only kilometers apart produce Rayleigh waves which are 180° out of phase [Rygg, 1979; Goforth, 1982; Helle and Rygg, 1984]. Those events which demonstrate the Rayleigh wave reversal are also accompanied by very high levels of Love wave excitation. Tectonic release from a thrust (reverse) fault is the generally accepted explanation for this reversal. Burger et al. [1986] studied the body waves from Novaya Zemlya Test Site explosions and found that tectonic release was as large as 1.6×10^{24} dyne-cm (equivalent to an m_b = 5.4 earthquake) for some events. Figure 3 shows the SH waves from an explosion (11/2/74, F = 0.52) at the southern Novaya Zemlya Test Site and synthetic waveforms for a strike-slip tectonic release model. Note that there are reversals of the polarity of the SH pulse. Recently,

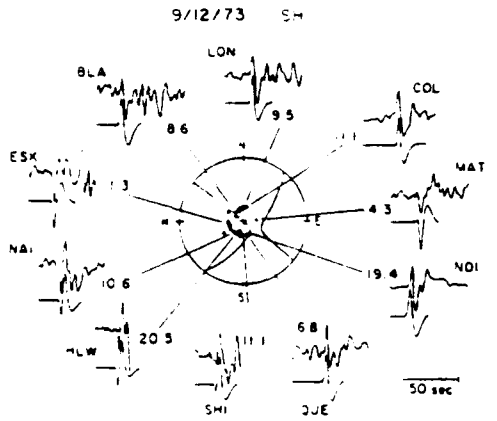

Fig. 3. Long-period SH observations and synthetic SH waveforms for a large Northern Novaya Zemlya explosion (9/12/73). The synthetics are for an oblique-normal double-couple mechanism dipping 55°. The number to the right of each seismogram pair give the moment (in units of 10^{16} Nt-m) necessary to match the observed amplitudes. From Burger et al. [1986].

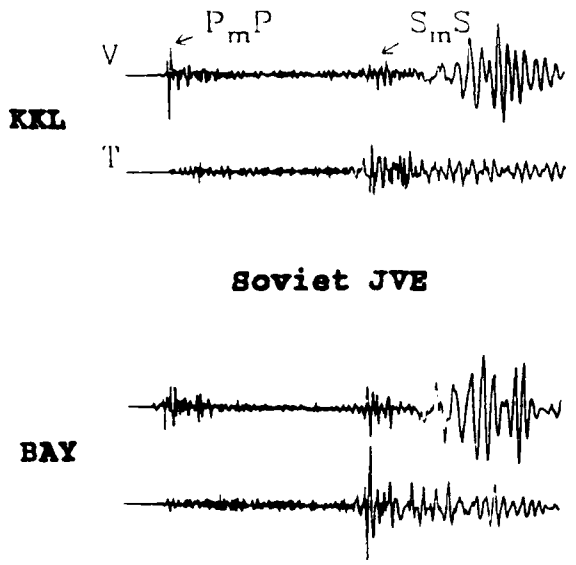

Fig. 4. Broadband, regional distance waveforms for the Soviet JVE. Both stations are approximately 260 km from the explosion. Note the very large SH wave identified as SmS. From Walter and Patton [1990].

Walter and Patton [1990] showed that the regional distance surface and body waves from the Joint Verification Experiment (JVE) required a significant component of tectonic release. High-frequency SmS (the SH Moho reflection) on the tangential component is shown in Figure 4; both stations are approximately 260 km from the explosion. This relatively high frequency observation of SH from an explosion shows clear azimuthal variability consistent with either a strike-slip or thrust mechanism for tectonic release.

In summary, SH waves from nuclear explosions are a common observation, and in general they are consistent with double-couple radiation patterns. If the SH-wave excitation for certain events is so similar to that of an earthquake, then it follows that the tectonic release should produce a P wavetrain also consistent with that of an earthquake. It is much more difficult to document the tectonic release signature of P waves because it is impossible to isolate the effects of the explosion (one can't simply look at the tangential component). As will be discussed later in this section, it is thought that for the large explosions at NTS the tectonic release has a nearly vertical strike-slip orientation. For a strike-slip earthquake recorded at teleseismic distances, the P wavetrain is dominated by the phase sP (both P and pP are small due to the vertical radiation pattern). Figure 5 shows the LPZ recordings of several Pahute Mesa explosions recorded at SHA (~24° away from NTS). These events are ordered on the basis of the ratio of the second positive upswing to the first upswing in the P wave (the ratio of the cd to ab amplitude). COBLY has the smallest ratio, BENHAM the largest. This also correlates with increasing amplitude of the SV pulse (approximately 4-1/2 minutes after the P-wave arrival). This ordering also happens to correspond roughly to an increasing F factor (F = 0.34 for COLBY, F = 0.85 for BENHAM). This strongly suggests that the size of the second upswing of the P wave is related to S-wave excitation. Wallace et al. [1983] interpret this second upswing of the P wave as sP from tectonic release. This interpretation has been questioned by Douglas et al. [1986], who notes that slap down from spall will also produce an arrival consistent with the timing of the second back swing in Figure 5. Although it is impossible to prove conclusively that sP is responsible for this arrival, Wallace et al. [1986] summarize a broad range of observations which favors coupling the arrival with SV. For example, the SV waveform from explosions BENHAM and GREELEY shows a phase reversal which is consistent with the orientation determined for the tectonic release double-couple. Further, this SV reversal is accompanied

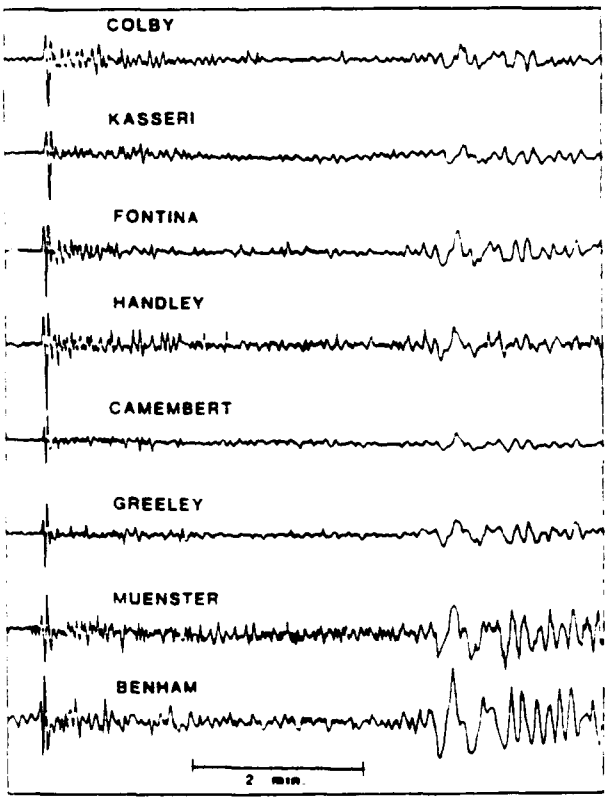

Fig. 5. The vertical component for eight large Pahute Mesa explosions recorded at SHA (15-100 instrument). SV arrives 4-1/2 minutes after the P wave. From Wallace et al. [1983].

by a reversal in polarity of the phase identified as sP.

Assuming that sP has been correctly identified in the explosion waveforms, it is possible to model the phase. Figure 6 shows a comparison of a high tectonic release event (BOXCAR) and an event with a much lower F factor (COLBY) recorded at LUB. COLBY and BOXCAR are separated by less than 3 km on Pahute Mesa and have approximately the same yield (~1000 kt; Dahlman and Israelson, 1977]. The main difference in the waveforms for the two explosions is the second upswing. This similarity suggests that the COLBY record can be used as an explosion "Green's function," and by simply adding a strike-slip synthetic waveform to simulate the tectonic release it is possible to model the BOXCAR record. In this modeling there is a trade-off between the relative timing of the explosion and tectonic release and the source S-wave velocity, but optimizing the fit produces a remarkable reproduction of the BOXCAR observation. Peak for peak, the predicted and observed seismograms of BOXCAR match to the PL arrivals. This near-perfect match indicates that tectonic release can have a strong signature on explosion P waves, at least in the period band of a WWSSN 15-100 instrument.

In general, it is difficult to determine the orientation of the tectonic release for a given explosion. As discussed earlier, the Love waves are ambiguous. The best body wave signature, SH, is similarly ambiguous. Nuttli [1969] showed that the SH radiation patterns for GREELEY and HALFBEAK are consistent with those generated by a double-couple but could not differentiate between a strike-slip or 45° dip-slip fault orientation. Hirasawa [1971] used the polarization angles of S waves from GREELEY, BOXCAR and BENHAM in an attempt to determine the orientation of the tectonic release double-couple for these events. Uncertainty in the size of the Ps phase from the explosion makes Hirasawa's results nonunique, but he argues that the polarizations are best fit with vertical north-south oriented strike-slip faulting for the tectonic release.

One way to alleviate the ambiguity of SH waveforms is to use the sP amplitudes as a constraint on the tectonic release orientation. sP amplitude is difficult to measure with precision, but the change in polarity is a powerful constraint. For individual explosions the data sets are sparse, but for most Pahute Mesa explosions, the SH waveforms are remarkably similar from event to event. Although the exact orientation may vary slightly from event to event, combining all the data allows for a robust inversion for a "characteristic" tectonic release mechanism for Pahute Mesa. Once the ambiguity of the tectonic release orientation is resolved, then the details of a tectonic release, such as stress drop, spatial extent of the source, and the source strength can be investigated.

Wallace et al. [1985] used the SH and sP waveforms from 21 Pahute Mesa explosions to determine the characteristic orientation for the Pahute Mesa tectonic release. On the basis of the SH waveforms and change in polarity of sP, there are three constraints on orientation: (1) the fault plane orientation must be approximately a vertical strike-slip or a 45° dip-slip fault; (2) there must be an SH nodal line striking N30°E; and (3) there must be a nodal surface in the sP radiation which separates azimuths of 15° and 97°. The only fault models which could satisfy all the criteria were predominantly strike-slip dislocations. The best "characteristic" solution is a pure strike-slip on a vertical plane striking N20°W. Figure 7 shows this plane and the extremal solution; the range of solutions between the average and extreme will satisfy the data to the 95% confidence level.

At first, the strike-slip mechanism for the tectonic release for the Pahute Mesa explosions is surprising considering the tectonic setting of NTS. Mapped Quaternary faults in the Basin and Range show predominantly normal-type slip. The Yucca fault in Yucca Valley, 20 km from Pahute Mesa, is a typical range-bounding, normal fault. Further, the displacements associated with the surface traces of faults which have moved during large explosions such as GREELEY are dominated by vertical slip [Dickey, 1969; McKeown and Dickey, 1969; Bucknam,

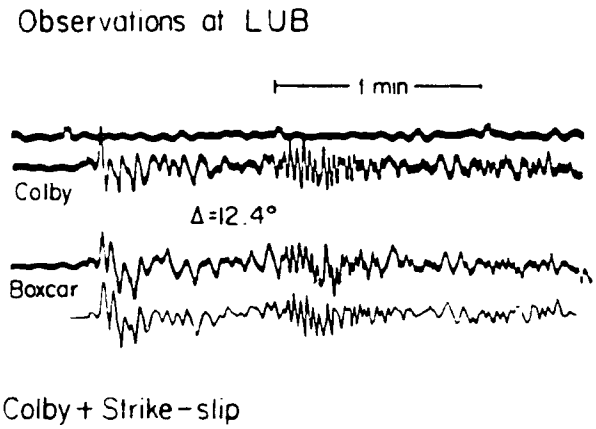

Fig. 6. A comparison of the P and PL waveforms for BOXCAR and COLBY at LUB. Also shown is a synthetic waveform constructed by summing the COLBY waveform and a synthetic calculated for a strike-slip double-couple (moment is 1.0×10^{17} Nt-m). From Wallace et al. [1983].

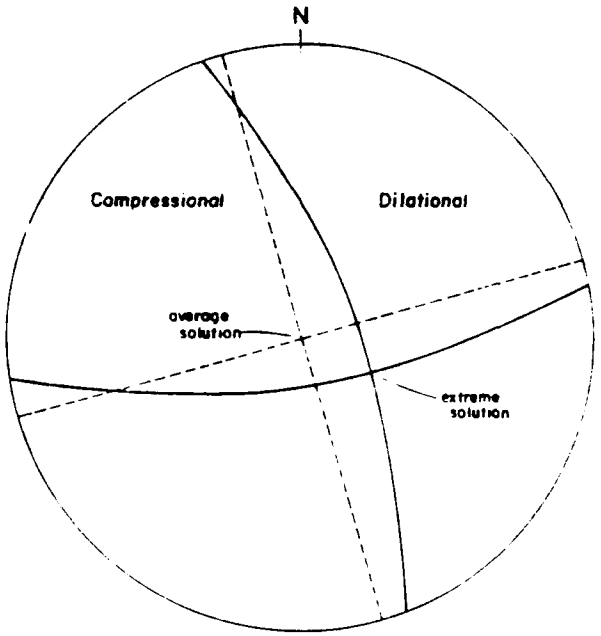

Fig. 7. Projection of the lower focal sphere for the average and extremal solutions for the "characteristic" tectonic release form the largest Pahute Mesa explosions. From Wallace et al. [1985].

1969; McKeown et al., 1970]. On the other hand, there are a number of factors which indicate that the strike-slip tectonic release mechanism is consistent with the present day, regional stress regime. The Massachusetts Mountain earthquake (8/5/71; $m_b = 4.2$) occurred 40 km south of Pahute Mesa. Fisher et al. [1972] used P wave first motions to determine a right-lateral focal mechanism with a plane striking N22°W. Patton [1982] confirmed this mechanism by an inversion of the short-period Rayleigh waves. The focal depth was very shallow (4.6 km), which is significant in that this depth corresponds to the likely depth of tectonic release for the largest explosions. A larger event (8/16/66), which occurred 200 km east of Pahute Mesa, was also a near-vertical,

right-lateral strike-slip earthquake, although the strike is somewhat shifted (N14°E). For several of the Pahute explosions there are significant aftershock sequences which are not symmetric about ground zero. For BENHAM and BOXCAR there is a north-south alignment [Hamilton and Healy, 1969; Ryall and Savage, 1969], and for BENHAM many of these aftershocks had right-lateral, strike-slip mechanisms.

It is very difficult to determine an "epicentral depth" for the Pahute Mesa tectonic release. Most of the analysis is based on long-period S waves which can be used to resolve depth to no better than approximately 5 km. On the basis of comparisons of waveforms with strike-slip earthquakes in the western U.S. the tectonic release must be shallow (<5 km). The aftershocks for BENHAM and BOXCAR extend to about 6 km depth, which is a maximum depth for the tectonic release. Analysis of the sP phase [Wallace et al., 1983] indicates a very short source duration for the tectonic release (<1 second). Assuming that the relative timing between the onset of the explosion P wave and sP is representative of the depth of the tectonic release, the centroid depth is between 2 and 4 km for the largest explosions. Because sP may be traveling through non-elastic material (fractured by the upgoing P wave), no better resolution is possible. The short source duration is indicative of high stress drops for the tectonic release. The high stress drop has important implications for the model of tectonic release.

Table 1 summarizes the long-period body wave observations of tectonic release. Although nearly every large underground explosion (Y > 300 kt) involves some amount of tectonic release, the effects on the first swing P waves, which might be used for magnitude, and thus yield determination, are subtle. The effects are much more pronounced later in the P-wave coda, and can have a significant effect on interpreting spall, slap down and near-source scattering. It is difficult to predict a priori what the tectonic release should be for a given explosion, and it depends on at least four factors: (a) the local stress field, (b) the size of explosion and depth of burial, (c) the proximity to previous explosions, and (d) the material in which the explosion is detonated. The details of tectonic release have only been investigated at NTS, but drawing from that experience, tectonic release appears to have a high stress drop, and to be associated with a volume of material surrounding the explosion.

Observations of Tectonic Release in Short-Period Body Waves

There are very few uncontroversial observations of tectonic release at short-periods (frequencies greater than 0.5 Hz). The most convincing are the SH waves at regional distances from events such as RULISON and the Soviet JVE. With the exception of Murphy and Archambeau [1986], it is usually assumed that m_b is not affected by tectonic release. There are two reasons for this: (1) there is not a single "phase" in the short-period P wave coda which can be unambiguously identified as sP from the tectonic release, and (2) early studies of the surface waves from tectonic release were interpreted in terms of low stress drops (~10 bars). Bache [1976] conducted a theoretical study of the potential effects of tectonic release on short-period P wave amplitudes and concluded that the effect was negligible for vertical strike-slip orientations (observed at Pahute Mesa). This represents a paradox: how can the tectonic release signature be so strong in the long-period P waves but be absent in the short-period P waves? Lay et al. [1984] investigated this problem by studying the details of the azimuthal variations of P wave amplitudes for 25 Pahute Mesa explosions. Using the first cycle (ab) amplitude of teleseismic short-period P waves, Lay et al. [1984] found an azimuthally varying pattern which could be fit with a $\sin(2\theta)$ curve. Figure 8 shows the azimuthal pattern for all Pahute events (average), GREELEY (high tectonic release) and HANDLEY (lower tectonic release). The amplitude pattern is enhanced by a factor of two between GREELEY and HANDLEY. The $\sin(2\theta)$ pattern is identical to the pattern expected for the radiation pattern from a vertical strike-slip fault. The position of the positive and negative lobes in the pattern are consistent with a right lateral fault striking N20°W; the same orientation derived from the long-period body waves. The significance of the $\sin(2\theta)$ fit can be evaluated by an f-test. Nearly all the Pahute Mesa events pass the test at the 99th % confidence level, but most importantly, the events with largest long-period tectonic release moments have the largest amplitude pattern. Figure 9 shows a simulation of the explosion plus tectonic release in an attempt to explain the GREELEY amplitude pattern. Although it is possible to fit the amplitude pattern with a simple point source tectonic release, the complexity it introduces into the waveform (especially a large sP) is inconsistent with the observed waveforms. One way to enhance the effect on the ab amplitude, but reduce the coda complexity, is to introduce directional rupture for the tectonic release. If the tectonic release ruptures downward at high velocities it will produce strong P waves but weaker sP phases. The bottom row of Figure 9 shows such a simulation.

There are alternative explanations for the $\sin(2\theta)$ amplitude behavior for Pahute Mesa explosions, such as lens-like upper mantle structure beneath Pahute Mesa [Lynnes and Lay, 1988]. But, the remarkable

TABLE 1. Long-Period Body Wave Observations of Tectonic Release

NTS:		
Smith [1969]	SH waves	Consistent with double couple strike-slip orientation
Imasawa [1971]	pS, sS	$\Delta\sigma$ (@ 130 bars
Wallace et al. [1983]	sP	$\Delta\sigma$ > 150 bars
Wallace et al. [1985]	SH, sP	Average orientation vertical strike-slip at Pahute Mesa; $\Delta\sigma$ > 150 bars for events in "new" regions
Novaya Zemlya		
Burger et al. [1986]	P, SV and SH	Northern NZ orientation is oblique normal, southern NZ orientation either strike-slip or thrust
Kazakhstan:		
Walter and Patton [1990]	SH	Strike-slip orientation for JVE
Colorado Plateau:		
Murphy and Archambeau [1986]	SH	Normal fault orientation; very high stress drop (>500 bars)

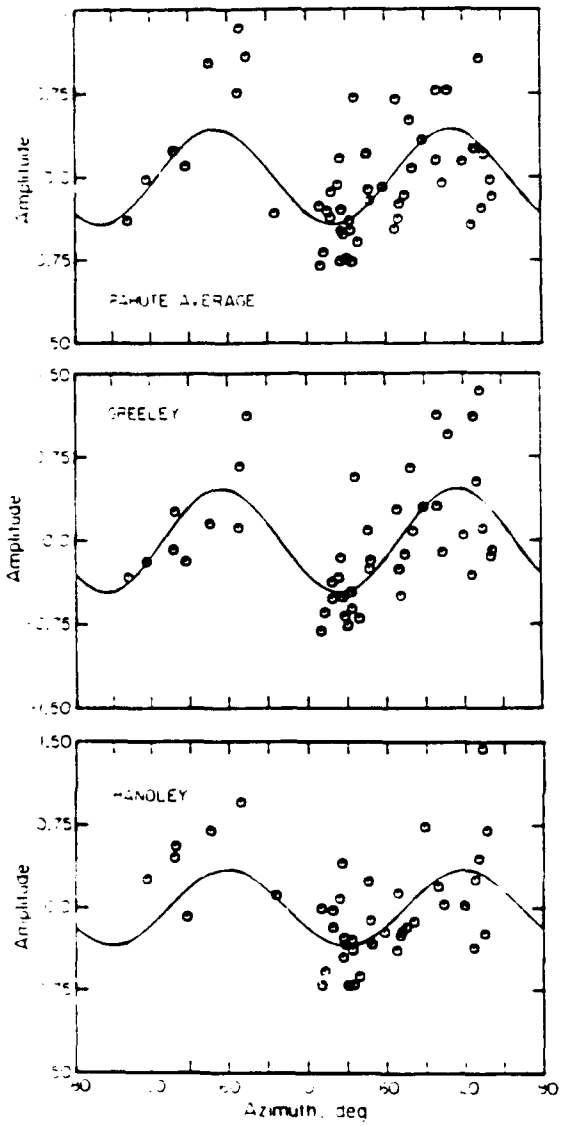

Fig. 8. Regression of sin(2Q) curves on short-period ab amplitudes for (a) average Pahute Mesa events; (b) GREELEY, a high tectonic release event; and (c) HANDLEY, a lower tectonic release event. From Lay et al. [1984].

consistency of the short-period pattern with the long-period SH arrivals favors at least some component of short-period tectonic release signature. Given and Mellman [1985] analyzed the surface waves from several Pahute Mesa events using sophisticated phase velocity and attenuation corrections developed for NTS by Stevens et al. [1982]. They determined the tectonic release orientation for many of the events studied by Lay et al. [1984]. Figure 10 shows the tectonic release orientation determined from the surface waves and the strike of the sin(2θ) pattern observed by Lay et al. [1984]. The strike of the double-couple varies from due north (90°) to N25°E for the different events. Although there are some differences in the absolute values of the strike as determined from surface and body waves, the agreement is good. More remarkable is the fact that as the strike varies the short-period measurement tracks the long periods very well. Using the argument of consistency between long- and short-period measurements, this is fairly strong (although indirect) evidence that the strike-slip tectonic release at NTS has a short-period signature.

The smallest explosion used in Figure 10 is PURSE (<80 kt). The technique of using SH waves at upper mantle and teleseismic distances to map the tectonic release becomes problematic at yields less than approximately 150 kt; the SH waves are simply too small. Patton [1988] developed a sophisticated inversion scheme for the six elements of the moment tensor utilizing regional surface wave data. When applied to Pahute Mesa explosions (Patton, 1990] the inversion yields a strike-slip

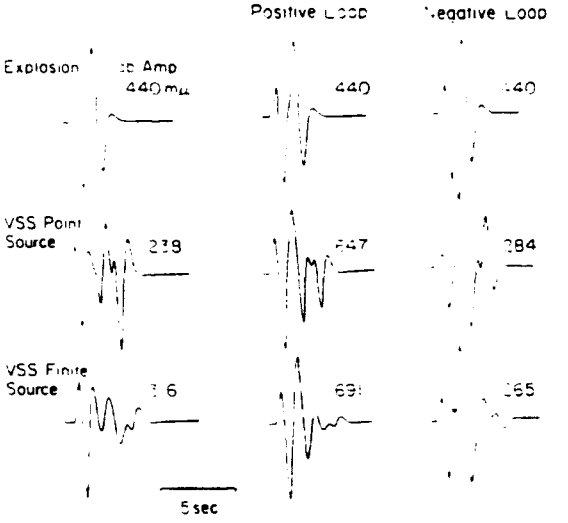

Fig. 9. A simulation of the short-period P waveforms for GREELEY assuming a vertical strike-slip (vss) orientation for the tectonic release. Top trace is the explosion alone. Next row is the effects of a point source tectonic release (left column is tectonic release alone, middle column is explosion plus tectonic release in the positive P loop direction, and the right column is the sum of the explosion and tectonic release in the negative P loop direction), and downward rupturing P wave synthetic. From Lay et al. [1984].

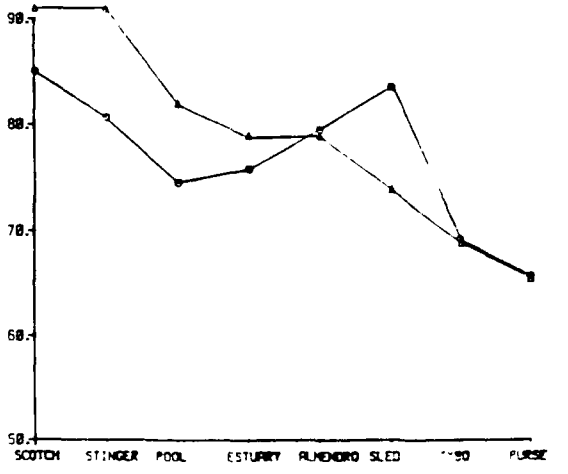

Fig. 10. Strike (in degrees) of tectonic release for different explosions. Triangles given the orientation as determined from surface waves, and the circles are the orientation of the sin(2Q) pattern determined from short-period ab amplitudes. From Wallace et al. [1986].

model for tectonic release as long as the yield of the explosion is greater than 200 kt. At yields less than 200 kt, the tectonic release appears to be characterized by a thrust type motion. A thrust mechanism is inconsistent with the regional stress pattern, so this must represent a different phenomenology than the tectonic release from large events. Masse [1981] reports thrust faults are observed above the working point of explosions detonated within Rainier Mesa. These thrust faults are initiated in the spall process of the explosion. As the upgoing compressional wave propagates away from the working point, joints, fractures or other planes of weakness are "driven" as large blocks of material move away from the expanding source cavity. There are also numerous examples of apparent shear-slip along bedding planes and joints for Rainier Mesa events. Stevens [1982] has shown that this driven motion will produce seismic waves which are equivalent to those produced by a double-couple. This process should occur in every explosion, but apparently there is a threshold above which regional stress dictates the form of non-isotropic radiation. Below this threshold only the block motion contributes to the seismic radiation.

Evidence for tectonic release at regional distances and in the near-field is difficult to document. At periods of 5-15 second, Wallace et al. [1983] show that the Pnl waveforms from Pahute Mesa explosions are sometimes strongly distorted by tectonic release. On the other hand, Alexander [1980], Pomeroy et al. [1982], and Gupta and Blandford [1983] present results which indicate that there is little evidence of non-isotropic seismic radiation in the Lg wavetrain. This implies that tectonic release has little effect on 3 Hz Lg amplitudes. A similar problem is rectifying the far-field representation of the tectonic release with the observations of the tangential component of the strong ground motions. The observed near-field SH waves from Pahute Mesa events are much more complicated and significantly smaller than expected. Figure 11 shows an example of this for BOXCAR. The observations (7.4 km from ground zero) show a very complicated tangential record. The synthetic seismograms shown below the observations were generated for an explosion source plus a strike-slip double-couple. The tangential component mismatch indicates two things: (1) significant off-azimuth energy, and (2) the inadequacy of a point source representation for the tectonic release. On the basis of the teleseismic modeling of SH from BOXCAR the tangential component can not simply be the result of scattering. If the tectonic release is purely a triggered fault motion, then it would be expected that the strong-motion SH waves would be similar to those produced by a similar sized earthquake, which they are not.

Wallace et al. [1987] attempted to rectify the near- and far-field SH waves by appealing to a distributed source. In Archambeau's [1972] model for tectonic release from a crushed zone about the working point, he defines the elastic radius, or extent of shear stress drop as:

$$R_e = F\rho\alpha^3 w_o \Delta\sigma \qquad (4)$$

where $\Delta\sigma$ is the stress drop, and ρ and α are the source density and P wave velocity respectively. For BOXCAR the elastic radius is on the order of 1 km if the stress drop is 200 bars. The distributed nature of the source can be modeled by placing a "cage" of point sources at the elastic radius. The resulting SH waves from such a distributed source are very complicated in the near-field due to the interference of the various sources. In the far-field, the long-period SH pulse is fairly simple because the wavelengths are long compared to the elastic radius. It is possible to make the near-field source arbitrarily complicated by choosing the number of distributed sources, elastic radius, etc., so there is not much gained by detailed tangential near-field modeling, but distributed sources offer a plausible explanation for differences in the near-field/far-field observations.

In summary, the short-period signature of tectonic release is much more subtle than at long periods. There is much indirect evidence that short-period P waves can be influenced by tectonic release, although direct evidence, such as an identifiable sP phase is lacking. The seismic moments which are required to explain the long-period body waves should produce a signature which is recognizable at short periods. This implies that the point source double-couple representation is incorrect. Apparently the rupture process or distributed character of the tectonic release strongly effects the short-period seismic radiation.

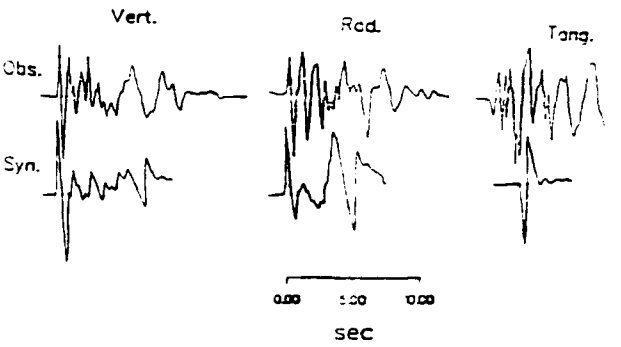

Fig. 11. Comparison of strong ground motion from BOXCAR observed at a recording site 7.4 km away from ground zero with synthetic seismograms calculated using the source model of Hartzell et al. [1983].

Models for Tectonic Release

The varied observations of the signature of tectonic release places numerous constraints on the physical processes which are generating the tectonic release. We can concentrate on the Pahute Mesa explosions studied for source orientation for further constraints. The explosions span an order of magnitude in the size of the explosion and the moment of tectonic release. The size of the tectonic release for these events is listed in Table 2. Figure 12a shows the size of the tectonic release versus explosion size. Explosion size is given by the world-wide average ab amplitude of the short-period P-waves normalized to 50°. BOXCAR is the master event; HANDLEY has the largest relative ab amplitude (1.41). In general, the tectonic release increases with yield. There is a trade-off between yield and depth of burial, since increasing yield usually results in greater burial depth. There is large scatter in the amount of tectonic release for a given yield. Note that JORUM, BOXCAR, KASSERI, FONTINA, MUENSTER and BENHAM are all approximately the same size, yet the tectonic release varies by an order of magnitude. Aki and Tsai [1972] found that for Yucca Flats explosions there was a yield threshold for tectonic release, and as time passed this threshold increased. In other words, tectonic release from the Yucca Flats test site decreased with time; the site "wore out." Wallace et al. [1983] suggested a similar phenomena occurred on Pahute Mesa; the tectonic release was significantly reduced when an event is detonated within a 4 to 5 km radius of the location of a previous explosion. For example, BOXCAR and JORUM, juxtaposed in the western part of Silent Canyon caldera, are about the same yield, yet BOXCAR has a tectonic release moment which is three times larger than JORUM. JORUM (9/16/69) was detonated after BOXCAR (4/26/68), supporting a hypothesis that tectonic release is a volume source. Figure 12b shows the same explosions as shown in Figure 12a except that they have been divided into two populations: (1) those events which are well separated (>4 km) from previous explosions (denoted with an H), and (2) those which are near a previous explosion (denoted with an L). There is a fairly systematic separation of the "H" and "L" populations. A least-squares fit of seismic moment (tectonic release) to explosion size for each population is also shown in Figure 12b; the lines are nearly parallel, but offset. STILTON and HANDLEY were excluded from this regression. Both of these events seem to belong to the low tectonic release population, but they are relatively isolated, implying that they should have high tectonic release.

TABLE 2. Moments for Tectonic Release from Pahute Mesa Explosions

Name	Date (m-d-yr)	Origin time	Lat. (°N)	Long. (°W)	Depth (km)	m_b	M_O[a]
Almendo	06-06-73	13:00	37.24	116.35	1.064	6.1	0.61
Benham	12-19-66	16:30	37.23	116.47	1.402	6.3	3.43
Boxcar	04-26-68	15:00	37.29	116.46	1.158	6.2	0.86
Camembert	06-26-75	12:30	37.28	116.37	1.311	6.1	0.86
Cheshire	02-14-76	11:30	37.24	116.47	1.167	5.8	0.43
Colby	03-14-75	12:30	37.31	116.47	1.273	6.2	0.49
Estuary	03-09-76	14:00	37.31	116.36	0.869	5.8	0.43
Fontina	02-12-76	14:45	37.27	116.49	1.219	6.1	1.35
Greeley	12-20-66	15:30	37.30	116.41	1.215	6.3	1.90
Halfbeak	06-30-66	22:15	37.32	116.30	0.819	6.1	0.61
Handley	03-26-70	19:00	37.30	116.53	1.206	6.4	1.47
Inlet	11-20-75	15:00	37.22	116.37	0.817	5.9	0.18
Jorum	09-16-69	14:30	37.31	116.46	1.158	6.1	0.31
Kassen	10-28-75	14:30	37.29	116.41	1.265	6.2	1.22
Mast	06-19-75	13:00	37.35	116.32	0.912	5.9	0.31
Muenster	01-03-76	19:15	37.30	116.33	1.451	6.2	1.96
Pipkin	10-08-69	14:30	37.26	116.44	0.617	5.6	0.12
Pool	03-17-76	14:15	37.26	116.31	0.879	6.0	0.12
Scotch	05-23-67	14:00	37.27	116.37	0.978	5.7	0.18
Stilton	06-03-75	14:20	37.34	116.52	0.731	5.8	0.07
Tybo	05-14-75	14:00	37.22	116.47	0.765	5.9	0.18

[a] M_O given in units of 10^{17} Nt-m (all values from Wallace et al., 1986).

STILTON and HANDLEY are the only Pahute Mesa explosions in Figure 12 which are not within Silent Valley Caldera. Although this may be coincidental, it is plausible that there is a different strain regime outside the caldera. Inspection of Figure 12 does not result in a threshold for tectonic release. PIPKIN has a yield on the order of 90 kt, which is below the yield threshold Patton [1990] would predict for the regional stress dominating tectonic release, thus one would expect a thrust type tectonic release mechanism. Unfortunately, there are not enough small yield events to reliably determine if tectonic release scales differently above and below some yield cut-off. For large explosions it appears that tectonic release is associated with a volume of material, and that volume is related to the size of the explosion. Toksöz and Kehrer [1972] noted that tectonic release is also related to source rock type. Explosions at NTS in granite appear to have much higher F factors. This is also true for Soviet explosions in the East Kazahkstan test site where events with the largest F factors are thought to occur in granitic rock and tend to be separated from previous explosions. Masse [1981] questions the conclusion of Aki and Tsai [1972] that the threshold for tectonic release increased in Yucca Flats with time. Rather, Masse suggested that the tectonic release variation is most likely the result of variations in the shot point depth relative to the saturated/unsaturated rock boundary. Although there does appear to be a volume associated with Yucca Flats events consistent with Pahute Mesa results, the source material probably plays an important role. As a first order approximation, tectonic release will apparently increase with rock type in the same way coupling increases with rock type.

If one accepts the volume-source observation for tectonic release, what does this imply for the "triggered slip" or "crushed zone relaxation" models for tectonic release? The volumes predicted on the basis of "isolated" or "influenced" populations at Pahute Mesa suggest that Archambeau's [1972] crushed zone is too small, yet the volume is not nearly large enough to be triggered slip on a single through going fault. A combination of these two models is the preferred kinematic model for tectonic release. If a distributed network of faults and joints within a region not much larger than Archambeau's [1972] radially cracked zone is "active" during the explosion process, it could account for the observation of tectonic release. The very high stress drops that appear to be required by the long-period sP phases can be explained as an artifact of assuming earthquake type rupture velocities. For example, the tectonic release moment from the teleseismic SH waves for BOXCAR is 3×10^{24} dyne-cm [Wallace et al., 1986]. If we assume that the volume which contributed to the generation of the tectonic release is $4/3\pi r^3$, where r = 1 km (the depth of burial for BOXCAR), and assume that the strain was released in the time it took the shock front to travel through this volume, the stress drop is on the order of 170 bars.

The distributed source model for tectonic release can also rectify the near-field observations of incoherent SH energy, and no systematic radiation pattern. The conclusion that tectonic release, associated with explosions at Pahute Mesa larger than 150 kt, is controlled by the regional stress regime is difficult to extend to other sites. Clearly, the seismic wavefield from all underground nuclear explosions will contain some contamination from non-isotropic radiation whether it be block motion or tectonic release. Further, rock type appears to be a very important parameter in controlling the size of tectonic release.

Conclusions and Problems

All underground nuclear explosions produce some non-isotropic seismic radiation. Part of this non-explosion component can be explained in terms of tectonic release, the radiation of seismic energy from equivalent shear-dislocation sources. These shear-sources are likely the result of three phenomena: (1) driven block or joint motion, (2) the release of the tectonic strain stored in a volume surrounding the explosion, and (3) the trigger of slip on prestressed faults. The driven block motion is observed in all explosions, and is dominated by thrust-type mechanisms, while the triggering of slip on faults is only rarely observed, and the sense of motion is dictated by the regional stress pattern. The volumetric stress release is also controlled by the regional stress pattern, and in general scales with yield. The reason for this is two fold: (1) the volume of rock which loses strength during an explosion scales with yield, and (2) as yield increases, depth of burial increases, which in turn, results in higher levels of stress. The tectonic release can produce a strong signature on the body waves from an explosion. This signature is a mixture of the three sources discussed above. For smaller

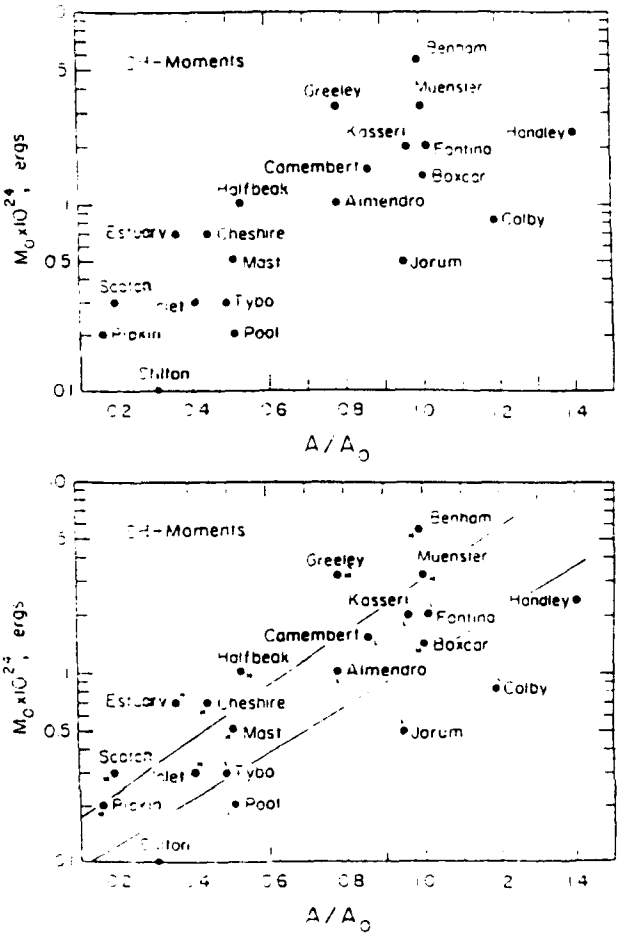

Fig. 12. (a) The seismic moment of the tectonic release for 21 Pahute Mesa explosions plotted against average ab amplitude. BOXCAR was used to normalize the amplitudes. (b) Data separated into two populations: "isolated" (predicted to have high tectonic release, labeled H) and "influenced" (predicted to have low tectonic release, labeled L).

events the driven block motion dominates. For larger explosions the volumetric stress-release can dominate, thus producing a seismic wavetrain which looks like a sum of an explosion and an earthquake. The earthquake can have any orientation (normal, thrust or strike-slip) depending on the regional level and orientation of stress.

At long periods, and in the far-field, the tectonic release can be represented by a point source. There is strong evidence that tectonic release will modify the long-period P waveform from an explosion. The volumetric component of tectonic release shows the largest variation between test sites, and even within test sites. On the basis of studies of Pahute Mesa events, the volume which produces the seismic wavefield appears to have a radius approximately 2 to 4 times the depth of burial. If an explosion is detonated within the source volume of a previous explosion it will have a reduced level of tectonic release. Rock type also appears to have a strong influence on the size of the tectonic release.

The evidence of a signature from tectonic release on short-period body waves is indirect. There are clear observations of short period SH pulses at regional distances, but Lg appears to be unaffected by tectonic release. In the near-field, the SH type energy is very complex and not coherent. The short-period observations favor a distributed source for the tectonic release, which is consistent with motion on many joints and bedding planes and the release of strain in a zone of fractured material around the working point. It is also apparent that the rupture process is important in explaining the short-period observations. It is likely that the rupture velocity is very high compared to an earthquake rupture, and downward directed energy (the direct P wave) is enhanced relative to upward directed energy (the sP and pP phases) which must travel through the spall zone (and hence a region of reduced strength) after reflecting on the free surface.

There are still several outstanding problems involving tectonic release. The most important is the qualification of the tectonic release signature on regional distance body waves. Why does the Lg yield estimator appear to be independent of tectonic release? Are new discriminates based on Pn and Pg sensitive to tectonic release (Taylor et al., 1989; Vergino et al., 1990)? As yield thresholds decrease, regional distance seismograms will become more important to monitoring, and at present there is little theoretical understanding of the factors which control the excitation of the various regional phases.

Acknowledgments. Much of the work presented in this paper represents collaborative efforts between the author and numerous coworkers. The author wishes to recognize Thorne Lay, Don Helmberger and Gladys Engen in particular. Comments by three anonymous reviewers and Howard Patton greatly improved the manuscript. Michelle Wallace provided significant editing of the manuscript.

References

Aki, K. and Y.B. Tsai, Mechanism of Love wave excitation by explosion sources, *J. Geophys. Res.*, *77*, 1452-1475, 1972.

Aki, K., P. Reasenberg, T. DeFazio, and Y.-B. Tsai, Near-field and far field seismic evidence for triggering of an earthquake by the BENHAM explosion, *Bull. Seism. Soc. Am.*, *59*, 2197-2207, 1969.

Alexander, S. S., Comparison of source and propagation characteristics in Eurasia, North Africa and the U.S. using regional and remote sensing observations, DARPA Symposium, Grand Island, New York, 1980.

Archambeau, C. B., The theory of stress wave radiation from explosions in prestressed media, *Geophys. J.*, *29*, 329-366, 1972.

Archambeau, C. B. and C. Sammis, Seismic radiation from explosions in prestressed media and the measurement of tectonic stress in the earth, *Rev. Geophys. Space Phys.*, *8*, 473-499, 1970.

Bache, T.C., The effect of tectonic stress release on explosion P wave signatures, *Bull. Seism. Soc. Am.*, *66*, 1441-1457, 1976.

Bucknam, R. C., Geologic effects of the BENHAM underground nuclear explosion, Nevada Test Site, *Bull. Seism. Soc. Am.*, *59*, 2209-2220, 1969.

Burger, R., T. Lay, T. Wallace, and L. Burdick, Evidence of tectonic release in long-period S waves from underground nuclear explosions at the Novaya Zemlya Test Sites, *Bull. Seism. Soc. Am.*, *76*, 733-755, 1986.

Brune, J. N. and P. W. Pomeroy, Surface wave radiation patterns for underground nuclear explosions and small-magnitude earthquakes, *J. Geophys. Res.*, *68*, 5005-5028, 1963.

Dahlman, O. and H. Israelson, *Monitoring Underground Nuclear Explosions*, Elsevier, New York, 440 pp., 1977.

Dickey, D. D., Strain associated with the BENHAM nuclear explosion, *Bull. Seism. Soc. Am.*, *59*, 2221-2230, 1969.

Douglas, A., J.B. Young and N.S. Lyman, Comments on a paper and a reply to a note by T.C. Wallace, D.V. Helmberger and T. Lay, *Bull. Seismo. Soc. Am.*, *76*, 305-311, 1986.

Fisher, F., P. Papanek, and R. Hamilton, *The Massachusetts Mountain earthquake of 5 August 1971 and its aftershocks, Nevada Test Site*, U.S.G.S. Rept. 474-149, 1972.

Given, J. W. and G. R. Mellman, Source parameters for nuclear explosions at NTS and Shagan River from observations of Rayleigh

and Love waves, presented at the DARPA/AFGL Seismic Research Symposium, May 6-8, 1985.

Goforth, T., Anomalous Rayleigh waves from presumed explosions at the Shagan River test site-A, abstract, DARPA symposium, Hampton, Virginia, 1982.

Gupta, I. N. and R. R. Blandford, A mechanism for generation of short-period transverse motion from explosions, *Bull. Seism. Soc. Am.*, *73*, 933-947, 1983.

Hamilton, R. M. and J. H. Healey, Aftershocks of the BENHAM nuclear explosion, *Bull. Seism. Soc. Am.*, *59*, 2271-2281, 1969.

Helle, H. and E. Rygg, Determination of tectonic release from surface waves generated by nuclear explosions in Eastern Kazakhstan, *Bull. Seism. Soc. Am.*, *74*, 1883-1898, 1984.

Hirasawa, T., Radiation patterns of S waves from underground explosions, *J. Geophys. Res.*, *76*, 6440-6454, 1971.

Johnson, L. R., T. V. McEvilly, and K. L. McLaughlin, Near-field recordings of ground accelerations from the Harzer explosion, abstract, *EOS*, *62*, 971, 1982.

Lay T., T. Wallace, and D. Helmberger, The effects of tectonic release on short-period P waves from NTS explosions, *Bull. Seism. Soc. Am.*, *74*, 819-847, 1984.

Lynnes, C. S. and T. Lay, Analysis of amplitude and travel-time anomalies for short-period P-waves from NTS explosions, *Geophys. J.*, *92*, 431-443, 1988.

Masse, R. P., Review of seismic source models for underground nuclear explosions, *Bull. Seism. Soc. Am.*, *71*, 1249-1268, 1981.

McKeown, F. A. and D. D. Dickey, Fault displacements and motion related to nuclear explosions, *Bull. Seism. Soc. Am.*, *59*, 2253-2269, 1969.

McKeown, F. A., P. P. Orkild, and R. C. Bucknam, Earthquake phenomena generated by nuclear explosions (abstract), *Earthquake Notes*, *41*, 10, 1970.

Muller, G., Seismic moment and long-period radiation of underground nuclear explosions, *Bull. Seism. Soc. Am.*, *63*, 847-857, 1973.

Murphy, J. and C. Archambeau, Variability in explosion body wave magnitudes: An analysis of the Rulison/Gasbuggy anomaly, *Bull. Seism. Soc. Am.*, *76*, 1087-1113, 1986.

Nuttli, O. W., Travel times and amplitudes of S waves from nuclear explosions in Nevada, *Bull. Seism. Soc. Am.*, *59*, 385-398, 1969.

Oliver, J., P. Pomerov, and M. Ewing, Long-period surface waves from nuclear explosions in various environments, *Science*, *131*, 1804-1805, 1960.

Patton, H. J., Measurements of Rayleigh-wave phase and the Massachusetts Mountain earthquake, *Bull. Seism. Soc. Am.*, *72*, 1329-1349, 1982.

Patton, H. J., Source models of the Harzer explosion from regional observations of fundamental-mode and higher mode surface waves, *Bull. Seism. Soc. Am.*, *78*, 1133-1157, 1988.

Patton, H. J., Seismic moment estimation and scaling of the long-period explosion source spectrum, AGU monograph, this volume, 1990

Pomeroy, R. W., W. J. Best, and T. V. McEvilly, Test Ban Treaty verification with regional data, *Bull. Seism. Soc. Am.*, *72*, 5089-5129, 1982.

Press, F. and C. Archambeau, Release of tectonic strain by underground nuclear explosions, *J. Geophys. Res.*, *67*, 337-343, 1962.

Ryall, A. and W. U. Savage, A comparison of seismological effects for the Nevada underground test BOXCAR with natural earthquakes in the Nevada region, *J. Geophys. Res.*, *74*, 4281-4289, 1969.

Rygg, E., Anomalous surface waves from underground explosions, *Bull. Seism. Soc. Am.*, *69*, 1995-2002, 1979.

Smith, S. W., Generation of seismic waves by underground explosions and the collapse of cavities, *J. Geophys. Res.*, *68*, 1477-1483, 1963.

Stevens, J. L., *A model for tectonic strain release from explosions in complex prestress fields applied to anomalous seismic waves from NTS and Eastern Kazakh explosions*, S-CUBED Technical Report SSS-R-5358, 1982.

Stevens, J., W. Rodi, J. Wang, B. Shkoller, E. Halda, B. Mason, and J. Minster, *Surface wave analysis package for Shagan River to SRO station path corrections*, S-Cubed Topical Report VSC-TR-82-81, 1982.

Taylor, S. R., M. D. Denny, E. S. Vergino, and R. E. Glaser, Regional discrimination between NTS explosions and Western U.S. earthquakes, *Bull. Seism. Soc. Am.*, *79*, 1142-1176, 1989.

Toksöz, M. N. and H. H. Kehrer, Tectonic strain release by underground nuclear explosions and its effect on seismic discrimination, *Geophys. J.*, *31*, 141-161, 1972.

Toksöz, M. N., A. Ben-Menahem, and D. G. Harkrider, Determination of source parameters of explosions and earthquakes by amplitude equalization of seismic surface waves, 1. Underground nuclear explosions, *J. Geophys. Res.*, *69*, 4355-4366, 1964.

Vergino, E. S. and Mensing, Yield estimation using regional m_b (Pn), *Bull. Seism. Soc. Am.*, *80*, 656-674, 1990.

Wallace, T., D. Helmberger, and G. Engen, Evidence of tectonic release from underground nuclear explosions in long-period P waves, *Bull. Seism. Soc. Am.*, *73*, 593-613, 1983.

Wallace, T., D. Helmberger, and G. Engen, Evidence of tectonic release from underground nuclear explosions in long period S waves, *Bull. Seism. Soc. Am.*, *85*, 157-174, 1985.

Wallace, T., D. Helmberger, and T. Lay, Reply to comments by A. Douglas, J. B. Young and N. S. Lyman and a note on the revised moments for Pahute Mesa tectonic release, *Bull. Seism. Soc. Am.*, *76*, 313-318, 1986.

Wallace, T., W. E. Holt, and K. Junkyoung, *Effects of tectonic release on broadband regional distance body waves*, AFGL-TR-87-0239, 50 p., 1987.

Walter, W. R. and H. J. Patton, Tectonic release from the Soviet Joint Verification Experiment, *Geophys. Res. Lett.*, *17*, 1517-1520, 1990.

DISTRIBUTION LIST

Prof. Thomas Ahrens
Seismological Lab, 252-21
Division of Geological & Planetary Sciences
California Institute of Technology
Pasadena, CA 91125

Prof. Keiiti Aki
Center for Earth Sciences
University of Southern California
University Park
Los Angeles, CA 90089-0741

Prof. Shelton Alexander
Geosciences Department
403 Deike Building
The Pennsylvania State University
University Park, PA 16802

Dr. Ralph Alewine, III
DARPA/NMRO
3701 North Fairfax Drive
Arlington, VA 22203-1714

Prof. Charles B. Archambeau
CIRES
University of Colorado
Boulder, CO 80309

Dr. Thomas C. Bache, Jr.
Science Applications Int'l Corp.
10260 Campus Point Drive
San Diego, CA 92121 (2 copies)

Prof. Muawia Barazangi
Institute for the Study of the Continent
Cornell University
Ithaca, NY 14853

Dr. Jeff Barker
Department of Geological Sciences
State University of New York
at Binghamton
Vestal, NY 13901

Dr. Douglas R. Baumgardt
ENSCO, Inc
5400 Port Royal Road
Springfield, VA 22151-2388

Dr. Susan Beck
Department of Geosciences
Building #77
University of Arizona
Tuscon, AZ 85721

Dr. T.J. Bennett
S-CUBED
A Division of Maxwell Laboratories
11800 Sunrise Valley Drive, Suite 1212
Reston, VA 22091

Dr. Robert Blandford
AFTAC/TT, Center for Seismic Studies
1300 North 17th Street
Suite 1450
Arlington, VA 22209-2308

Dr. G.A. Bollinger
Department of Geological Sciences
Virginia Polytechnical Institute
21044 Derring Hall
Blacksburg, VA 24061

Dr. Stephen Bratt
Center for Seismic Studies
1300 North 17th Street
Suite 1450
Arlington, VA 22209-2308

Dr. Lawrence Burdick
Woodward-Clyde Consultants
566 El Dorado Street
Pasadena, CA 91109-3245

Dr. Robert Burridge
Schlumberger-Doll Research Center
Old Quarry Road
Ridgefield, CT 06877

Dr. Jerry Carter
Center for Seismic Studies
1300 North 17th Street
Suite 1450
Arlington, VA 22209-2308

Dr. Eric Chael
Division 9241
Sandia Laboratory
Albuquerque, NM 87185

Prof. Vernon F. Cormier
Department of Geology & Geophysics
U-45, Room 207
University of Connecticut
Storrs, CT 06268

Prof. Steven Day
Department of Geological Sciences
San Diego State University
San Diego, CA 92182

Marvin Denny
U.S. Department of Energy
Office of Arms Control
Washington, DC 20585

Dr. Zoltan Der
ENSCO, Inc.
5400 Port Royal Road
Springfield, VA 22151-2388

Prof. Adam Dziewonski
Hoffman Laboratory, Harvard University
Dept. of Earth Atmos. & Planetary Sciences
20 Oxford Street
Cambridge, MA 02138

Prof. John Ebel
Department of Geology & Geophysics
Boston College
Chestnut Hill, MA 02167

Eric Fielding
SNEE Hall
INSTOC
Cornell University
Ithaca, NY 14853

Dr. Mark D. Fisk
Mission Research Corporation
735 State Street
P.O. Drawer 719
Santa Barbara, CA 93102

Prof Stanley Flatte
Applied Sciences Building
University of California, Santa Cruz
Santa Cruz, CA 95064

Dr. John Foley
NER-Geo Sciences
1100 Crown Colony Drive
Quincy, MA 02169

Prof. Donald Forsyth
Department of Geological Sciences
Brown University
Providence, RI 02912

Dr. Art Frankel
U.S. Geological Survey
922 National Center
Reston, VA 22092

Dr. Cliff Frolich
Institute of Geophysics
8701 North Mopac
Austin, TX 78759

Dr. Holly Given
IGPP, A-025
Scripps Institute of Oceanography
University of California, San Diego
La Jolla, CA 92093

Dr. Jeffrey W. Given
SAIC
10260 Campus Point Drive
San Diego, CA 92121

Dr. Dale Glover
Defense Intelligence Agency
ATTN: ODT-1B
Washington, DC 20301

Dr. Indra Gupta
Teledyne Geotech
314 Montgomery Street
Alexanderia, VA 22314

Dan N. Hagedon
Pacific Northwest Laboratories
Battelle Boulevard
Richland, WA 99352

Dr. James Hannon
Lawrence Livermore National Laboratory
P.O. Box 808
L-205
Livermore, CA 94550

Dr. Roger Hansen
HQ AFTAC/TTR
Patrick AFB, FL 32925-6001

Prof. David G. Harkrider
Seismological Laboratory
Division of Geological & Planetary Sciences
California Institute of Technology
Pasadena, CA 91125

Prof. Danny Harvey
CIRES
University of Colorado
Boulder, CO 80309

Prof. Donald V. Helmberger
Seismological Laboratory
Division of Geological & Planetary Sciences
California Institute of Technology
Pasadena, CA 91125

Prof. Eugene Herrin
Institute for the Study of Earth and Man
Geophysical Laboratory
Southern Methodist University
Dallas, TX 75275

Prof. Robert B. Herrmann
Department of Earth & Atmospheric Sciences
St. Louis University
St. Louis, MO 63156

Prof. Lane R. Johnson
Seismographic Station
University of California
Berkeley, CA 94720

Prof. Thomas H. Jordan
Department of Earth, Atmospheric &
Planetary Sciences
Massachusetts Institute of Technology
Cambridge, MA 02139

Prof. Alan Kafka
Department of Geology & Geophysics
Boston College
Chestnut Hill, MA 02167

Robert C. Kemerait
ENSCO, Inc.
445 Pineda Court
Melbourne, FL 32940

Dr. Max Koontz
U.S. Dept. of Energy/DP 5
Forrestal Building
1000 Independence Avenue
Washington, DC 20585

Dr. Richard LaCoss
MIT Lincoln Laboratory, M-200B
P.O. Box 73
Lexington, MA 02173-0073

Dr. Fred K. Lamb
University of Illinois at Urbana-Champaign
Department of Physics
1110 West Green Street
Urbana, IL 61801

Prof. Charles A. Langston
Geosciences Department
403 Deike Building
The Pennsylvania State University
University Park, PA 16802

Jim Lawson, Chief Geophysicist
Oklahoma Geological Survey
Oklahoma Geophysical Observatory
P.O. Box 8
Leonard, OK 74043-0008

Prof. Thorne Lay
Institute of Tectonics
Earth Science Board
University of California, Santa Cruz
Santa Cruz, CA 95064

Dr. William Leith
U.S. Geological Survey
Mail Stop 928
Reston, VA 22092

Mr. James F. Lewkowicz
Phillips Laboratory/GPEH
Hanscom AFB, MA 01731-5000(2 copies)

Mr. Alfred Lieberman
ACDA/VI-OA State Department Building
Room 5726
320-21st Street, NW
Washington, DC 20451

Prof. L. Timothy Long
School of Geophysical Sciences
Georgia Institute of Technology
Atlanta, GA 30332

Dr. Randolph Martin, III
New England Research, Inc.
76 Olcott Drive
White River Junction, VT 05001

Dr. Robert Masse
Denver Federal Building
Box 25046, Mail Stop 967
Denver, CO 80225

Dr. Gary McCartor
Department of Physics
Southern Methodist University
Dallas, TX 75275

Prof. Thomas V. McEvilly
Seismographic Station
University of California
Berkeley, CA 94720

Dr. Art McGarr
U.S. Geological Survey
Mail Stop 977
U.S. Geological Survey
Menlo Park, CA 94025

Dr. Keith L. McLaughlin
S-CUBED
A Division of Maxwell Laboratory
P.O. Box 1620
La Jolla, CA 92038-1620

Stephen Miller & Dr. Alexander Florence
SRI International
333 Ravenswood Avenue
Box AF 116
Menlo Park, CA 94025-3493

Prof. Bernard Minster
IGPP, A-025
Scripps Institute of Oceanography
University of California, San Diego
La Jolla, CA 92093

Prof. Brian J. Mitchell
Department of Earth & Atmospheric Sciences
St. Louis University
St. Louis, MO 63156

Mr. Jack Murphy
S-CUBED
A Division of Maxwell Laboratory
11800 Sunrise Valley Drive, Suite 1212
Reston, VA 22091 (2 Copies)

Dr. Keith K. Nakanishi
Lawrence Livermore National Laboratory
L-025
P.O. Box 808
Livermore, CA 94550

Dr. Carl Newton
Los Alamos National Laboratory
P.O. Box 1663
Mail Stop C335, Group ESS-3
Los Alamos, NM 87545

Dr. Bao Nguyen
HQ AFTAC/TTR
Patrick AFB, FL 32925-6001

Prof. John A. Orcutt
IGPP, A-025
Scripps Institute of Oceanography
University of California, San Diego
La Jolla, CA 92093

Prof. Jeffrey Park
Kline Geology Laboratory
P.O. Box 6666
New Haven, CT 06511-8130

Dr. Howard Patton
Lawrence Livermore National Laboratory
L-025
P.O. Box 808
Livermore, CA 94550

Dr. Frank Pilotte
HQ AFTAC/TT
Patrick AFB, FL 32925-6001

Dr. Jay J. Pulli
Radix Systems, Inc.
2 Taft Court, Suite 203
Rockville, MD 20850

Dr. Robert Reinke
ATTN: FCTVTD
Field Command
Defense Nuclear Agency
Kirtland AFB, NM 87115

Prof. Paul G. Richards
Lamont-Doherty Geological Observatory
of Columbia University
Palisades, NY 10964

Mr. Wilmer Rivers
Teledyne Geotech
314 Montgomery Street
Alexandria, VA 22314

Dr. George Rothe
HQ AFTAC/TTR
Patrick AFB, FL 32925-6001

Dr. Alan S. Ryall, Jr.
DARPA/NMRO
3701 North Fairfax Drive
Arlington, VA 22209-1714

Dr. Richard Sailor
TASC, Inc.
55 Walkers Brook Drive
Reading, MA 01867

Prof. Charles G. Sammis
Center for Earth Sciences
University of Southern California
University Park
Los Angeles, CA 90089-0741

Prof. Christopher H. Scholz
Lamont-Doherty Geological Observatory
of Columbia University
Palisades, CA 10964

Dr. Susan Schwartz
Institute of Tectonics
1156 High Street
Santa Cruz, CA 95064

Secretary of the Air Force
(SAFRD)
Washington, DC 20330

Office of the Secretary of Defense
DDR&E
Washington, DC 20330

Thomas J. Sereno, Jr.
Science Application Int'l Corp.
10260 Campus Point Drive
San Diego, CA 92121

Dr. Michael Shore
Defense Nuclear Agency/SPSS
6801 Telegraph Road
Alexandria, VA 22310

Dr. Matthew Sibol
Virginia Tech
Seismological Observatory
4044 Derring Hall
Blacksburg, VA 24061-0420

Prof. David G. Simpson
IRIS, Inc.
1616 North Fort Myer Drive
Suite 1440
Arlington, VA 22209

Donald L. Springer
Lawrence Livermore National Laboratory
L-025
P.O. Box 808
Livermore, CA 94550

Dr. Jeffrey Stevens
S-CUBED
A Division of Maxwell Laboratory
P.O. Box 1620
La Jolla, CA 92038-1620

Lt. Col. Jim Stobie
ATTN: AFOSR/NL
Bolling AFB
Washington, DC 20332-6448

Prof. Brian Stump
Institute for the Study of Earth & Man
Geophysical Laboratory
Southern Methodist University
Dallas, TX 75275

Prof. Jeremiah Sullivan
University of Illinois at Urbana-Champaign
Department of Physics
1110 West Green Street
Urbana, IL 61801

Prof. L. Sykes
Lamont-Doherty Geological Observatory
of Columbia University
Palisades, NY 10964

Dr. David Taylor
ENSCO, Inc.
445 Pineda Court
Melbourne, FL 32940

Dr. Steven R. Taylor
Los Alamos National Laboratory
P.O. Box 1663
Mail Stop C335
Los Alamos, NM 87545

Prof. Clifford Thurber
University of Wisconsin-Madison
Department of Geology & Geophysics
1215 West Dayton Street
Madison, WS 53706

Prof. M. Nafi Toksoz
Earth Resources Lab
Massachusetts Institute of Technology
42 Carleton Street
Cambridge, MA 02142

Dr. Larry Turnbull
CIA-OSWR/NED
Washington, DC 20505

Dr. Gregory van der Vink
IRIS, Inc.
1616 North Fort Myer Drive
Suite 1440
Arlington, VA 22209

Dr. Karl Veith
EG&G
5211 Auth Road
Suite 240
Suitland, MD 20746

Prof. Terry C. Wallace
Department of Geosciences
Building #77
University of Arizona
Tuscon, AZ 85721

Dr. Thomas Weaver
Los Alamos National Laboratory
P.O. Box 1663
Mail Stop C335
Los Alamos, NM 87545

Dr. William Wortman
Mission Research Corporation
8560 Cinderbed Road
Suite 700
Newington, VA 22122

Prof. Francis T. Wu
Department of Geological Sciences
State University of New York
at Binghamton
Vestal, NY 13901

AFTAC/CA
(STINFO)
Patrick AFB, FL 32925-6001

DARPA/PM
3701 North Fairfax Drive
Arlington, VA 22203-1714

DARPA/RMO/RETRIEVAL
3701 North Fairfax Drive
Arlington, VA 22203-1714

DARPA/RMO/SECURITY OFFICE
3701 North Fairfax Drive
Arlington, VA 22203-1714

HQ DNA
ATTN: Technical Library
Washington, DC 20305

Defense Intelligence Agency
Directorate for Scientific & Technical Intelligence
ATTN: DTIB
Washington, DC 20340-6158

Defense Technical Information Center
Cameron Station
Alexandria, VA 22314 (2 Copies)

TACTEC
Battelle Memorial Institute
505 King Avenue
Columbus, OH 43201 (Final Report)

Phillips Laboratory
ATTN: XPG
Hanscom AFB, MA 01731-5000

Phillips Laboratory
ATTN: GPE
Hanscom AFB, MA 01731-5000

Phillips Laboratory
ATTN: TSML
Hanscom AFB, MA 01731-5000

Phillips Laboratory
ATTN: SUL
Kirtland, NM 87117 (2 copies)

Dr. Michel Bouchon
I.R.I.G.M.-B.P. 68
38402 St. Martin D'Heres
Cedex, FRANCE

Dr. Michel Campillo
Observatoire de Grenoble
I.R.I.G.M.-B.P. 53
38041 Grenoble, FRANCE

Dr. Kin Yip Chun
Geophysics Division
Physics Department
University of Toronto
Ontario, CANADA

Prof. Hans-Peter Harjes
Institute for Geophysic
Ruhr University/Bochum
P.O. Box 102148
4630 Bochum 1, GERMANY

Prof. Eystein Husebye
NTNF/NORSAR
P.O. Box 51
N-2007 Kjeller, NORWAY

David Jepsen
Acting Head, Nuclear Monitoring Section
Bureau of Mineral Resources
Geology and Geophysics
G.P.O. Box 378, Canberra, AUSTRALIA

Ms. Eva Johannisson
Senior Research Officer
National Defense Research Inst.
P.O. Box 27322
S-102 54 Stockholm, SWEDEN

Dr. Peter Marshall
Procurement Executive
Ministry of Defense
Blacknest, Brimpton
Reading FG7-FRS, UNITED KINGDOM

Dr. Bernard Massinon, Dr. Pierre Mechler
Societe Radiomana
27 rue Claude Bernard
75005 Paris, FRANCE (2 Copies)

Dr. Svein Mykkeltveit
NTNT/NORSAR
P.O. Box 51
N-2007 Kjeller, NORWAY (3 Copies)

Prof. Keith Priestley
University of Cambridge
Bullard Labs, Dept. of Earth Sciences
Madingley Rise, Madingley Road
Cambridge CB3 OEZ, ENGLAND

Dr. Jorg Schlittenhardt
Federal Institute for Geosciences & Nat'l Res.
Postfach 510153
D-3000 Hannover 51, GERMANY

Dr. Johannes Schweitzer
Institute of Geophysics
Ruhr University/Bochum
P.O. Box 1102148
4360 Bochum 1, GERMANY

END